

Copyright is owned by the Author of the thesis. Permission is given for a copy to be downloaded by an individual for the purpose of research and private study only. The thesis may not be reproduced elsewhere without the permission of the Author.



Massey University

SCHOOL OF ENGINEERING AND
ADVANCED TECHNOLOGY

**Design and Development of a Food Texture
Analyser**

A thesis presented in partial fulfillment of the requirements

for the degree of

**Master of Engineering
in
Mechatronics**

at Massey University, Manawatu, New Zealand

Weizhong Shi

August 2015

SUPERVISORS

a. Gourab Sen Gupta

b. Ken Mercer

c. John Bronlund

ACKNOWLEDGEMENTS

In completing this Master's degree in Mechatronics Engineering I would like to take this opportunity to sincerely thank several people.

I sincerely thank Associate Professor Gourab Sen Gupta from the School of Engineering and Advanced Technology (SEAT), Massey University, Palmerston North, New Zealand for his guidance and expertise throughout this project from start to finish.

I would like to thank Professor John Brounlund for giving me insight into food texture and its measurement. He also helped me to develop the specifications of a practical texture analyser.

I would like to acknowledge the contributions of Mr. Ken Mercer, Mr. Colin Plaw, Bruce Collins, Anthony Wade and Clive Bardell, and thank them a lot. I would also like to thank the SEAT IT support staff for providing me with the required IT tools to run software for my study.

Sincere thanks to Debraj Basu for proof reading my thesis and helping me to improve it.

I would like to thank my friend Vicky Yue. Thanks for accompanying me to the national park for a visit, during the hardest period of my project.

Finally, and most importantly, I would like to thank my parents, for their unconditional love and support throughout my time at university. Thank you for all the sacrifices you have made to give me a better chance in life.

Abstract

Texture is an important attribute of food and is one of the several dimensions of food quality. In today's world of sensing and automated measurements, it is becoming increasingly common to analyse food by using a texture analyser. A variety of texture analysers is in use by researchers and industry for the purpose of quality assurance and improvements.

This thesis is on the design, development and implementation of a food texture analyser with a focus on enhancing response time, increasing measurement flexibility, and reducing equipment cost.

Several enhancements have been done to an existing texture analyser. A high-end 24-bits ADC (Analogue to Digital Converter) has been used to measure the output of a load cell very accurately. The output of the ADC is coupled to a modern microcontroller using the industry standard SPI bus. A touch screen has been incorporated to provide an easy user interface. A completely new motor controller/driver has been employed for the movement of the robotic arm and an infra-red sensor has been used to detect its position. A unique and novel contribution is in the form of a new command-language that has been developed which makes it extremely flexible for the user to control the motor movements. An enhancement, not found in existing commercial texture analysers, is the real-time graphing of measurement data which is displayed on the PC. Additionally all the data can be saved to a text file or a CSV file for subsequent retrieval and processing.

The complete system has been realised and tested. Several different fruits were used for experiments and the measurement data compared with a commercial texture analyser. The system is simple to use, versatile and low cost for use in research and industry.

Table of Contents

ACKNOWLEDGEMENTS	i
Abstract.....	ii
Chapter 1 Introduction.....	6
1.1 What is a fruit texture measurement system?	11
Chapter 2 Review of Texture Analysers	13
2.1 Introduction to Texture Analyser	13
2.2 Limitations of existing Texture Analysers	16
2.3 Specifications	18
2.4 Summary	19
Chapter 3 Mechanical Design	21
3.1 Methods for movement	22
3.2 Mechanical Component Description	23
3.2.1 Material selection.....	23
3.2.2 Ball screw.....	25
3.2.2 Stepper motor	28
3.2.4 Base of the instrument.....	30
3.2.2 Infra-red sensor holder	32
3.2.3 Load cell.....	32
3.3 Summary	34
Chapter 4 Electronic design.....	35
4.1 Electronic design and overview.....	35
4.2 Master board	38
4.2.1 Microcontroller	38

4.2.2 Stepper Motor Driver.....	40
4.2.3 ADC.....	44
4.2.4 Pull-up Resistor.....	50
4.2.5 Infra-Red sensor	51
4.2.6 Using diode to realise an OR Gate	52
4.2.7 Power supply	52
4.3 Slave Board	58
4.3.1 Touchscreen	58
4.4 Protection System and Circuits.....	61
4.5 Schematic and PCB	61
4.6 Summary	67
Chapter 5 Software Implementation.....	68
5.1 SPI Bus:.....	68
5.2 Microcontroller programming	69
5.2.1 Stepper Motor Driver.....	69
5.2.2 Analogue to Digital Converter.....	72
5.2.3 Touch Screen.....	74
5.2.4 Control Modes and the Interpreter	75
5.3 Graphical User Interface for Instrument Control.....	81
5.3.1 Functions and Features of the Graphical User Interface.....	81
5.3.2 Serial Port.....	83
5.4 Summary	84
Chapter 6 Experiments and Results.....	85
6.1 Initial force test using pressure ball.....	85
6.2 Repeat tests and comparison.....	88
6.3 Experimentations with fruits.....	89
6.3.1 Avocado	89
6.3.2 Kiwifruit	93

6.3.2 Persimmon.....	97
6.4 Summary	102
Chapter 7 Summary and Future Possibilities	103
References	106
Appendix.....	109
Appendix 1: Critical Component Data Sheets.....	109
Appendix 2: PCB design.....	116
Appendix 3: Test results	118
Appendix4: ADC code	136

List of Figures

Chapter 1

FIGURE 1.1: PUNCTURE FORCE VS PUNCH AREA (REPRINTED FROM J.FOOD SCI.31, 286, 1966; COPYRIGHT BY INSTITUTE OF FOOD TECHNOLOGIST.).....	8
FIGURE 1.2: FOOD TEXTURE AND VISCOSITY: CONCEPT AND MEASUREMENT: ACADEMIC PRESS FROM BOURNE, M. (2002).....	11
FIGURE 1.3: SIMPLE DIAGRAM OF THE WHOLE SYSTEM.....	12

Chapter 2

FIGURE 2.1: POWDER FLOW ANALYSER [18]	13
FIGURE 2.2: TA.XT PLUS TEXTURE ANALYSER [18]	14

Chapter 3

FIGURE 3.1: TEXTURE ANALYSER	21
FIGURE 3.2: THE MODIFIED TEXTURE ANALYSER	23
FIGURE 3.3: DIMENSIONS OF THE IEC CONNECTOR	30
FIGURE 3.4: DIMENSIONS OF DB9	31
FIGURE 3.5: DIMENSIONS OF DB15	31
FIGURE 3.6: THE BASE IN SOLIDWORKS.....	31
FIGURE 3.7: SOLIDWORKS DESIGN OF THE INFRA-RED SENSOR HOLDER	32
FIGURE 3. 8: LOAD CELL.....	33
FIGURE 3.9: THE PRINCIPLE OF THE LOAD CELL WORKING [36]	33
FIGURE 3.10: THE SPECIFICATIONS OF THE LOAD CELL	34

Chapter 4

FIGURE 4.1: FUNCTIONAL BLOCK DIAGRAM OF THE ELECTRONIC DESIGN	36
FIGURE 4.2: THE SIZE OF EXECUTABLE FILE OF MASTER BOARD	37
FIGURE 4.3: THE SIZE OF EXECUTABLE FILE OF SLAVE BOARD.....	37
FIGURE 4.4: ARDUINO NANO [40]	39
FIGURE 4.5: L6472 MICROSTEPPING MOTOR DRIVES[42]	41
FIGURE 4.6: TYPICAL CIRCUIT OF L6472	42
FIGURE 4.7: THE CHARGE PUMP CIRCUIT [42]	43
FIGURE 4.8: THE SCHEMATIC OF L6472	44
FIGURE 4.9: THE INTERNAL STRUCTURE OF THE ADC	45
FIGURE 4.10: TYPICAL CIRCUIT OF THE ADC 7192[45]	48
FIGURE 4.11: THE SCHEMATIC OF ADC 7192 CIRCUIT	49
FIGURE 4.12: EXAMPLE CODE OF ADC 7192.....	49
FIGURE 4.13: THE RESULT FROM ADC	50
FIGURE 4.14: THE SCHEMATIC OF PULL UP RESISTORS	51
FIGURE 4.15: INFRA-RED SENSOR.....	52
FIGURE 4.16: THE SCHEMATIC OF OR GATE.....	52
FIGURE 4.17: THE TYPICAL CIRCUIT OF LM2594.....	53

FIGURE 4.18: THE SCHEMATIC OF LM2594.....	53
FIGURE 4.19: THE RIPPLE BEFORE LC FILTER.....	54
FIGURE 4.20: THE RIPPLE AFTER LC FILTER	54
FIGURE 4.21: TYPICAL CIRCUIT FOR 7805.....	55
FIGURE 4.22: THE POWER-SUPPLY REJECTION RATIO (TPSA4901) [53].....	55
FIGURE 4.23: THE SCHEMATIC OF TPSA4901 [53]	56
FIGURE 4.24: THE RIPPLE AFTER LDO FILTER	56
FIGURE 4.25: THE SCHEMATIC OF REF5050.....	57
FIGURE 4.26: THE SCHEMATIC OF THE POWER SUPPLY.....	57
FIGURE 4.27: TOUCH SCREEN	58
FIGURE 4.28: THE PRINCIPLE OF TOUCH SCREEN OPERATION [56].....	59
FIGURE 4.29: 4 WIRE TOUCH SCREEN.....	60
FIGURE 4.30: PROTECT SYSTEM.....	61
FIGURE 4.31: THE SCHEMATIC OF THE PROTECTION SYSTEM [57].....	61
FIGURE 4.32: THE FORMATTING OF MIXED SIGNAL [63].....	63
FIGURE 4.33: THE DIAGRAM OF MIXED SIGNAL [63]	63
FIGURE 4.34: THE COMPLETE SCHEMATIC OF THE MASTER BOARD [63].....	65
FIGURE 4.35: THE SCHEMATIC OF THE SLAVE BOARD	65
FIGURE 4.36: TOP LAYER OF THE MASTER BOARD	66
FIGURE 4.37: BOTTOM LAYER OF THE MASTER BOARD	66
FIGURE 4.38: THE PCB DESIGN OF THE SLAVE BOARD	67

Chapter 5

FIGURE 5.1: SPI BUS CONNECTIONS BETWEEN MASTER AND SLAVE DEVICES	68
FIGURE 5.2: SPI TIMING DIAGRAM OF L6472 STEPPER MOTOR DRIVER CHIP	69
FIGURE 5.3: CONTINUOUS CONVERSION MODE	72
FIGURE 5.4: CONTINUOUS READ	73
FIGURE 5.5: THE VISUAL BUTTONS OF THE TOUCH SCREEN.....	75
FIGURE 5.6:PROGRAM CONTROL MODE STRUCTURE.....	78
FIGURE 5.7: AN EXAMPLE OF RECURSIVE CODE IN C.....	80
FIGURE 5.8: THE STRUCTURE OF THE SOFTWARE DESIGN.....	80
FIGURE 5.9 : SNIPPET OF CODE TO PARSE THE COMMAND STRING AT THE MICROCONTROLLER END.....	81
FIGURE 5.10: CODE TO SEND COMMAND STRING ON RS232 PORT.....	81
FIGURE 5.11: THE GRAPHICAL USER INTERFACE (GUI) FOR THE INSTRUMENT.....	82
FIGURE 5.12 REAL TIME MEASUREMENT DATA AND GRAPH	82
FIGURE 5.13 THE TEXTBOX FOR DISPLAYING THE DATA FROM THE LOAD CELL	82
FIGURE 5.14 SAMPLE CODE OF SERIAL PORT INITIALIZATION	83

Chapter 6

FIGURE 6.1: SQUEEZE/BOUNCY BALL USED FOR INITIAL EXPERIMENTATION	86
FIGURE 6.2: THE COMPRESSION PROBE USED WITH THE SQUEEZE BALL.....	86
FIGURE 6.3: THE RESULT FROM TESTS DONE USING STANDARD TEXTURE ANALYSER (FORCE VS. TIME)	

.....	86
FIGURE 6.4: THE RESULT FROM TESTS DONE USING THE NEWLY DEVELOPED TEXTURE ANALYSER	87
FIGURE 6.5: COINCIDING THE TEST CURVES.....	88
FIGURE 6.6: TESTING AVOCADO USING STANDARD TEXTURE ANALYSER.....	89
FIGURE 6.7: TESTING AVOCADO USING THE NEW TEXTURE ANALYSER	90
FIGURE 6.8: RESULTS OF FORCE MEASUREMENT OF AVOCADO USING THE STANDARD TEXTURE ANALYSER	90
FIGURE 6.9: RESULTS OF FORCE MEASUREMENT OF AVOCADO USING THE NEW TEXTURE ANALYSER	91
FIGURE 6.10: COMBINING THE RESULTS OF THE TEXTURE ANALYSER AND THE NEW INSTRUMENT FOR AVOCADO	91
FIGURE 6.11: TESTING KIWIFRUIT USING STANDARD TEXTURE ANALYSER	94
FIGURE 6.12: TESTING KIWIFRUIT USING THE NEW ANALYSER.....	94
FIGURE 6.13: RESULTS OF FORCE MEASUREMENT OF KIWIFRUIT USING THE STANDARD TEXTURE ANALYSER	94
FIGURE 6.14: RESULTS OF FORCE MEASUREMENT OF KIWIFRUIT USING THE NEW TEXTURE ANALYSER	95
FIGURE 6.15: COMBINING THE RESULTS OF THE TEXTURE ANALYSER AND THE NEW INSTRUMENT FOR KIWIFRUIT	95
FIGURE 6.16: PERSIMMON BEING TESTED USING A STANDARD TEXTURE ANALYSER.....	98
FIGURE 6.17: RESULTS OF FORCE MEASUREMENT OF PERSIMMON USING THE STANDARD TEXTURE ANALYSER	98
FIGURE 6.18: RESULTS OF FORCE MEASUREMENT OF PERSIMMON USING THE NEW TEXTURE ANALYSER	98
FIGURE 6.19: COMBINING THE RESULTS OF THE TEXTURE ANALYSER AND THE NEW INSTRUMENT FOR PERSIMMON.....	99

List of Tables

Chapter 1

TABLE 1.1: THE PUNCTURE FORCE FOR SAMPLE NUT (FROM BOURNE, M. (2002). FOOD TEXTURE AND VISCOSITY: CONCEPT AND MEASUREMENT: ACADEMIC PRESS.	8
TABLE 1.2: THE EXAMPLES OF ROME APPLES WHEN SQUEEZED. FROM BOURNE, M. (2002). FOOD TEXTURE AND VISCOSITY: CONCEPT AND MEASUREMENT: ACADEMIC PRESS [13]	10

Chapter 2

TABLE 2.1: BASIC PARAMETERS OF TA.XT PLUS	15
TABLE 2.2: TECHNICAL SPECIFICATIONS OF TA.HD PLUS	16
TABLE 2.3: THE SPEED OF ORIGINAL TEXTURE ANALYSER	17
TABLE 2.4: THE SPEED OF NEW TEXTURE ANALYSER	17
TABLE 2.5: AVERAGE FORCE PER TOOTH DURING MASTICATION[13]	19

Chapter 4

TABLE 4.1: SPECIFICATIONS OF NANO	39
TABLE 4.2: COMMUNICATIONS REGISTER OF ADC 7192	47
TABLE 4.3: MODE REGISTER OF ADC 7192.....	47
TABLE 4.4: CONFIGURATION REGISTER OF ADC 7192.....	48

Chapter 5

TABLE 5.1: THE REGISTERS OF L6472	70
TABLE 5.2: COMMAND SET OF L6472	71
TABLE 5.3: PROGRAMMING THE CHANNEL SELECTION BITS FOR THE ADC.....	74
TABLE 5.4: SETTING THE GAIN FOR THE ADC.....	74
TABLE 5.5: POLARITY SELECT BIT.....	74

Chapter 6

TABLE 6.1: THE CONDITIONS OF THE PRESSURE BALL TEST	85
TABLE 6.2: THE MAXIMUM, MINIMUM, MEAN ERROR AND STANDARD DEVIATION FOR MEASUREMENTS DONE ON SQUEEZE BALL WITH THE STANDARD AND THE NEW INSTRUMENT	87
TABLE 6.3: THE CONDITIONS OF THE AVOCADO TEST	89
TABLE 6.4: THE MAXIMUM, MINIMUM, MEAN ERROR AND STANDARD DEVIATION FOR MEASUREMENTS DONE ON AVOCADO WITH THE STANDARD AND THE NEW INSTRUMENT	92
TABLE 6.5: THE CONDITIONS OF TESTING KIWIFRUIT.....	93
TABLE 6.6: THE MAXIMUM, MINIMUM, MEAN ERROR AND STANDARD DEVIATION FOR MEASUREMENTS DONE ON KIWIFRUIT WITH THE STANDARD AND THE NEW INSTRUMENT.....	95
TABLE 6.7: THE CONDITIONS OF TESTING PERSIMMON.....	97
TABLE 6.8: THE MAXIMUM, MINIMUM, MEAN ERROR AND STANDARD DEVIATION FOR MEASUREMENTS DONE ON PERSIMMON WITH THE STANDARD AND THE NEW INSTRUMENT ...	99

Chapter 7

TABLE 7.1: COMPARISON BETWEEN TWO TEXTURE ANALYSERS.....	105
--	-----

Chapter 1

Introduction

In general, food texture measurement is a way to know the physical structure of food. Malcolm Bourne[1] said that the texture properties are perceived by the human senses. Nowadays, texture analyzers are used to imitate the feeling and perception of human by using them that measure the properties of texture in a scientific way. Textures affect consumer preference of accepted foods and every food manufacturer strives to make his product of the highest level of texture and flavour [2]. For product developers, it can let them transfer the target texture from the lab to the consumer's kitchen in a scientific way.

Food texture measurement is a well-established technique that can evaluate the physical properties of the food structure and raw ingredients [1]. The application of food texture measurement is across a wide range of food types, including fruit, meat, confectioneries, snack, cheese, etc. Bourne [2] indicated that since the texture is a property related to the sense of touch, it can be measured easily by using a mechanical method such as force [3]. The standard tests in food texture measurement, such as compression, puncture and penetration, cutting and shearing, and extrusion are used to measure the hardness, softness, crispness and other properties of food [4]. The user can collect the data of the mechanical food texture measurement in a variety of ways. Bourne indicates that the texture is not a single-dimensional attribute; it is a multidimensional attribute [3]. The textual properties of foods have the following characteristics [4]:

1. They are a group of physical properties
2. They derive from the structure of the food
3. Belong under the mechanical or rheological subheading of physical properties.
4. Sensed by the feeling of touch
5. Objective measurement is usually by using functions of mass, distance and time.

The five characteristics that are mentioned above mean that the food scientists should consider the whole characteristics of food, which can be utilized in the measurement, and choose the most appropriate one for the product of interest [5]. Then it is necessary to select an instrument that is suitable to measure these characteristics. The result of data is required to be logged in a file and displayed on the screen to help scientists to do their analysis.

The most common form of texture measurement is by measuring force [2]. The sub-classifications of force measurement include puncture, compression-extrusion, cutting-shear, compression, tensile, TPA (Texture Profile Analysis), bending and snapping, and deformation [5].

Compression

There are two main kinds of compression tests. These are:

- **Uniaxial compression**
- **Bulk compression**

In uniaxial compression, the samples are compressed and cause a change in shape [5]. This method is usually used in solid foods testing [6]. In bulk compression testing, sample will be compressed in three dimensions [7]. That causes a change in volume but usually no change in shape. However, compression is seldom used in testing food, because of the slowness and difficulty in using the technique [1].

Puncture

The puncture test measures the force required to push a punch or probe into food [1]. In this test, a thin instrument is made to penetrate into the sample. A resistant force is achieved from a certain depth of penetration [8]. Under certain conditions and at a specific time, the depth of penetration is measured and used as an index of hardness, firmness, toughness etc [1].

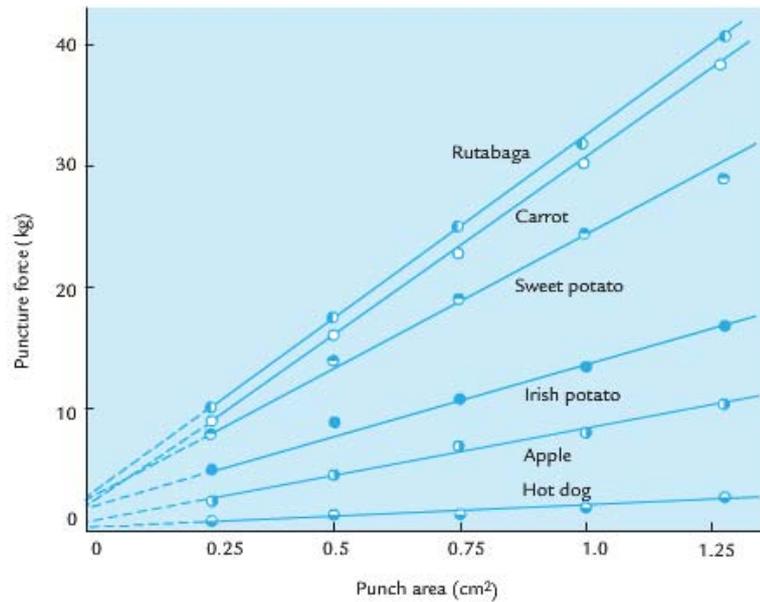


Figure 1.1: Puncture force VS punch area (Reprinted from J.Food Sci.31, 286, 1966; copyright by Institute of Food Technologist.)

Figure 1.1 shows the relationship of force and punch area of some daily food as consequence of puncher test. Table 1.1 illustrates puncture force of different types of nuts.

Table 1.1: The Puncture force for Sample nut (from Bourne, M. (2002). Food texture and viscosity: concept and measurement: Academic Press.

Nut	Puncture force and standard deviation (N)
Almond	20.3 ± 4.7
Brazil nut	17.0 ± 5.8
Cashew	11.1 ± 3.2
Hazelnut	19.9 ± 4.2
Macadamia	13.6 ± 1.4
Peanut	13.3 ± 2.9
Pecan	6.7 ± 1.3
Pine nut	4.5 ± 0.7
Walnut	5.0 ± 0.9

Tests were performed in a TA.XT2 Texture Analyzer using a 1.17-mm diameter circular punch with a flat face. Crosshead speed 3.0 mm s⁻¹. (Unpublished data from M. C. Bourne.)

It can be seen from table 1.1 that the hardest nut is almond and has a puncture force of 20.3 N on it. The softest nut is walnut; it can be penetrated with just using 5.0 N force. The puncture principle is the most frequently used principle for measuring food texture [1].

Cutting and Shearing

In some specific conditions, it is necessary to attach a single or multiple blades to cut or shear through the sample of food to achieve the maximum test force [9]. It is indicated that the food technologists sometimes use the shear force to describe any cutting action that causes the product to be divided into two or more pieces [1]. The sharper the blade, higher the pressure that will be applied on the food.

Compression-extrusion

The compression-extrusion test consists of applying force to a food until it flows through an outlet (or number of outlets) that may be in the form of one or more slots or holes that are in the test cell [10]. The food is compressed until the structure of the food is disrupted, and it extrudes through these outlets [1]. The pattern of forces that are involved in such a test is complex. Usually, the maximum force required to accomplish extrusion is measured and used as an index of textural quality.

Tensile

The tensile test is not widely used with food because the process of mastication has already created compression, not the tension of the food between the molars.

Tensile is defined as a force normal to the surface on which it acted and directed outwards from the body [3].

The pattern of force is collected and transferred to the computer as the material is being tensed. The relationship of force and time will be displayed immediately at the end of the test.

Fracture and Bending/Snapping

The ability of fracture is a parameter that was initially called brittleness. Texture analyser will crumble the material such as peanuts. Foods that exhibit the ability to fracture are products that possess a high degree of hardness and low degree of adhesiveness [1]. The level of fracture ability of food is measured as the horizontal force with which food moves away from the point where the vertical force is applied. Another factor that helps to determine fracture ability is the suddenness (i.e. the distance from fracture) with which the food breaks.

Deformation

Deformation is a test that is the change the height or diameter of food under the application of force [11].

Table 1.2 demonstrates the change in dimensions of Rome apples (table 1.2), when they are squeezed.

Table 1.2: The examples of Rome Apples when squeezed. From Bourne, M. (2002). Food texture and viscosity: concept and measurement: Academic Press [12]

Force range (kg)	Deformation of flaccid apple (mm)	Deformation of firm apple (mm)	Ratio $\frac{\text{Flaccid apple deformation}}{\text{Firm apple deformation}}$
0-2	2.7	0.85	3.2
2-4	1.0	0.4	2.5
4-6	0.7	0.3	2.3
6-8	0.55	0.3	1.8
8-10	0.45	0.3	1.5
10-12	0.4	0.3	1.3
12-14	0.4	0.3	1.3
14-16	0.3	0.3	1.0
16-18	0.3	0.3	1.0
18-20	0.3	0.3	1.0

Source: Data from Bourne (1967b); reprinted with permission of New York State Agricultural

As can be seen, when the force on the apples was in the range of 0 to 8 kg, the deformation of flaccid apple is more obvious than that in firm apple, especially when the range of force was between 0-2 kg. The ratio gets smaller as the force range increases; at the range of 14 – 16 kg and beyond, the ratio equals 1.

Texture Profile Analysis

Bourne indicated that Texture Profile Analysis (short for TPA) is a kind of test that imitates the action of the jaw. He extracted a number of textural parameters from the resulting force-time curve that correlate well with sensory evaluation of those parameters [13]. This test method is frequently used in texture analysis.

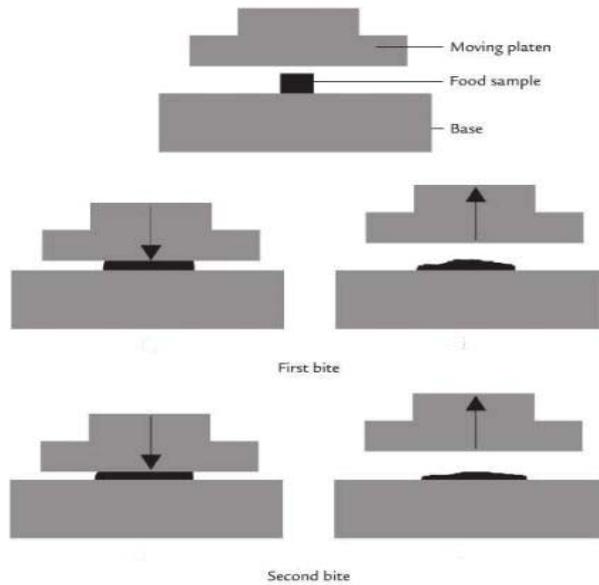


Figure 1.2: Food texture and viscosity: concept and measurement: Academic Press From Bourne, M. (2002).

Figure 1.2 shows the action of the TPA. As illustrated in Figure 1.2, a 'bite-size 'sample of the food of standard size and shape is placed on the platform. Compressed and Decompressed two times by a platen attached to the drive system [1]. To imitate the chewing action of the teeth, a high compression is needed. Bourne recommended a 90% compression when performing TPA test.

1.1 What is a food texture measurement system?

A fruit texture measurement system focuses on the food. It includes the analyser, which is capable of measuring the tested material and also collect data [14]. The data is transferred simultaneously to the computer through a standard protocol as the analyser is running. The simple structure (Figure 1.3) of a food texture measurement system is illustrated:

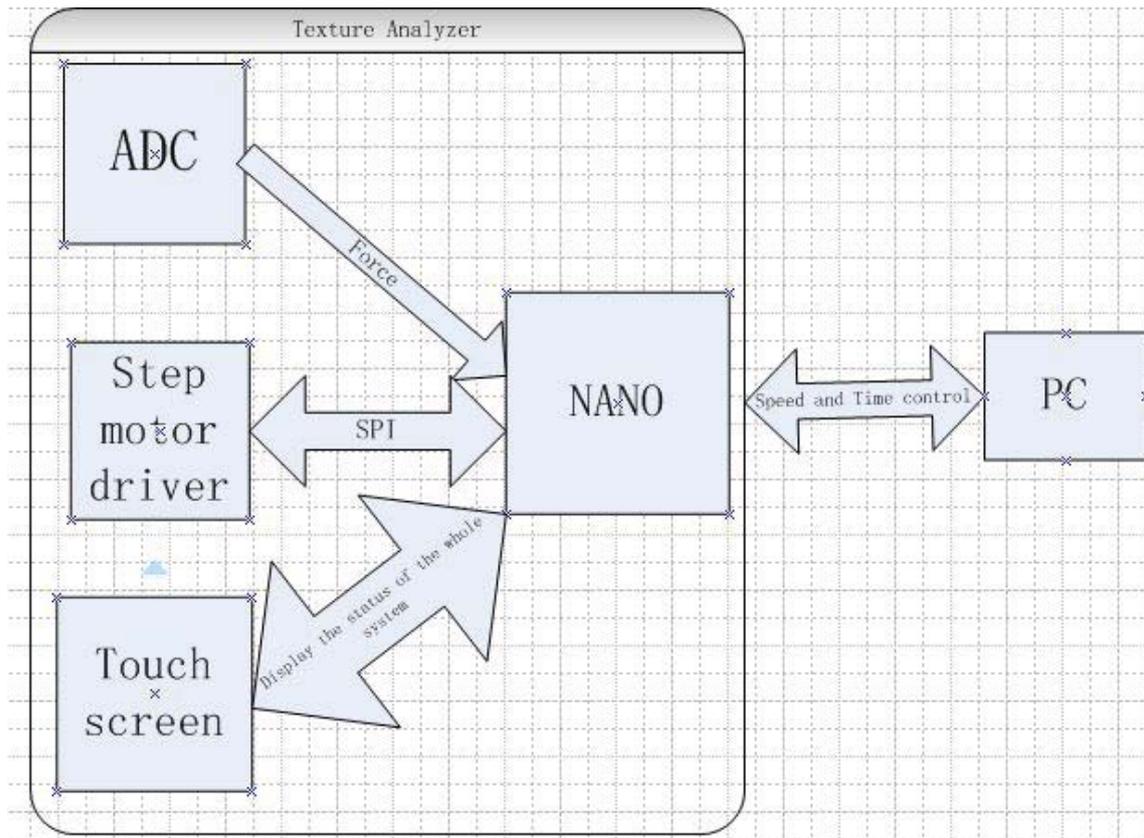


Figure 1.3: Simple diagram of the whole system

In general, a texture analyser consists of four core elements [5]:

1. A probe in contact with the sample: for example, penetrating probe, a spindle, or a cutting blade.
2. A driving machine that can provide motion (vertical and horizontal)
3. A sensory instrument that can detect the resistance given by the food
4. A readout system that can display the result of the test.

Chapter 2

Review of Texture Analysers

In today's world, it is increasingly common to analysis fruit by using texture analyser. A variety of texture analysers for different purposes is provided to institutes, universities, and companies to help researchers achieve high quality of measurement data for study and analysis.

2.1 Introduction to Texture Analyser

A texture analyser is the machine that imitates the chewing action of human, which is capable of measuring virtually any physical product characteristic such as hardness [15], fracture ability, adhesiveness, gel strength, extensibility of foods, cosmetics, pharmaceuticals, and other consumer products [13]. As an example, the texture analyser from Texture Technologies [17] will be demonstrated as the prevalent texture analyser in the following section:

Powder Flow Analyser:

The Powder Flow Analyser in figure 2.1, is used to measure and analyse powder flow, powder flowability, and the rheological properties of the powder. It features helical blade (sensor) and the arm of the equipment guarantees accurate repetition. The result can be transferred immediately to the screen (PC or other embedded system terminal).

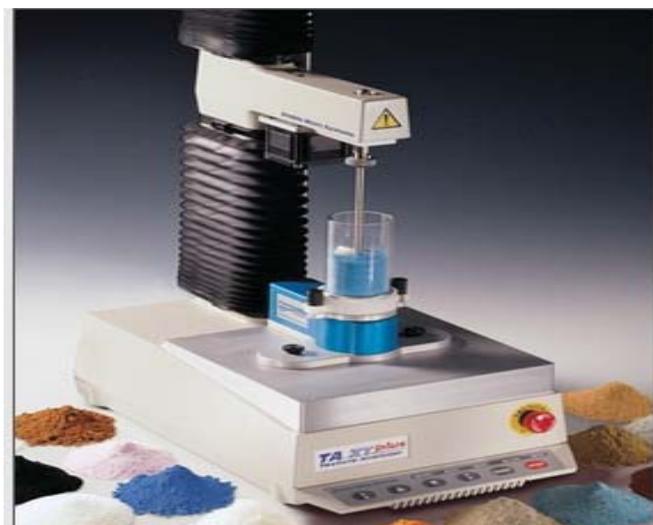


Figure 2.1: Powder Flow Analyser [16]

The characteristics of the texture analyser:

- (1) The sample tests can be done, including slicing, shearing, compressing, compacting, mixing, and aerating. Users can program their codes for specific tests.
- (2) Provide the measurement and analysis of force, time, and distance parameters that define the sample behaviour when the equipment is in use.
- (3) Objective, numeric and automated analysis.
- (4) The arm of this equipment can hold a very light and sensitive sensor; hence it can only test soft stuff.

TA.XT plus Texture Analyser

As the flagship food texture measurement product, TA.XT plus Texture Analyser [18] in figure 2.2 has the ability to measure virtually any physical product characteristic or materials testing metric.

It is extremely efficient and has a very easy-to-use comprehensive software package.



Figure 2.2: TA.XT plus Texture Analyser [18]

Table 2.1 shows the basic parameters of TA.XT plus [17]:

Table 2.1: Basic parameters of TA.XT plus

	5 Kilo Load Cell	30 Kilo Load Cell	50 Kilo Load Cell
Max Force	+/- 5 kg	+/- 30 kg	+/- 50 kg
Force Sensitivity	0.1 g	1 g	1~3 g
Load Cell	Directly interchangeable by the user. All load cells store their unique calibration and identification information in 'onboard' non-volatile memory		
Speed Range	0.05 – 40 mm-second (20 mm/second at 50 kg max. range)		
Speed Accuracy	Better than 0.1%		
Position Range Setting	0.001-295 mm		
Range Resolution	0.001 mm		

At Massey University, this type of TA is frequently used to measure the characteristics of fruit or food which is not very hard.

TA.HD plus Texture Analyser [18]

As the most powerful Texture Analyser, TA.HD plus, is shown in Figure 2.3. It has the ability to penetrate thick and tough materials. Using two high quality ball screws and one powerful motor, this equipment is designed and manufactured for long-term reliability and accuracy to address the needs of testing heavy duty stuff. However, this one is not commonly used in the food texture analysis on a daily basis. Because most of the food can be tested by using the TA_XT plus, this analyser is for the testing of special hard food or other material only.



Figure 2.3: TA.HD plus Texture Analyser

Some technical specifications are summarized in table 2.2

Table 2.2: Technical Specifications of TA.HD plus

Speed Range	0.01 ~ 20 mm/sec up to 250 kg 0.01 – 13 mm/sec from 250 kg to 750 kg
Speed Accuracy	Better than 0.1%
Position Range Setting	0.1 – 524 mm
Position Range Setting	0.001 – 295 mm
Range Resolution	0.001 mm

2.2 Limitations of existing Texture Analysers

The principle of operating a texture analyser is necessary to be introduced before the discussion on the limitations. Initially the robotic arm will go down at the *pre-test* speed. The speed of the robotic arm will change to *test speed* after the probe touches the test sample and the force exceeds the trigger force. The speed will change to *pre-test* speed after the robotic arm finishes the test and go back to the home position. Low speed is the primary disadvantage of the current texture analysers. Though it has extremely high precision, the speed range is 0.01 – 40 mm per second. As the datasheet of the texture analyser indicated, the pre-test speed should be lower than the

test speed, because high speed can crush test sample or affect the result of test. It always takes a long time when doing the repeatability experiments. Hence, one of the aims of this project is to enhance the speed of the equipment but not lose the precision. An infrared sensor will be used to detect the speed change and will be described in a subsequent chapter.

Table 2.3 and table 2.4 show the time-saving when promoting the speed of motor. Table 2.3 shows the classic relationship between speed and time.

Table 2.3: The speed of original texture analyser

Measurement Steps		Speed	Time (s)
1	move 100 mm to sample standard	40 mm/s	2.5
2	compress 10 mm at 1 mm/s	1 mm/s	10
3	go back to the test standard		10
4	repeat step 2	1 mm/s	10
5	go back to initial position	40 mm	2.75
6	Total time		35.25

The V_{max} is 0.1 m/s when the machine does not hold the load.

Table 2.4: The speed of new texture analyser

Measurement Steps		Speed	Time (s)
1	move 100 mm to sample standard	100 mm/s	1
2	compress 10 mm at 1 mm/s	1 mm/s	10
3	go back to the test standard	1 mm/s	10
4	repeat step 2	1 mm/s	10
5	go back to initial position	100 mm	1.1
6	Total time		32.1

So we can save 3.15 s for each measurement at most.

If the whole measurement is done 2000 times, the time saved will be 1.75 hours!

Now a day a texture analyser is quite expensive. The one used at Massey University is about \$10,000. Also, the software of the texture analyser is expensive. Hence, in this

project, a free open source system should be developed so that every user can just use their laptop to control the system, using the common serial port interface. Users should be able to type some commands and then can collect data from the machine.

Additionally, the push buttons on the original texture analyser are replaced by the visual buttons that are displayed on a touch screen. Since, the existing equipment is quite old the PCB needs to be redesigned in a smaller form factor

2.3 Specifications

This project is to rebuild the existing fruit texture analyser. As the thesis has mentioned, the fruit texture analyser is the instrument used to imitate the human feeling of the food (such as chewing or biting). Hence, some knowledge of teeth should be known. Most food is bitten by incisors. The maximum force exerted on the teeth is 15 kg between the incisors [1]. Table 2.5 displays the average force per tooth during mastication. As a consequence, the range of the full-scale of force used on most fruits is from 1 to 200 N (the extra 50 N need to be given), which means that at least 200 N of force should be provided by the motor. Puncture and TPA (texture profile analysis) are the most frequently used testing methods in food testing. Hence, the design of the new machine will focus on the puncture and TPA more than the other testing methods.

The comparison of specifications between the new instrument and the original one is as follows:

	Original instrument	New instrument
Force	The minimum force the motor provide is 15kg	Motor: the minimum force the motor should provide is 20 kg
The range of speed	0.05 – 40 mm-second (20 mm/second at 50 kg max. range)	The lowest speed of the motor is 0.02 mm/s
Protocol between PC and instrument	Use serial com port (RS232)	Use serial com port (RS232)

Instrument Accuracy	Accuracy: 0.1% for load cell	Accuracy : 0.01% for load cell ([1], [16])
Software	Need to purchase from company	Open source system can receive the code from the PC

Table 2.5: Average force per tooth during mastication [13]

Food	Force (kg)	Food	Force (kg)
French roll	1.8	Ham on white bread	1.0
Tender steak	1.4	Lobster	0.8
Pear (hard)	1.4	Apple (Macintosh)	0.7
Celery (raw)	1.3	Cucumber (raw)	0.7
Carrot (raw)	1.3	Raised doughnut	0.7
Bologna on roll	1.2	Broccoli	0.6
White bread (with crusts)	1.1	Potato (boiled)	0.6
Tomato	1.1	Crabmeat	0.5
Hard rye bread	1.0	Tuna fish	0.5
Hamburger (broiled)	1.0	Shrimp	0.5
Coleslaw	1.0	Cake	0.5
Lettuce	1.0	Cabbage (boiled)	0.4
Orange section	1.0	Carrot (boiled)	0.4
French roll (with liquid)	1.0	Beets (boiled)	0.3

2.4 Summary

From the survey of existing texture analysers, a clear idea was developed as to how to undertake this project. There are three kinds of prevalent texture analysers used in our school for different force scale. The force scale of Powder Flow Analyser is from 0~5 kg, whereas that of TA.XT plus Texture Analyser and TA.HD plus Texture Analyser are from 0~50 kg and 0~750 kg respectively.

The principle of texture analyser is that the equipment should work with a linear motion independent of compression or extension. The key issues that should be concentrated on are the power supply and motor drivers used by the TA.XT plus texture analyser. The texture analyser is very powerful to give the sufficient force to the test, which will be one main point to consider in my new project. In addition, due to the design of the machine for multiple-purpose (cater every range of load cell - 5 ~ 25 kg), an infrared detector will be attached to the texture analyser to modulate the speed of the robotic arm to prevent damage from the high speed crushing on the test fruit. For the precision of the force, an ADC is required for this project.

A touch screen is needed for some visual buttons to control the motion of the equipment and display the status of the equipment.

Chapter 3

Mechanical Design

In this chapter, the mechanical design is described in details, starting with the selection of ball screw and ends with the load cell. To prove the suitability of using ball screw and stepper motor for this project, scientific methods of choosing these components were followed by using the datasheets from THK company and stepper motor datasheets respectively. A new base platform has been created to fit the new PCB design dimensions. The details of the load cell would be described at the end.

The new food texture analyser is shown in figure 3.1. As can be seen, attached with the sensor and the load cell, the robotic arm can do the linear motion with speed control and has the ability to do the food test. The infra-red sensor can detect when the speed of the arm should be slowed down. The touch screen with a very user friendly interface, confronts the equipment.

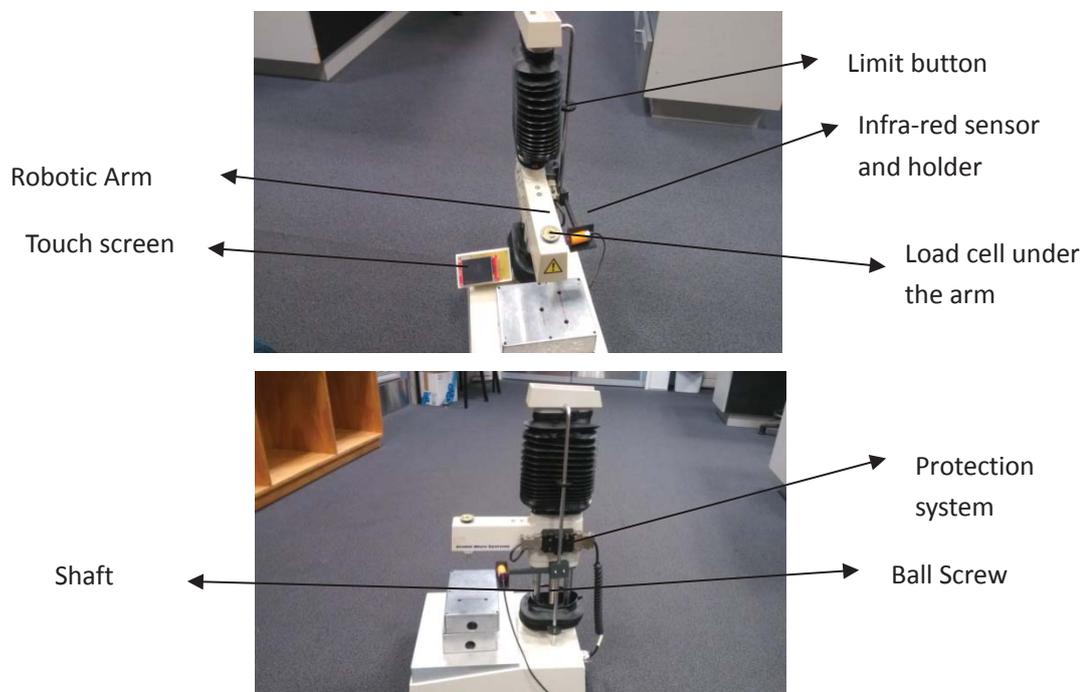


Figure 3.1: Texture analyser

The functions of the various parts of the machinery are as follows:

1. **Motor:** gives the whole rotary motion for the ball screw to let the arm ascend or descend.
2. **Ball screw:** to translate the rotational motion to linear motion with minimal friction
3. **Robotic Arm:** attached to the ball screw tightly, and holds the load cell
4. **Load cell:** to measure the force when the probe, which is attached to the load cell, touches the food.
5. **Infra-red holder:** to hold infra-red sensor at a certain height
6. **Shaft:** to keep ball screw stable.
7. **Limit button:** to limit the position of the robotic arm.

3.1 Methods for movement

Rotation:

A rotation is a circular movement of an object around a centre of rotation [19, 20]. The movement of motors is rotational. Motors, especially the ones with high torque, are widely used source of motion. They are compact and easy to manage. However, for this project, rotational motion has to be converted to linear to test the texture of the sample under test (figure 3.1). As a consequence, the first problem is how to convert the rotation generated by stepper motor to linear motion with minimal energy consumption.

Linear motion:

Linear motion is a motion along a straight line, and can be depicted as one dimensioned in mathematics [21]. It is the most fundamental of all motions. In this project, the motion of ball screw is translated into vertical linear motion. The robotic arm is attached to the ball screw so that it can move up and down the ball screw.

A ball screw is a mechanical linear actuator that can translate rotational motion to linear motion with very little friction and energy loss (less than 2% of the total energy consumption) [22]. A threaded shaft provides a helical raceway for the ball bearing which acts as a precision screw [22]. We modified an existing machine without

changing the ball screw.

3.2 Mechanical Component Description

A number of key mechanical components are required to allow for this machine to be constructed; the use of linear motion on the Y axis, and a powerful driver to give the force and speed to the whole machine. An arm protection system is also required.

As shown in the picture below (figure 3.2), the function of the robotic arm is to attach the load cell and probe. Some parameters, like the material selection, dimensions, and weight should be considered.



Figure 3.2: The modified Texture Analyser

3.2.1 Material selection

Normally, plastic, stainless steel, and aluminium are the most common material for an engineering project. In this project, plastic is utilized for the box of the touch screen and the holder of the infra-red sensor.

The ball screw and the shaft are made of stainless steel. Also, the base is made of aluminium. The reasons for choosing the different material for different parts are illustrated as follows:

Stainless steel

Stainless steel is a steel alloy with a minimum of 10.5% chromium content by mass [23, 24]. Stainless steel has sufficient corrosion resistance to resist rusting in countless applications; also it can resist high temperature better than most other materials [25]. Factors that prompted the use of stainless steel for ball screw and shaft are-

Density:

The density of stainless steel is about the same as carbon or low-alloy steels, which is 7.85 cm/s^2 [27].

Structure:

Stainless steels have ferrite (low carbon), martensitic (high carbon), or duplex structures [25]. Some of the stainless alloys are not ferromagnetic. However in this project, it is not necessary to consider it.

Expansion:

The linear temperature expansion of stainless steel is about 0.4 inches/100 feet [26]. It is not uncommon to hear complain of the instability of stainless steel [23]. However, in this project, it is just used in linear motion. This problem can be ignored.

Corrosion:

Mixed with chromium and nickel, stainless steel has an exceptional quality of resistance to corrosion.

With the features mentioned above, stainless steel is appropriate for manufacturing the ball screw and shaft. The ball screw and shaft on the original equipment are made of stainless.

Plastic

Because of the light weight of plastic, the infra-red sensor holder and the enclosure for touch screen are made of plastic using a 3D printer. This is the cheapest way to realise the design.

Aluminum

In order to reduce the cost of the whole equipment, aluminium has been used to design the base. Moreover, aluminium is very easy to shape. Hence, it is used for the base of the texture analyser.

Comparisons between stainless steel, plastics, and aluminium

1. Plastic (Acrylic): it is too soft and fragile to design the whole system.
2. Stainless Steel: the properties are the same as the steel, and cannot rust easily.
3. Although it is much lighter than steel, aluminium alloy is one-third the stiffness

of steel, which means it is quite soft, and also it costs more compared to using steel.

In conclusion, stainless steel will be used in this project for designing the ball screw, shaft, and the structure of the box.

3.2.2 Ball screw

Linear motion, as an essential requirement of this project, can be accomplished by two different methods. One is by using a ball screw, the other using oil cylinder. In this project, the ball screw has been selected because it is cheap and meets the accuracy requirements for this project. The original ball screw is 1605 manufactured by THK. It is necessary to understand the suitability of using this ball screw for this project.



Figure 3.3 ball screw 1605

Ball screw selection:

There are some parameters which should be considered when choosing a suitable ball screw. These are discussed below.

(1) Lead:

The wider the pitch, the faster the speed ball screw will travel. However, wider lead means lower load can be handled. It also means lower accuracy. When the driving motor's rated rotational speed is 1,000 rpm (revolutions per minute) and the maximum speed is 0.1 m/s, the Ball Screw lead is obtained from the equation (1).

$$lead = \frac{1000 * 60 * speed}{rev} \quad (1)$$

The lead should be more than 2 mm. In order to maintain the load and avoid reduction

of speed, the 5 mm lead has been chosen.

Permissible Axial load [27]

As a vertical linear motion, the direction of moving is on Y axis. The weight of the arm which the force holds on the ball screw should be identified at first. The weight of the arm includes the weight of the arm itself (without load), the weight of the load cell, and the weight of the probe. The heaviest load cell is 3 kg (most of them are only 0.2 kg ~ 0.3 kg; the one used in this project is less than 1 kg). The heaviest weight of probe is 0.7 kg. The weight of the arm (without load) is 5 kg. Hence, the weight of the arm is 8.3 kg (the heaviest load cell plus sensor and arm). To keep the machine safe, 10 kg will be used to do all the calculations.

Now the axial load should be calculated to ensure the ball screw is stable when running.

The calculations below will show the maximum tolerance undergone by the ball screw.

Guide surface resistance: $f = 20 \text{ N}$ (without load)

The maximum force of food: $m_1 = 20 \text{ kg}$

Work mass (maximum): $m_2 = 10 \text{ kg}$ (including nut + arm + load cell)

Maximum speed: $V_{\max} = 0.1 \text{ m/s}$

Acceleration time $t_1 = 0.2 \text{ s}$

Position accuracy = $0.35 \text{ mm}/300 \text{ mm}$

$g = 9.8 \text{ N}$

Frictional coefficient $\mu = 0.003$

$$\alpha = \frac{V_{\max}}{t_1} = 0.5 \text{ m/s}^2 \quad (2)$$

During the upward acceleration

$$Fa1 = (m_1 + m_2) \cdot g + f + (m_1 + m_2) \cdot \alpha = 588 + 30 = 318 \quad (3)$$

During upward uniform motion:

$$Fa2 = (m_1 + m_2) \cdot g + f = 308 \text{ N} \quad (4)$$

During upward deceleration:

$$Fa3 = (m_1 + m_2) \cdot g + f - (m_1 + m_2) \cdot \alpha = 278 \text{ N} \quad (5)$$

During downward acceleration:

$$Fa_4 = (m_1 + m_2) \cdot g - f - (m_1 + m_2) \cdot \alpha = 238 \text{ N} \quad (6)$$

During downward uniform motion:

$$Fa_5 = (m_1 + m_2) \cdot g - f = 268 \text{ N} \quad (7)$$

During downward deceleration:

$$Fa_6 = (m_1 + m_2) \cdot g - f + (m_1 + m_2) \cdot \alpha = 298 \text{ N} \quad (8)$$

Thus, the maximum axial load applied on the Ball Screw is as follows:

$$Fa_{\max} = Fa_1 = 318 \text{ N} \quad (9)$$

According to the THK ball screw datasheet of 1603, the static load rating C_{0a} is 25.2 kN which is far more than 318 N. It means that this ball screw can tolerate the weight of the arm; hence the ball screw 1603 was selected for this project. Therefore the original ball screw can be used for my new design.

(2) Buckling load of the Screw Shaft

Because the ball screw is used for vertical linear motion, the support unit is chosen as a fixed type unit at the bottom of the ball screw and also a fixed unit at the top of the ball screw.

Assume buckling load of the screw shaft is P1.

Distance between two mounting surfaces $L = 400 \text{ mm}$

Screw-shaft thread minor diameter $d_1 = 12.5 \text{ mm}$

η is the factor of mounting, and is 20 (according to the THK datasheet of 1603).

$$P1 = \eta * \frac{d_1 * d_1 * d_1 * d_1}{L} = 1220 \text{ N} \quad (10)$$

(3) Permissible Compressive and Tensile Load of the screw Shaft (P2) [27]

$$P2 = 116 * d_1^2 = 181 \text{ N} \quad (11)$$

Where 116 is the coefficient of tensile, according to the manual of THK.

P1 and P2 are far more than the maximum axial load. Therefore, it is not an issue to use this ball screw.

3.2.2 Stepper motor

To prove the stepper motor that has installed on the original equipment is suitable for my project; the torque needs to be decided. The motion of the arm can be broken into three steps or stages as follows:

1. The robotic arm descends in the pre-test speed.
2. When the infra- red sensor detects the position of the robotic arm, the arm then goes down slowly till it reaches the test speed. Then the probe will penetrate the tested stuff till the load cell detects the force touching on the food exceeds the trigger force.
3. The arm rises up, leaving the food at the test speed, and then when the arm rises up to a certain distance (detected by infra-red sensor), it will home in at a very fast speed (pre-test speed).

So the activity mentioned above can be visualized as:

In stage 1, the motor is driving the arm (which includes the load cell and the probe) down at a very fast speed. Then the robotic arm tests the sample, by penetration or compression, at the test speed, which is much lower than the previous speed. Finally the arm goes up at a very high speed.

In this case, the force is divided into three parts for calculation. They are

First case:

$$F_{a1} = m_2 * g + \mu * m_2 * g = 100.3 \text{ N} \quad (12)$$

F_{a1} is the force when the arm descends in the pre-test speed

The torque that motor need for this case is:

$$T_1 = \frac{(F_{a1} * \text{lead})}{(2 * 3.14 * N_1)} = 177.5 \text{ N} * \text{mm} \quad (13)$$

N_1 it is the coefficient of the ball screw efficiency. It is 90%

Hence $T_1 = 177.5 \text{ N}$. T_1 is the force when robotic arm descent in a constant speed.

The next thing is calculated the force when the probe is touching the fruit:

Before calculating T_2 , let us calculate the inertial moment when robotic arm slow down [28]:

Since the inertial moment per unit length of the screw shaft is $J_s = 3.9 \times 10^{-4}$ kg•cm²/mm (it is provided by THK manual) [27], the inertial moment of the screw shaft with an overall length of 300 mm is obtained as follows:

The maximum force of food: $M_1 = 20$ kg

Work table mass (maximum): $M_2 = 10$ kg (including nut + arm + load cell)

Lead = 3 mm

$$J = (m_1 + m_2) * \left(\frac{\text{Lead}}{2 * \pi}\right)^2 * 10^{-6} + J_s \quad (14)$$

$$J = 0.56 * 10^{-4} \text{ Kg} * \text{M}^2 \quad (15)$$

Angular acceleration

$$\omega = \frac{(2 * \pi * \text{rev})}{60} = 104 \text{ rad/s} \quad (16)$$

where Rev is 1000 rad*min⁻¹

Based on the above, the torque (T_2) required for acceleration is obtained as follows:

$$F1 \text{ (the force of acceleration)} = (J + J_m) * \omega = 13.2 \text{ N} * \text{mm} \quad (17)$$

Where J_m is the inertial moment of the motor

$$J_m = 5 * 10^{-5} \text{ Kg} * \text{m}^2$$

In stage (2):

$$Fa2 = m_2 + m_1 * g + \mu * (m_2 + m_1 * g) = 702.1 \text{ N} \quad (18)$$

$$T2 = \frac{(Fa2 * \text{Lead})}{(2 * 3.14 * N1)} + Fa1 = 1238 \text{ N} \quad (19)$$

Where m_2 is the weight of the arm, m_1 is the force of food (20 kg).

Hence, the torque is 1238.51 N x mm in this stage.

In stage (3) is same as the first one. Hence, as the result, the torque of the motor should be more than 1238.51 N x mm. The torque of the stepper motor installed on the original equipment is 3 N x m which is more than what be needed. Thus the original stepper motor can be used in this project.

All the improvement above shows that the original equipment can be the structure of the new equipment. Hence, the structure of the original equipment is still used in this project.

3.2.4 Base of the instrument

The base of the original equipment should be redesigned to suit the new PCB. In this project, as mentioned above, the load cell, the touch screen and the infra-red sensor should be located on the outside of the equipment. The connectors were required for the communication between the main PCB and sensors. Also, the connectors were needed for power supply and microcontroller. These would be considered in the base designing.

The connector that is used for power supply was called IEC, which combine two elements: the switch and the socket. Given the ultra-compact design, this component is ideal for low-profile designs. According to the data sheet, the parameter of the IEC connector is shown in figure 3.3:

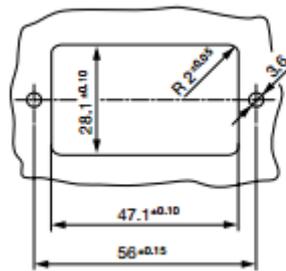


Figure 3.3: Dimensions of the IEC connector

The DB15 connector is for the load cell, and the DB 9 connector is for the touch screen. A standard USB interface should be on the base plate to be the bridge between microcontroller and computer. Figure 3.4 and figure 3.5 display the dimension of DB9 and DB15 respectively.

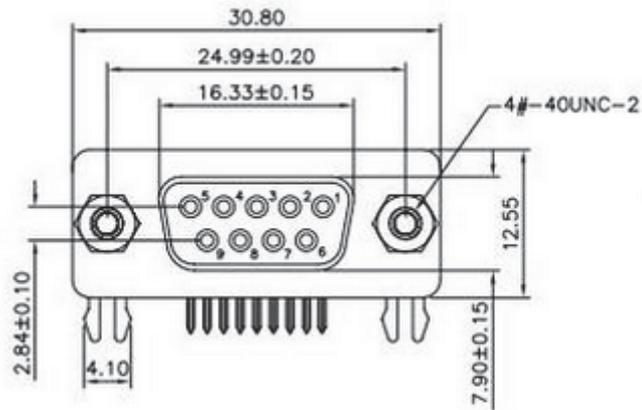


Figure 3.4: Dimensions of DB9

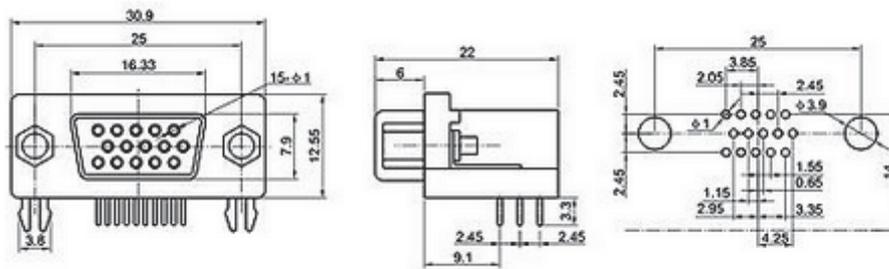


Figure 3.5: Dimensions of DB15

Infrared sensor needs three pins (VCC, GND and INPUT) to connect with the PCB; hence it requires a small space. Figure 3.6 below shows the base design in SolidWorks.

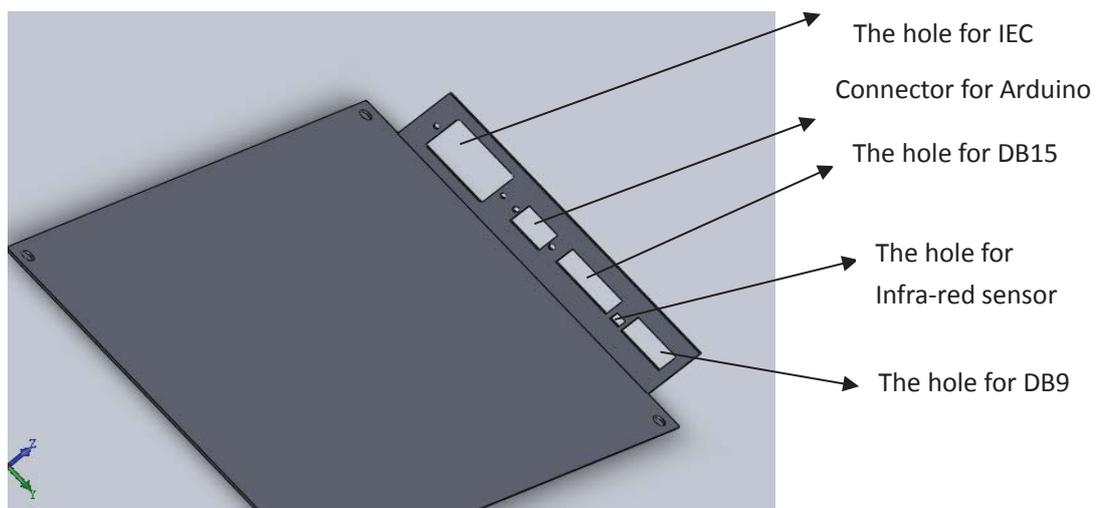


Figure 3.6: The base in SolidWorks

The fabricated base plate machined on a CNC machine required G-code. This was generated by using software called SolidCam with the code based on the SolidWorks drawing and dimensions. The CNC machine was then able to do very precise (with an accuracy of 0.01 mm) cuts and profiles using a range of cutting tools.

3.2.2 Infra-red sensor holder

To keep the infrared sensor at a certain height, a holder is necessary to be made. To reduce damage to the original equipment, the holder would be attached to the roll that already holds two protection buttons on it. 3D printer was used to print the holder. The project was saved as .STL file. The 3D printer can convert the binary picture (the STL file) into binary code so that it can print the stuff easily. Figure 3.7 shows the infra-red sensor holder in SolidWorks.

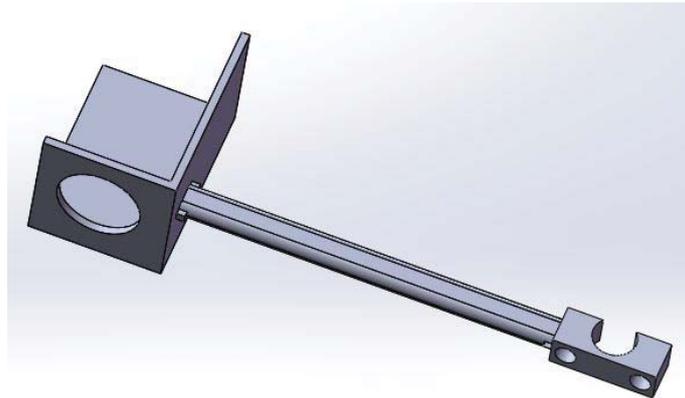


Figure 3.7: SolidWorks design of the infra-red sensor holder

3.2.3 Load cell

In this project, a four-wire load cell is used to test the texture of food. Figure 3.8 displays the load cell used in this project.

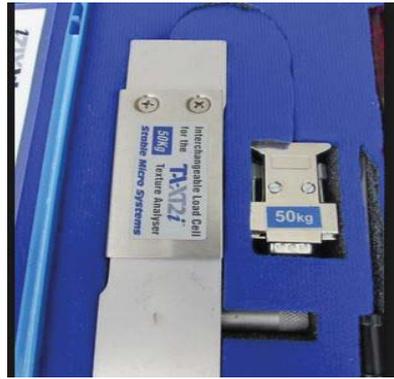


Figure 3. 8: Load cell

As figure 3.9 illustrates, a load cell is a sensor or a transducer that converts a load or force on it into an electrical signal[29]. This electrical signal can be a voltage change, current change or frequency change depending on the type of load cell, and circuitry used [30]. Traditionally, load cells are built using resistive bonded foil strain gauges. Strain gauges are essentially resistors built using standard semiconductor etching techniques and are bonded to a metallic member such as a cantilever beam or a diaphragm [30].

A 4-wire load cell, as can be seen in the figure 3.9, includes excitation+, excitation-, signal+ and signal- lines. It is connected to the ADC to get a digital signal that can be analysed by the microcontroller.

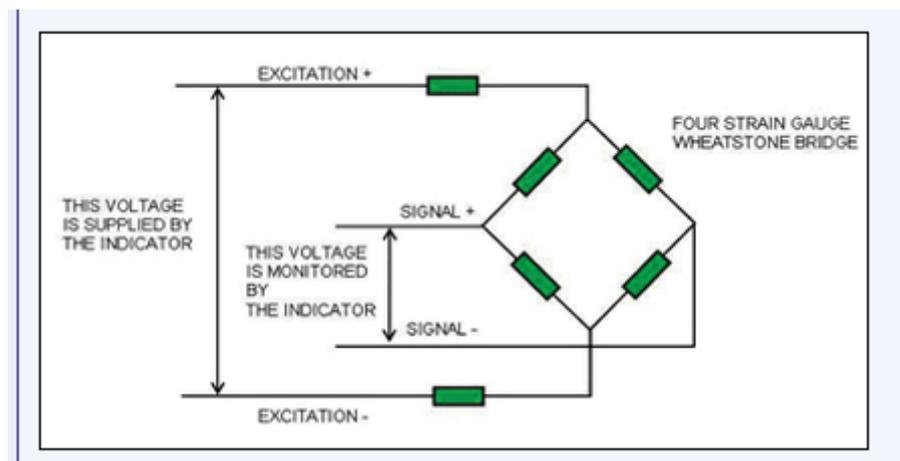


Figure 3.9: The principle of the load cell working [31]

Figure 3.10 shows the features of the load cell

Specifications			
Signal Output at Capacity.....	2±0.2 mV/V	Service Load.....	100% Capacity
Linearity Error.....	< 0.017% FSO	Safe Load.....	150% Capacity
Non-Repeatability.....	< 0.010% FSO	Ultimate Load.....	300% Capacity
Combined Error.....	< 0.020% FSO	Input Resistance.....	409Ω ± 6Ω
Off Centre Load Error.....	< 0.017% FSO	Output Resistance.....	350Ω ± 3Ω
Creep/(30 mins.).....	< 0.015% FSO	Insulation Resistance.....	> 5000 MΩ (@50 VDC)
Zero Balance.....	< 2% Capacity	Excitation Voltage(Rec).....	5~12V AC/DC
Temperature Effect on Span(/10C).....	< 0.014% FSO	Excitation Voltage(Max.).....	18 V AC/DC
Temperature Effect on Zero(/10C).....	< 0.017% FSO	Cable.....	0.4m long, Ø3.8 mm
Operating Temperature Range.....	-35 ~ +65 C	4 core screened PVC
Compensated Temperature Range.....	-10 ~ +40 C	Material.....	Aluminium Alloy
Storage Temperature Range.....	-50 ~ 85 C	Sealing.....	IP65
Wiring Connections			
Excitation +ve.....	Red	Signal +ve.....	Green
Excitation -ve.....	Black	Signal -ve.....	White

Figure 3.10: The specifications of the load cell

3.3 Summary

The aim of this chapter was to prove that every original machinery part is suitable for the new project. The material selections for the ball screw, the base and the infra-red sensor holder are presented. The calculations of the forces based on the manual of THK prove that the original ball screw can be used in the new project. Original motor with enough torque also can be used as new actuator in the new project. A new base is designed to suit the new PCB board, whereas a new infra-red holder is made, attached on the shaft of the texture analyser.

The electronic circuit and its design details are covered in the next chapter. To allow movement of the arm, some electronic components were required. A stepper motor driver was required to interface the stepper motor to a computer allowing for custom software to be developed to control the stepper motors. Also, a powerful microcontroller should be used for this complicated project.

The next chapter will depict the automation components selected in this project with a detailed overview of how each of the electronic components is used and integrated into the system.

Chapter 4

Electronic design

The whole system is controlled electronically. The complex electronics for the system is described in details in this chapter starting with the schematic and finishing with the PCB.

A novel contribution of this thesis is the design and implementation of a motor controller/driver circuit which has been designed with generic use and application in mind for motor control.

A very high-end ADC has been used to measure the output of the load cell and it has been described in details.

The special requirements of the power supply and its circuits are also discussed.

4.1 Electronic design and overview

The functional block diagram, figure 4.1, shows two independent sections. They are:

1. The master board, which connects with the user interface terminal (slave board), controls the whole system, and transfers data, generated from the load cell to the PC by using RS232 communication protocol.
2. The slave board that controls the touch screen functions as a visual button and displays the basic status of the whole system.

The protocol for connection between these two boards is visual SPI bus, which uses normal GPIO to imitate the data transfer methods of a SPI bus. There are two reasons for using the two boards. Firstly, the memory size of the executable code of Arduino Nano is 32KB (including 2K bootloader). The code for touch screen is about 20 KB (Figure 4.2), while the code for stepper motor driver and ADC is more than 13K (Figure 4.3). Secondly, the code for the touch screen always crashes for some unknown reasons when all the components are integrated into one board. Making the PCBs separate keeps every part of the board working well.

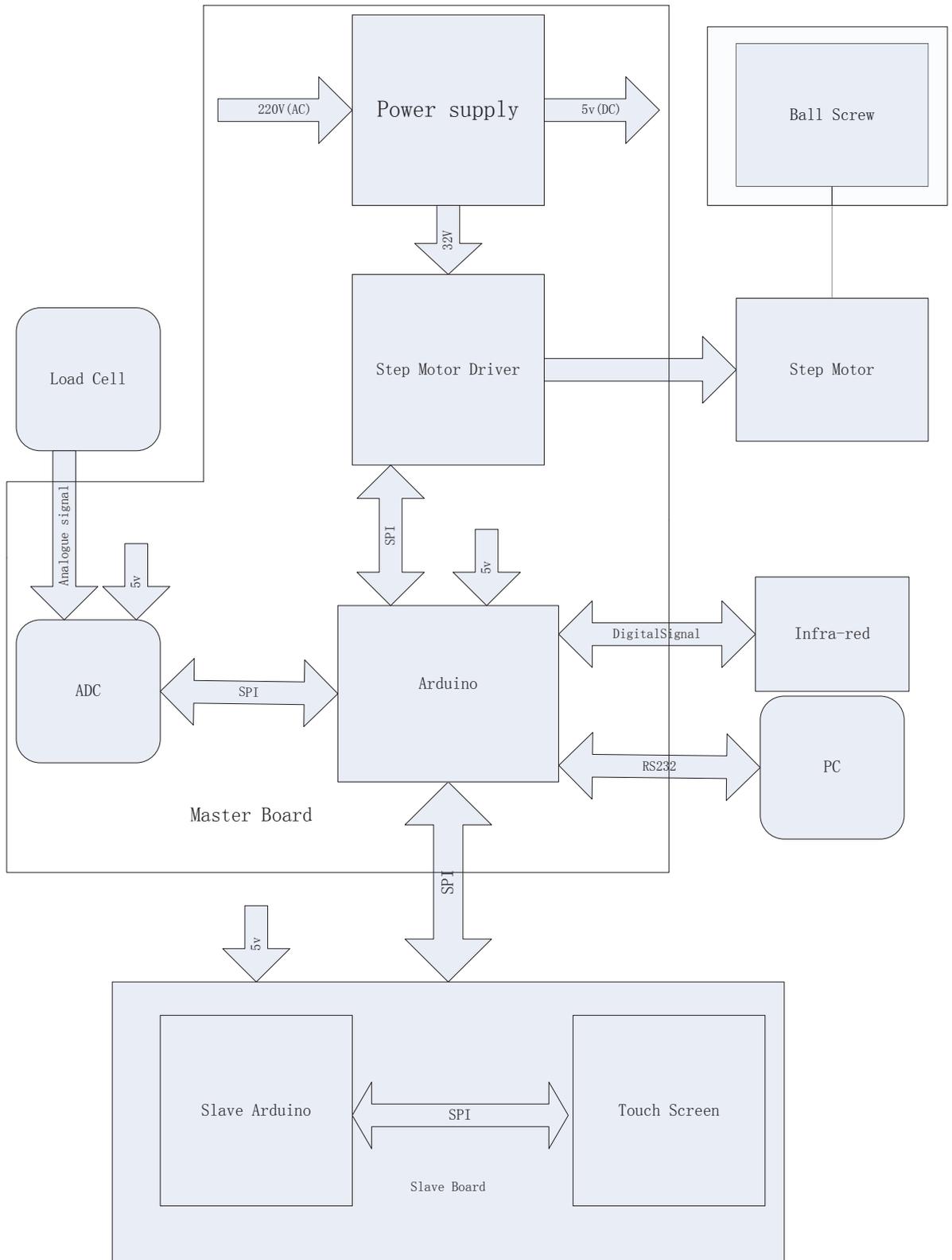


Figure 4.1: Functional Block Diagram of the electronic design

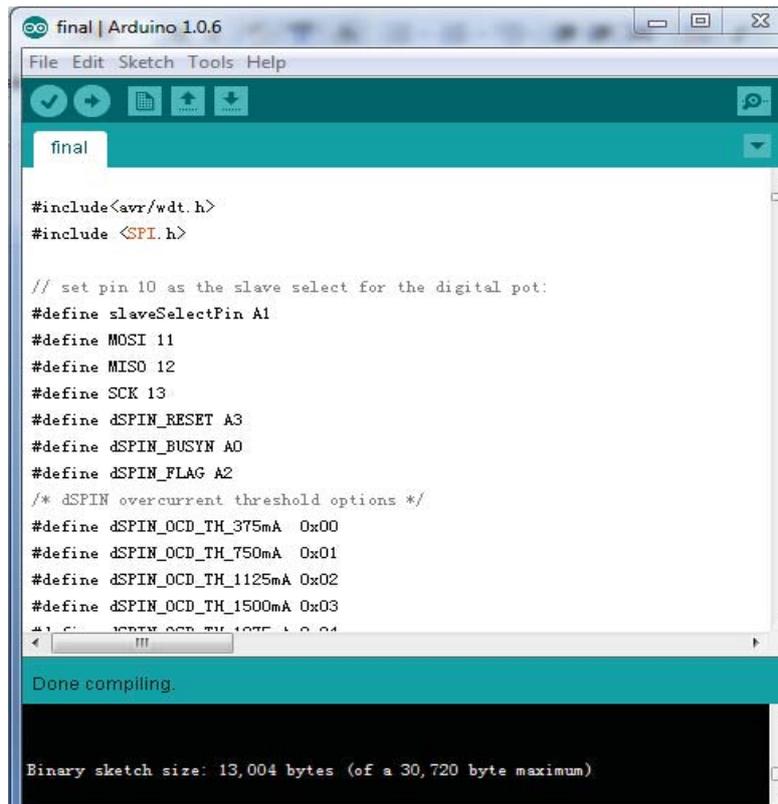


Figure 4.2: The size of executable file of master board

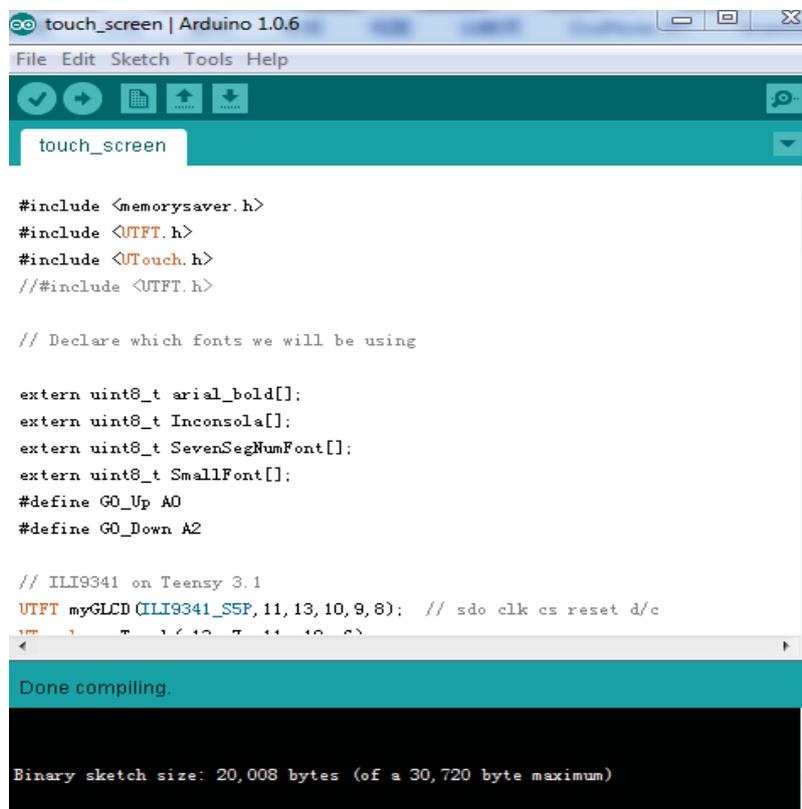


Figure 4.3: The size of executable file of slave board

4.2 Master board

To allow movement of the robot arm, and to receive data from the load cell and infra-red sensor, some electronic components and a complex circuit design were required. The master board includes four parts: Microcontroller, ADC, stepper motor driver and the power supply. The Stepper Motor Driver is for actuating the stepper motor. The function of the ADC is to convert the analogue signal generated from the load cell to a digital signal; whereas the microcontroller, the core of the whole system, collects data from all of the other parts and transfers the data to the computer. The power supply unit is to provide sufficient and stable power to all the components on both the master board and the slave board. The next subsection describes every element of the master and slave board in detail.

4.2.1 Microcontroller

Arduino Nano (Figure 4.4) is the microcontroller in this project. As the website of Arduino indicated [32], this microcontroller is an open-source electronics prototyping platform based on flexible, easy-to-use hardware and software. It is intended for artists, designers, hobbyists and anyone interested in creating interactive objects or environments [33, 34].

Compared with other microcontrollers, the advantage of a Nano is that the programmers are not required to be worried about programming the driver code of hardware protocol (such as SPI, TWI(I2C), and serial port) by themselves [33]. The designer only needs to call the functions of the hardware protocol from the Arduino library. Hence, this microcontroller can promote the efficiency of the programming.

In addition, in the world of Arduino (mega168/328), Nano is the smallest one that could be found, and it is very easy to install it into a PCB. However, in my project, two Nano boards have been used because of the narrow space. One of them for the master board controlling the ADC and the stepper motor driver, the other is for driving the touch screen individually. The parameters of a Nano are listed in Table 4.1.

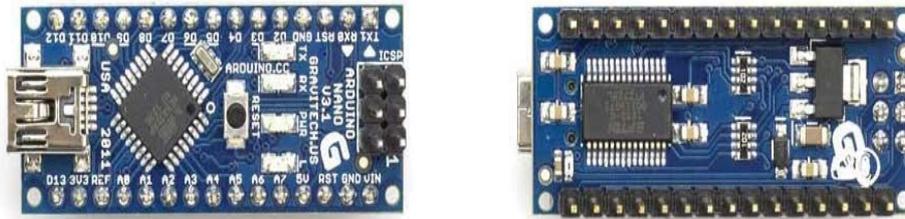


Figure 4.4: Arduino Nano[35]

Table 4.1: Specifications of Nano

Microcontroller	Atmel ATmega168 or ATmega328(Nano)
Operating Voltage (logic level)	5 V
Input Voltage (recommended)	7-12 V
Input Voltage (limits)	6-20 V
Digital I/O Pins	14 (of which 6 provide PWM output)
Analog Input Pins	8
DC Current per I/O Pin	40 mA
Flash Memory	16 KB (ATmega168) or 32 KB (ATmega328) of which 2 KB used by bootloader
SRAM	1 KB (ATmega168) or 2 KB (ATmega328)
EEPROM	512 bytes (ATmega168) or 1 KB (ATmega328)
Clock Speed	16 MHz
Dimensions	0.73" x 1.70"
Length	45 mm
Width	18 mm
Weight	5 g

Operating Voltage	5 V
Input Voltage (limits)	6-20 V
Digital I/O Pins	14 (of which 6 provide PWM output)
Analog Input Pins	8
DC Current per I/O Pin	40 mA
Flash Memory	16 KB (ATmega168) or 32 KB (ATmega328) of which 2 KB used by bootloader
SRAM	1 KB (ATmega168) or 2 KB (ATmega328)
EEPROM	512 bytes (ATmega168) or 1 KB (ATmega328)
Clock Speed	16 MHz
Dimensions	0.73" x 1.70"
Length	45 mm
Width	18 mm
Weight	5 g

4.2.2 Stepper Motor Driver

The motor controller has two parts. They are:

1. Control circuitry and
2. Stepper motor driver

Nano was used as the control part, and L6472 was utilized as a micro step driver. The control part will be depicted in the software implement section.

The L6472 device (figure 4.5), realized in analogue mixed signal technology, is an advanced fully integrated solution suitable for driving two-phase bipolar stepper motors with micro stepping [36]. The device can generate the motion profiles defined by the users, such as acceleration, deceleration, speed or target position and is very easy to be programmed through a dedicated register set. Some of the features of L6472 are as follows:

1. Operating Voltage: 8 - 45 V
2. A output peak current (3.0 A rms)
3. Programmable speed profile
4. Programmable Power MOSFET slew rate
5. Up to 1/16 micro stepping
6. Predictive current control with adaptive deceleration
7. Non dissipative current sensing
8. SPI interface
9. Low quiescent and stand by currents
10. Programmable non dissipative overcurrent protection on all the power MOSFETs
11. Two levels of over temperature protection

From all the the features mentioned above, what needs to be focused on are the operating voltage, which decides how much torque can be provided; peak current which is related to the maximum speed, and the micro stepping, which tells us the precision that L6472 can provide. In our project, the precision is 0.002 mm. The lead of the ball screw is 3 mm. Each step of the stepper motor is 1.8° , which means the stepper motor should run 200 steps for one rotation (3 mm) (when the micro stepping is full-scale step). When the micro stepping is 1/16, the motor will run $16*200 = 3200$ steps for one rotation (3 mm), which means the precision is 0.0015 mm (3/3200), more accurate than the precision mentioned in the specifications of the machine.



Figure 4.5: L6472[37]

The designing of L6472

Figure 4.6 illustrates the typical circuit of the L6472 [38]

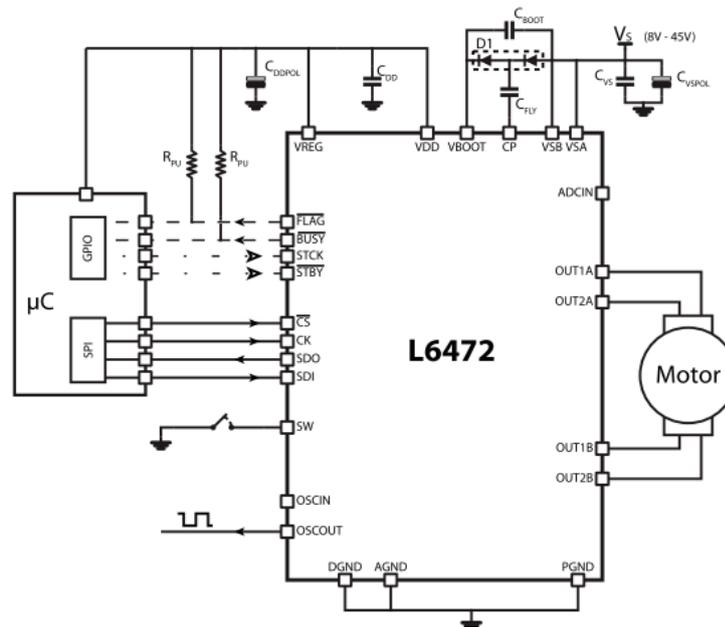


Figure 4.6: Typical circuit of L6472

As can be seen, C_{DDPOL} , C_{DD} , C_{vs} , and C_{vspol} are the decoupling capacitors for reducing the noise from the power supply. Two R_{pu} are pull-up resistors to enhance the quality of signal input and output.

The function of each of the pin is shown as following:

1. Flag Pin

By default an internal open drain transistor pulls the FLAG pin to ground when at least one of the following conditions occurs:

- Power-up or standby / reset exit
- Overcurrent detection
- Thermal warning
- Thermal shutdown
- UVLO (under-voltage lockout)
- Switch turn-on event
- Wrong command
- Non-performable command

2. Busy\SYNC pin

This pin is an open drain output that can be used as the busy flag or synchronization signal according to the SYNC_EN bit value. When SYNC_EN bit is set low, this pin can be used as the busy flag, whereas when SYNC_EN is set high, this pin can be regarded as in a SYNC mode.

3. $\overline{\text{STBY}}$

The device can be reset and put into standby mode through this pin. When the $\overline{\text{STBY}}$ pin is driven low, the bridges are left open (High Z state), the internal charge pump is stopped, the SPI interface and control logic are disabled, and the internal 3 V voltage regulator maximum output current is reduced as a result, the L6472 heavily reduces the power consumption.

4. CS, SDO, SDI, CLK: They are the pins of the SPI bus.

To ensure the correct driving of the high-side integrated MOSFETs, a voltage higher than the motor power supply voltage needs to be applied to the Vboot pin. The high-side gate driver supply voltage Vboot is obtained from an oscillator and a few external components realizing a charge pump (figure 4.7).

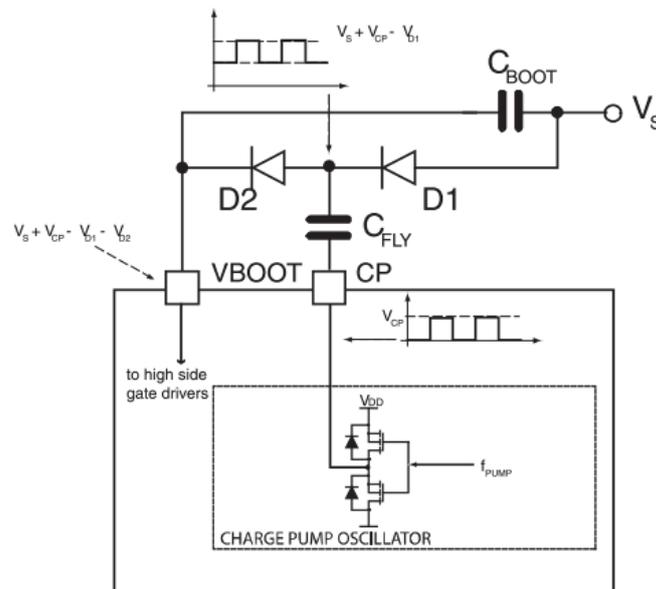


Figure 4.7: The charge pump circuit[37]

Figure 4.8 illustrates the schematic of L6472.

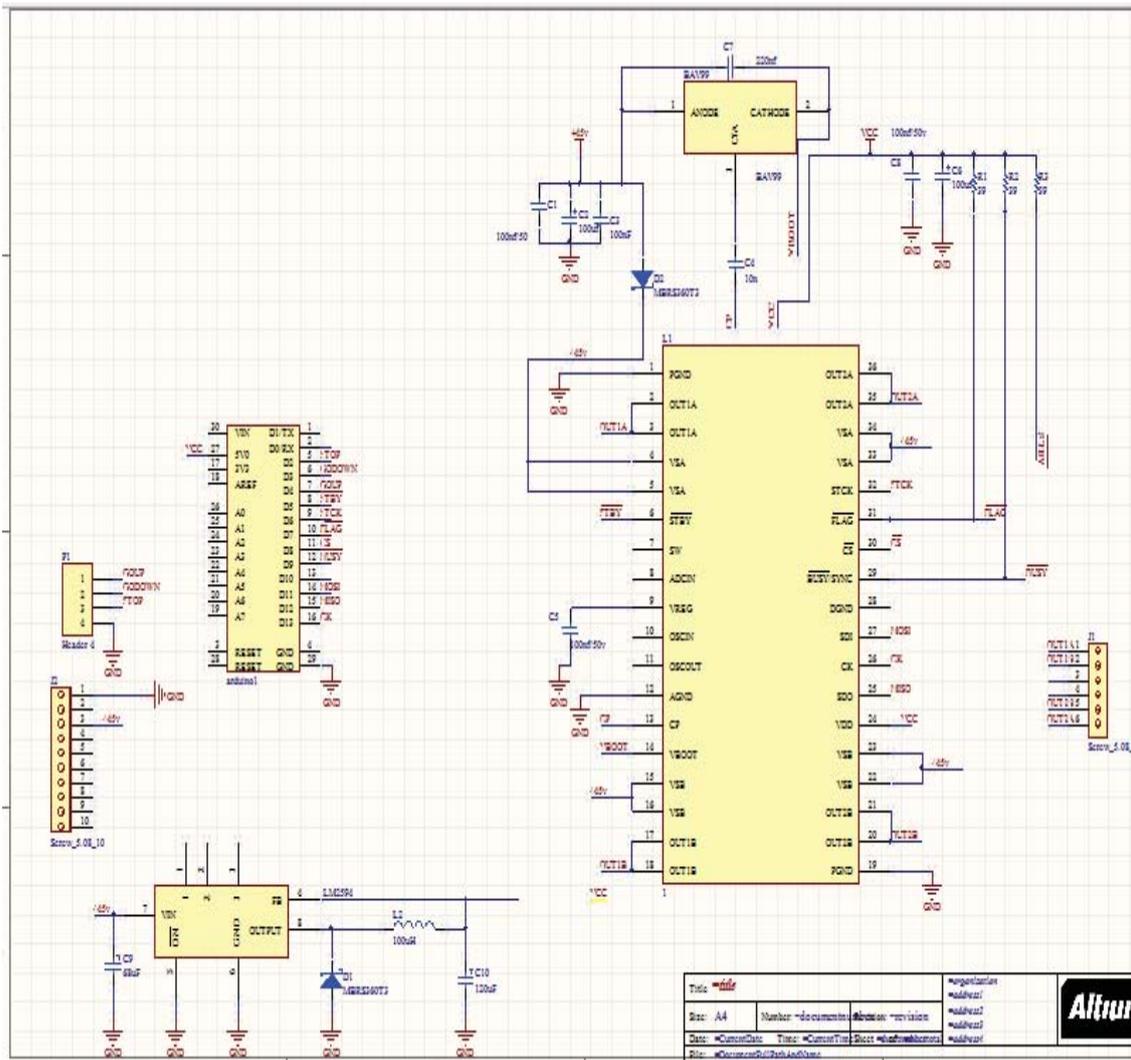


Figure 4.8: The schematic of L6472

In this schematic, according to the recommendation from L6472 datasheet, the selected diode for the voltage charge pump up is BAV99.

4.2.3 ADC

The output signal of the load cell is an analogue signal, which cannot be processed by a digital microcontroller [39]. As per the specifications of this project detailed in section 2.3, the accuracy of the load cell is 0.01%, which means for a 25 kg load cell, the accuracy of the result is ± 2.5 g. Signal output of the load cell used in this project is 2 mV/V. The reference voltage for the Analogue to Digital (AD) converter is 5 V, thus the signal output at capacity is 10 mv in full scale. A 24-bit ADC, which can achieve that accuracy (0.002 g ideally), is selected for this project. The specifications for the ADC selection are:

1. Being highly accurate and stable (the accuracy cannot be lower than ± 2.5 g)
2. Having a high range of adjustable sampling rate
3. Can process data and communicate between devices

To receive accurate data from the load cell, a 24-bit AD converter, AD7192 [45], is selected for this project. The AD7192 is a low noise, complete analogue front end for high precision measurement applications[40]. It contains a low noise, 24-bit sigma-delta (Σ - Δ) analogue-to-digital converter (ADC) [41, 42]. The on-chip low noise gain stage means that signals of small amplitude can be interfaced directly to the ADC. The device can be configured to have two differential inputs or four pseudo differential inputs. The on-chip channel sequencer allows several channels to be enabled, and the AD7192 sequentially converts on each enabled channel [43]. This simplifies communication with the components. The on-chip 4.92 MHz clock can be used as the clock source to the ADC. Alternatively, an external clock or crystal can be used. The output data rate from the part can be varied from 4.7 Hz to 4.8 kHz. The load cell is a high precision load cell that outputs 2 mV/V, hence over the entire load range of the load cell (0~25 kg) the input of the ADC will not exceed $2 \times 5 = 10$ mV. Figure 4.9 displays the internal structure of the ADC.

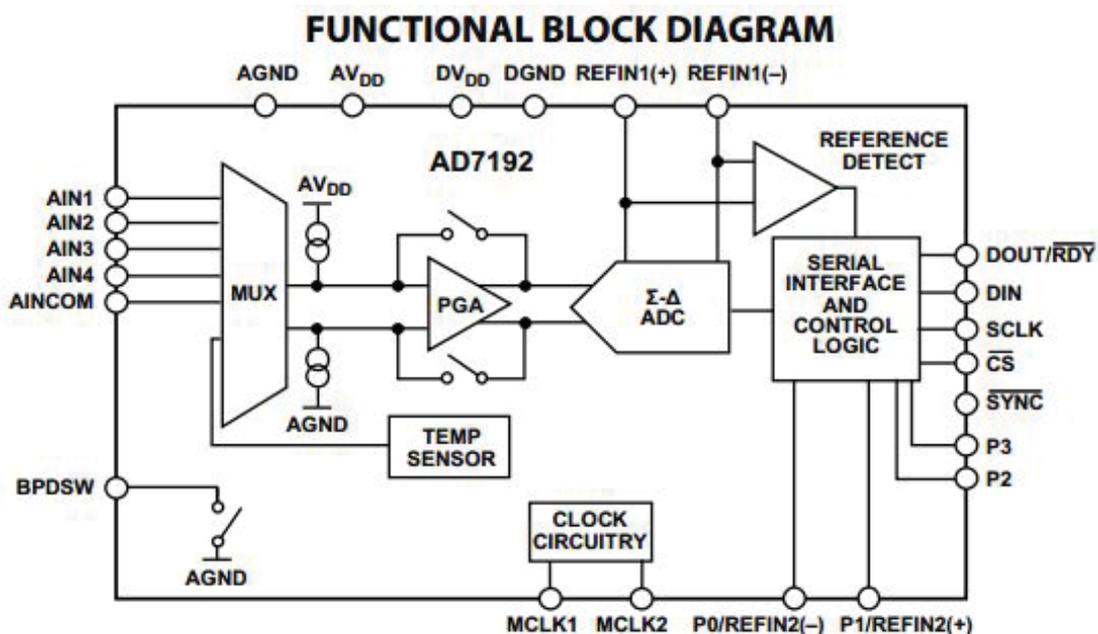


Figure 4.9: The Internal structure of the ADC

There are a number of registers in AD7192. In this project, we have used the

following registers.

1. Communications register
2. Mode register
3. Configuration register
4. Data register.

Communications register

The communication register is an 8-bit write-only register. All communications to the part must start with a write operation to the communications register. The data written to the communications register determines whether the next operation is a read or a write operation and in which register this operation takes place [44]. For read or write operations (\overline{WEN}) when the subsequent read or write operation to the selected register is complete, the interface returns to where it expects a write operation to the communications register. This is the default state of the interface. On power-up or after a reset, the ADC is in this default state waiting for a write operation to the communications register (Table 4.2).

\overline{WEN} : Write enable bit. A 0 must be written to this bit so that the write to the communications register actually occurs. If a 1 is the first bit written, the part does not clock on to subsequent bits in the register. It stays at this bit location until a 0 is written to this bit. After a 0 is written to the \overline{WEN} bit, the next seven bits are loaded to the communications register. Idling the DIN pin high between data transfers minimizes the effects of spurious SCLK pulses on the serial interface.

$R/\overline{W}(0)$: A 0 in this bit location indicates that the next operation is a write to a specified register. A 1 in this position indicates that the next operation is a read from the designated register.

RS2 to RS0: Register addresses bits. These address bits are used to select which registers of the ADC are selected during the serial interface communication.

CREAD: Continuous read of the data register. When this bit is set to 1 (and the data register is selected), the serial interface is configured so that the data register can be continuously read

CR1 and CR0: These bits must be set to 0 for correct operation.

Table 4.2: Communications register of ADC 7192

CR7	CR6	CR5	CR4	CR3	CR2	CR1	CR0
WEN(0)	R/W(0)	RS2(0)	RS1(0)	RS0(0)	CREAD(0)	0(0)	0(0)

Mode register

The mode register is a 24-bit register which supports both read and write operations. As the table 4.3 shows, this register is used to select the operating mode, the output data rate, and the clock source. MR0 through MR23 indicate the bit locations where MR denotes that the bits are the mode register bits. MR23 denotes the first bit of the data stream. The number in parentheses indicates the power-on/reset default status of that bit. Any write to the mode register resets the modulator and filter, and sets the RDY bit.

Table 4.3: Mode Register of ADC 7192

MR23	MR22	MR21	MR20	MR19	MR18	MR17	MR16
MD2(0)	MD1(0)	MD0(0)	DAT_STA(0)	CLK1(1)	CLK0(0)	0	0
MR15	MR14	MR13	MR12	MR11	MR10	MR9	MR8
SINC3(0)	0	ENPAR(0)	CLK_DIV(0)	SINGLE(0)	REJ60(0)	FS9(0)	FS8(0)
MR7	MR6	MR5	MR4	MR3	MR2	MR1	MRO
FS7(0)	FS6(1)	FS5(1)	FS4(0)	FS3(0)	FS2(0)	FS1(0)	FS0(0)

The description below presents the significant bits used in this project:

MR19, MR18:

These bits are used to select the clock source for the AD7192. Either the on-chip 4.92 MHz clock or an external clock can be used. The ability to use an external clock allows several AD7192 devices to be synchronized. Also, 50 Hz/60 Hz rejection is improved when an accurate external clock drives the AD7192.

MR12:

It is the CLK_DIV, Clock Divide by 2. When CLK_DIV is set, the master clock is divided by 2. For normal conversions, this bit should be set to 0.

MR21 - MR23:

When these bits are all set to 0, the ADC operates in the continuous conversion mode (default). In continuous conversion mode, the ADC continuously performs conversions and places the result in the data register.

Configuration register

The configuration register in Table 4.4 is a 24-bit register from which data can be read or to which data can be written. This register is used to configure the ADC for unipolar or bipolar mode (U/\bar{B}), to enable or disable the buffer (BUF), to enable or disable the burnout currents (BURN), to select the gain ($G2-G0$), and to select the analog input channel ($CH7\sim CH0$) [44].

Table 4.4: Configuration register of ADC 7192

CON23	CON22	CON21	CON20	CON19	CON18	CON17	CON16
CHOP(0)	0(0)	0(0)	REFSEL(0)	0(0)	0(0)	0(0)	0(0)
CON15	CON14	CON13	CON12	CON11	CON10	CON9	CON8
CH7(0)	CH6(0)	CH5(0)	CH4(0)	CH3(0)	CH2(0)	CH1(0)	CH0(1)
CON7	CON6	CON5	CON4	CON3	CON2	CON1	CON0
BURN(0)	REFDET(0)	0(0)	BUF(1)	U/\bar{B} (0)	G2(1)	G1(1)	G0(1)

Data register

The conversion result from the ADC is stored in this data register. This is a read-only, 24-bit register. On completion of a read operation from this register, the RDY pin/bit is set. When the DAT_STA bit in the mode register is set to 1, the contents of the status register are appended to each 24-bit conversion. This is advisable when several analogue input channels are enabled, because the three LSBs of the status register (CHD2 to CHD0) identify the channel from which the conversion originated.

Circuit design of the ADC

Figure 4.10 shows the typical circuit of ADC 7192 [45].

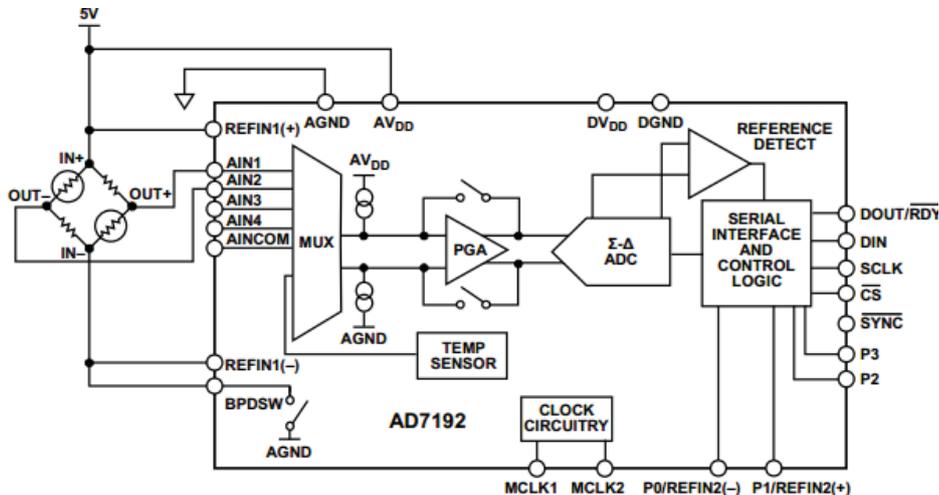


Figure 4.10: Typical circuit of the ADC 7192 [45]

The ADC transfers data to the microcontroller using the SPI interface bus. AIN1 connects to out+, and out- is connected to AIN2, the negative side. BPDSW is the bridge power-down switch to AGND. It is not used in this project; hence, it is not connected. Figure 4.11 illustrates the circuit of the ADC in this project:

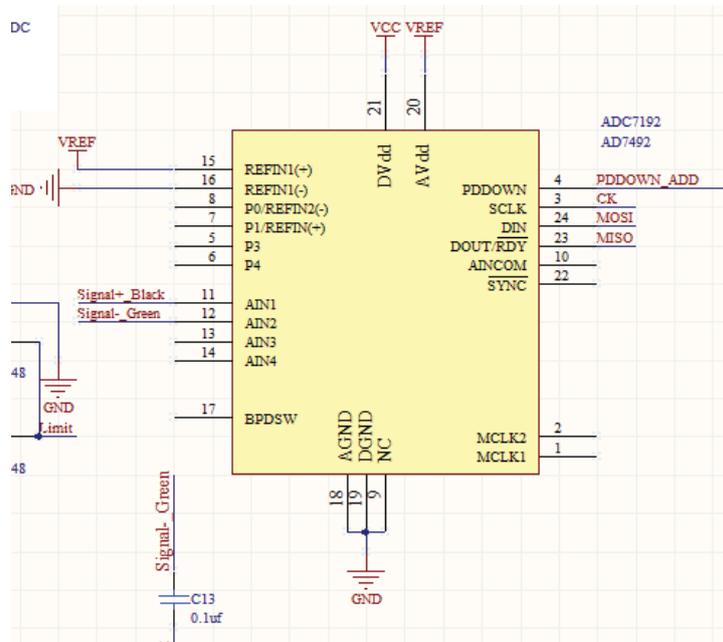


Figure 4.11: The schematic of ADC 7192 circuit

To reduce the effect of noise, the decoupling capacitors should be added between the AIN1 and AIN2 and also between the ground and AIN1 and AIN2. An example ADC code is illustrated in figure 4.12. To test if the program was working as designed, a serial monitor was used to show that the 24 bit result changed value when a force was generated from the load cell.

```

AD_CS_ON(); //open the CS of ADC

While (digitalRead (MISO == 1) // waiting for data transformation
done

SPI.transfer(0x58);          // open the Mode

Val = SPI.transfer(0xff);

Val = (val<<8) | SPI.transfer(0xff);

Val = (val<<8) | SPI.transfer(0xff);

Serial.print(val);

```

Figure 4.12: Example code of ADC 7192

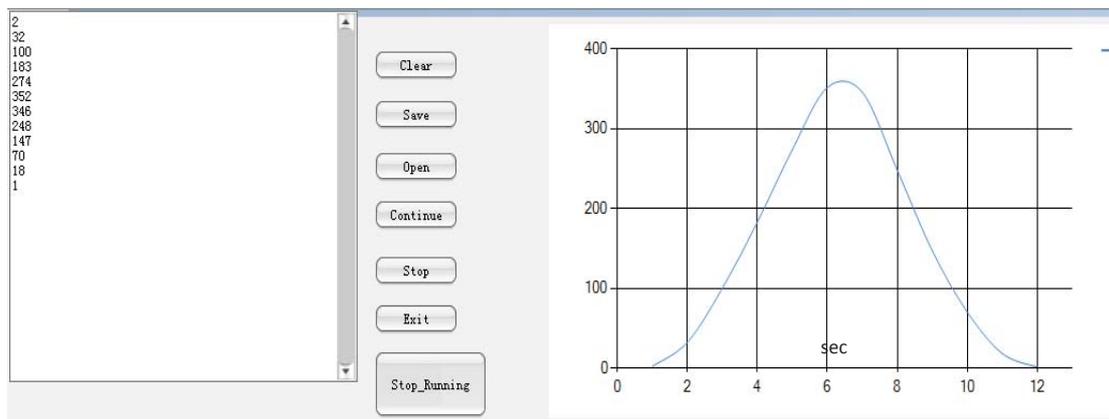


Figure 4.13: The result from ADC

Figure 4.13 shows the test of the ADC. The textbox displays the data transferred from the load cell (the unit is gram). At the right side, the real time graph shows the trend of the force; y axis is the value of the applied force and x axis is time.

In this project, the ADC is configured for unipolar operation, the output codes are natural (straight) binary with a zero differential input voltage resulting in a code of 00...00, a midscale voltage resulting in a code of 100...000, and a full-scale input voltage resulting in a code of 111...111. The output code for any analogue input voltage can be represented as:

$$\text{Code} = (2N \times \text{AIN} \times \text{Gain})/\text{VREF} \quad (20)$$

In this project, the VREF is 5 V, Gain is 128, N = 24. The output voltage AIN value can be calculated from this formula. The code would be described in the software implement section in detail.

4.2.4 Pull-up Resistor

During the period of testing the PCB, the protocol of ADC (SPI bus) did not work. No output was received from ADC. The pull-up resistor should be added to reduce the effect of noise and promote capability of the SPI bus. Normally, SPI bus does not need a pull-up resistor. However, the performance of SPI is lower either due to so many via holes drilled on the board or when SPI drives more than one IC. Hence, the pull-up resistor would be needed to enhance the capability of the SPI driver. Usually the bigger the value of pull-up resistor better is the performance.

Figure 4.14 displays the schematic of pull up resistors for the SPI bus of the ADC. R6, R7, and R16 are the pull-up resistors.

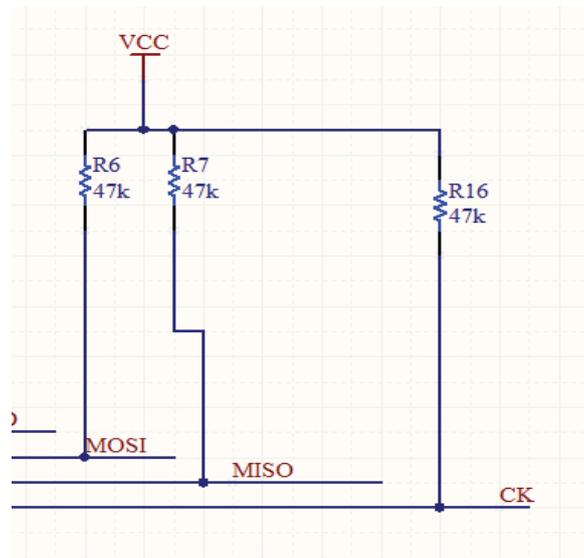


Figure 4.14: The schematic of pull up resistors

4.2.5 Infra-Red sensor

Infrared is the invisible radiant energy. It is electromagnetic radiation with longer wave lengths than those of visible light [45]. In this project, a small infra-red sensor was used to detect the location of the robotic arm. The robotic arm must not touch the test food when it is in a high speed (pre-test speed) mode because it may crush or destroy the food, especially fragile samples. The function of the infra-red sensor is to detect the position of the arm so that the arm can reduce its speed to the test speed before the probe touches the test food. Hence, the sensor is provided to the users so that they can adjust the height of the infra-red sensor manually according to the different size of food sample.

Figure 4.15 shows the infra-red sensor used in this project, which just has 3 pins (VCC, GND, and OUTPUT). When the robotic arm is detected, the infra-red sensor will generate a high voltage. The sensor output will give a low signal when there is nothing detected.



Figure 4.15: Infra-red sensor

4.2.6 Using diode to realise an OR Gate

During the time of designing the PCB, the number of pins in the Arduino Uno appeared to be insufficient. It is required to keep some spare pins. In the protection system, there are two outputs, one is for the top limit, and the other is for the bottom limit. Using two diodes as an OR gate, one less pin can be used. Figure 4.16 below displays the circuit of the OR gate.

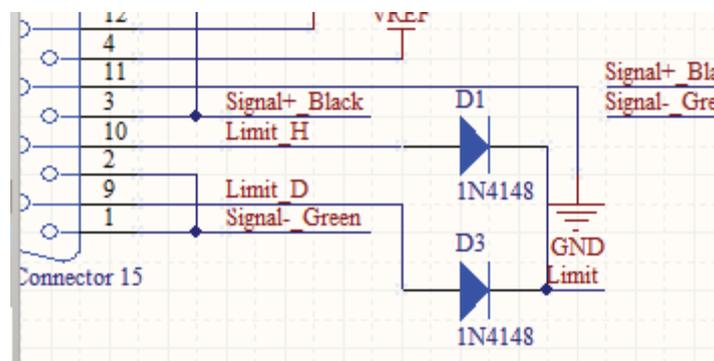


Figure 4.16: The schematic of OR gate

4.2.7 Power supply

According to the specification of the L6472 ADC, the input voltage is 36 V to drive the stepper motor. The Arduino needs 5 V and the ADC needs 5 V for its analogue reference voltage. The current must be flat and smooth to keep the noise from power supply affecting the results from ADC. The slave board also needs 5 V for the Arduino and the touch screen.

The switching regulator LM2594HV, with 57 V maximum input voltage is found to be suitable for the project. Switch regulators are more efficient than the linear ones

[46].

Requiring a minimum number of external components, this regulator is simple to use and features internal frequency compensation, a fixed-frequency oscillator, and improved line and load regulation specifications [46, 47]. The output ripple from switch regulator is about 5 mV after attaching an LC filter, including 3 uH inductor and 100 uF capacitor. Figure 4.17 displays the typical circuit of LM2594.

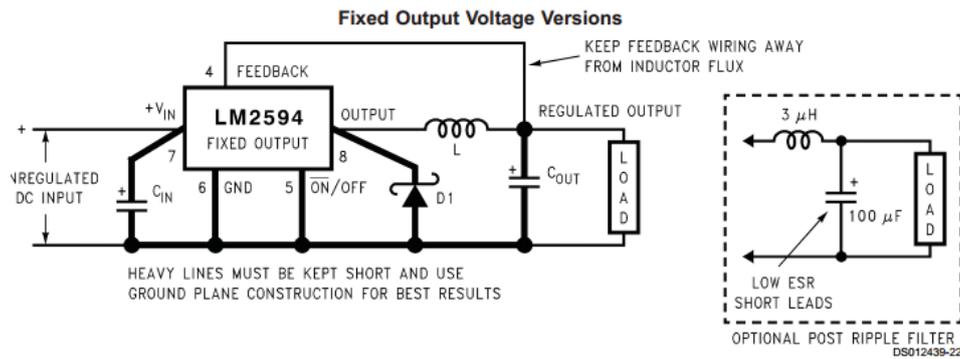


Figure 4.17: The typical circuit of LM2594

Figure 4.18 shows the schematic of LM2594.

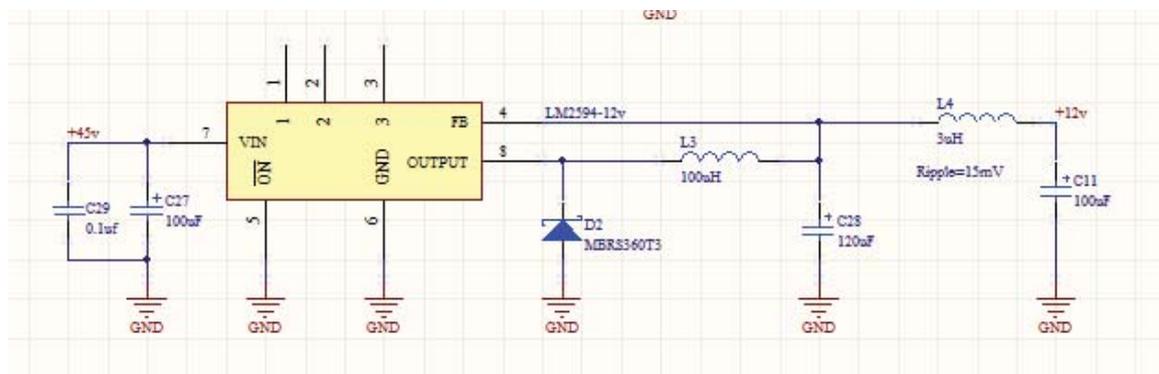


Figure 4.18: The schematic of LM2594

The C29 and C27 are the decoupling capacitors. The diode (D2) and inductor (L3) work together as a feedback circuit of the switch regulator. L4 and C11 combine together as a low pass filter to reduce the ripple generated from the switch regulator to 5 mV. Figure 4.19 below presents the ripple before the LC filter.

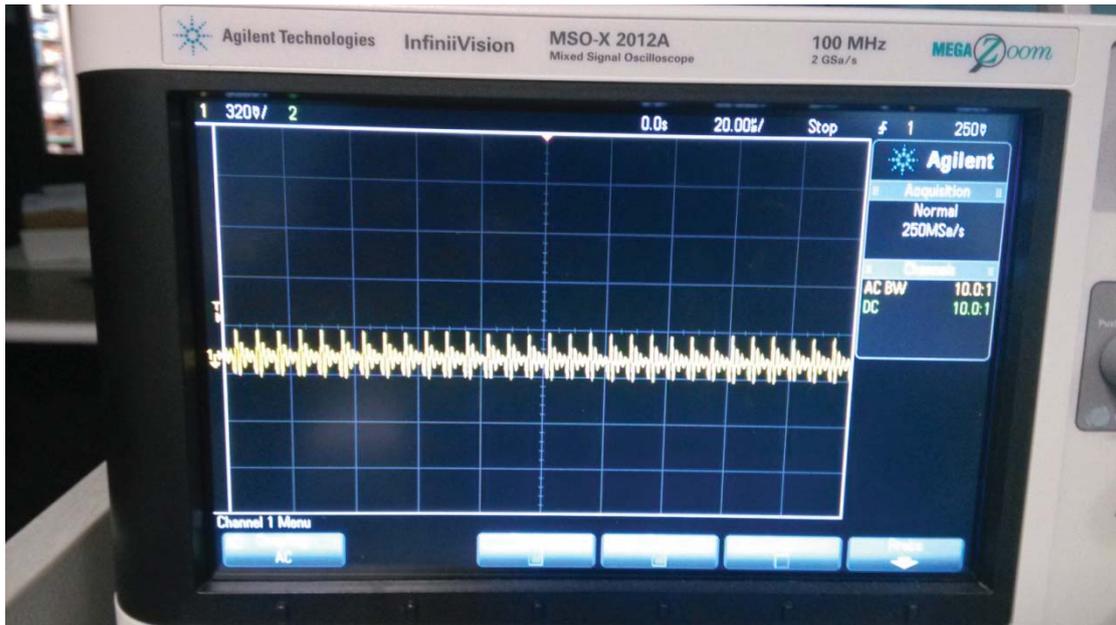


Figure 4.19: The ripple before LC filter

The ripple shown in Figure 4.19 is the input ripple of the power supply (the power supply used in this project is HRP-1 5 0). It is about 320 mV. Figure 4.20 depicts the output of ripple after the LC filter. As can be seen, the average ripple is about 5 mV.

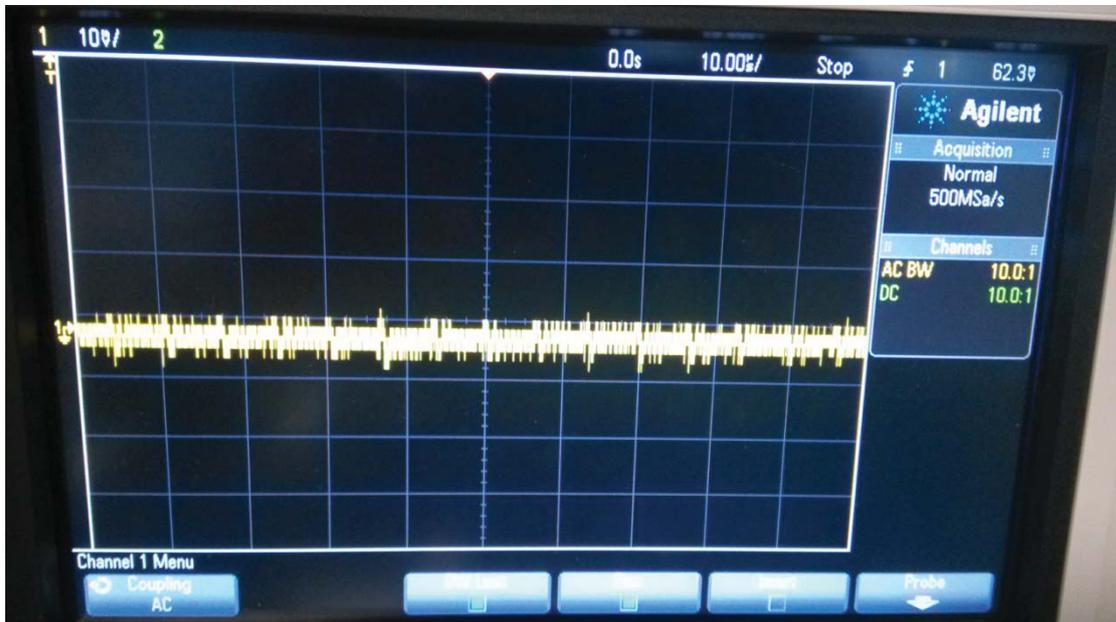


Figure 4.20: The ripple after LC filter

Linear regulator (12 V to 5 V), 7805, is used to power the Arduino board (figure 4.21).

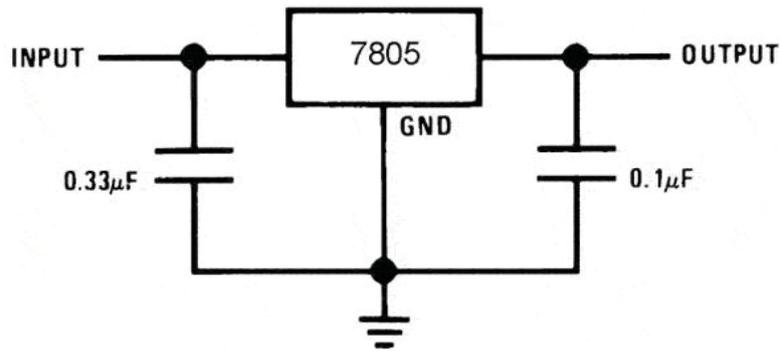


Figure 4.21: Typical circuit for 7805

ADC needs a constant current and stable voltage to ensure error-free data transfer. Hence, a LDO (low-dropout regulator) is necessary to be used to reduce the ripple from the switch regulator. To reduce the ripple produced by the switch regulator, a LDO with high ripple rejection (60 dB) is selected in this project.

An LDO, TPSA4901, is chosen for rejecting the ripple. It is an ultra-low noise positive linear regulator. The input is from 3 V to 36 V and just has 15.3 μV noise when the input frequency is 10 Hz to 100 kHz on average. Furthermore, according to the datasheet, the application of it is to supply rails for op amps, DACs, ADCs, and other high-precision analogue circuitry. As the datasheet suggests, the power-supply ripple rejection in 120 Hz is 72 dB, and from 10 Hz to 400 kHz is more than 60 dB (Figure 4.22) [48]. The output ripple from LM2594HV is 5 mV. The power-rejection of TPS4901 is 60 dB at 150 kHz, which is the frequency of LM2594. Hence, the output ripple is $5 \text{ mV}/1000 = 0.005 \text{ mV}$ which is too small to influence the result from the AD converter.

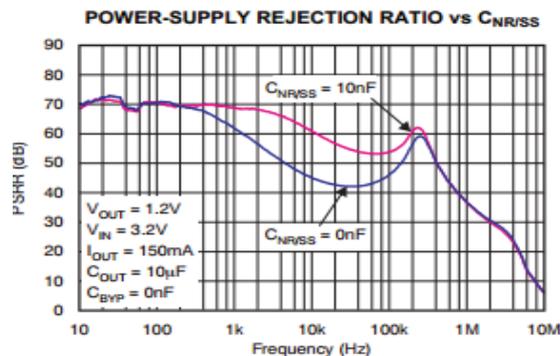


Figure 4.22: The power-supply rejection ratio (TPSA4901) [53]

According to the datasheet of LM2594, the ripple frequency is about 150 kHz. Hence

the power supply rejection ratio is, as figure 4.22 shows, about 60 dB.

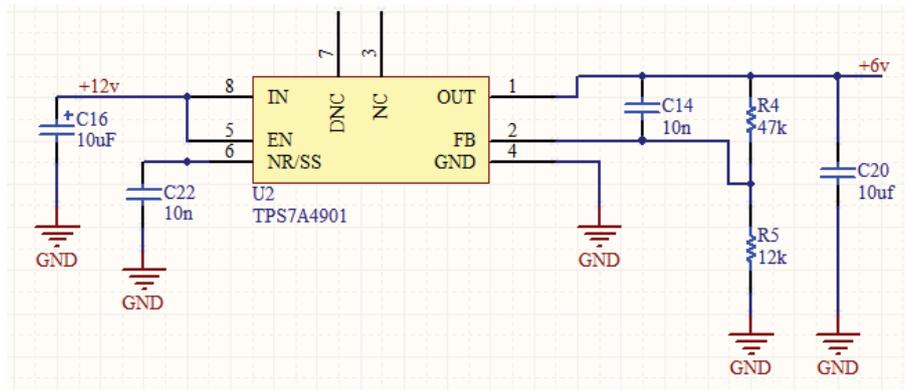


Figure 4.23: The schematic of TPSA4901 [53]

As can be seen in figure 4.23, C16 and C20 are the decoupling capacitors and the capacitor C14 is the noise reduction capacitor. The function of C14 is to bypass noise generated by the internal band gap generator. Figure 4.22 shows the relationship between PSRR (Power-supply rejection ratio) and Frequency. As can be seen, the performance is better when C22 (10 nF) is added than when no capacitor is used. This capacitor allows RMS noise to be reduced to very low levels. C14 can reduce the ripple of the output voltage.

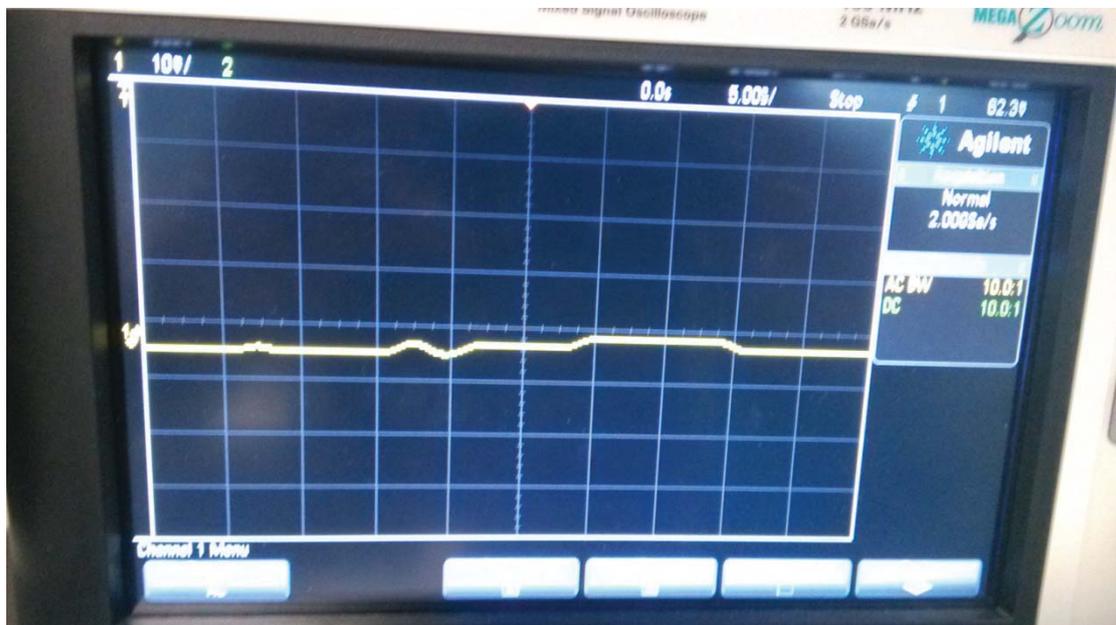


Figure 4.24: The ripple after LDO filter

Figure 4.24 illustrates the output ripple from TPS7A4901. The ripple is quite small that hardly affects the ADC result.

REF5050

The REF5050 is a low-noise, low-drift, very high precision voltage reference. This reference is capable of both sinking and sourcing, and is very robust with regard to line and load changes. Since load cells need high precision [78] the REF5050 was used to give the power for the ADC analogue reference voltage and load cell. REF5050 is a low temperature drift (high-grade: 3 ppm/°C(max)), and high accuracy component. It is used for the ADC power supply (analogue part). Table 4.5 shows the parameter of REF5050:

Table 4.5: The parameter of REF5050

ABSOLUTE MAXIMUM RATINGS⁽¹⁾

	REF50xx	UNIT
Input Voltage	+18	V
Output Short-Circuit	30	mA
Operating Temperature Range	-55 to +125	°C
Storage Temperature Range	-65 to +150	°C
Junction Temperature (T _J max)	+150	°C
ESD Rating	Human Body Model (HBM)	3000
	Charged Device Model (CDM)	1000

Figure 4.25 displays the schematic of REF5050.

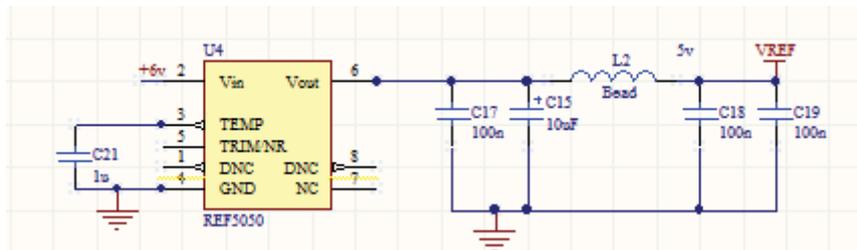


Figure 4.25: The schematic of REF5050

The bead (inductor), C17, C15, C18 and C19 together implement a passive low pass filter to reduce the effect of ripple, make voltage and current constant and stable. The complete power supply system is displayed in figure 4.26:

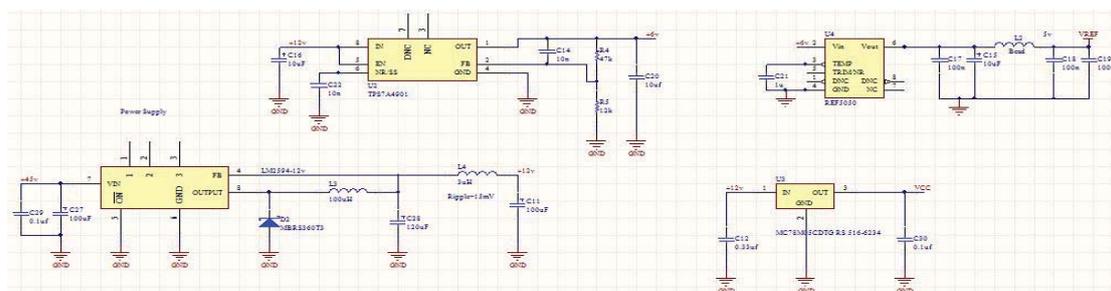


Figure 4.26: The schematic of the power supply

4.3 Slave Board

4.3.1 Touchscreen

A touchscreen is an electronic visual display that the user can control through simple or multi-touch gestures by touching the screen with a special stylus/pen and-or one or more fingers [49, 50]. Figure 4.27 presents the touch screen that is used in this project



Figure 4.27: Touch Screen

Some touchscreens require an ordinary or specially coated glove to work while others use a special stylus/pen only. The user can use the touchscreen to react to what is displayed on it and to control how it is displayed (for example zooming the text size) [51]. The touch screen used in this project is a resistor sense surface, and is cheap. Using the SPI protocol, the data can be transferred in a serial operation, which means it can save pins compared with parallel connections. The purpose of this is to display the status of the machine, and the visual buttons will help users to control the whole equipment.

The driver of the touch screen used in this project is called ILI9341, a 262, 144-colour single-chip SOC driver for a-TFT liquid crystal display with a resolution of 240x320 RGB dots, comprising of a 720-channel source driver, a 320-channel gate driver, 172,800 bytes GRAM for graphic display data, and power supply circuit [52, 53]. ILI9341 supports parallel 8-/9-/16-18-bit bus MCU interface, and also SPI protocol. In this project, for the reason of saving IO pins, the SPI has been used.

The range of I/O interface voltage of ILI9341 is from 1.65 to 3.3 V, hence the 20 k Ω resistors should be added to convert 5 V to 3.3 V.

The principle of the touch screen

As figure 4.28 shows, the screen is formed by two plastic films, each coated with a conductive layer of metal, usually indium tin oxide (ITO), that are separated by an air gap [54]. One plate, the X-plate in the diagram, is excited by the supply voltage [55]. When the screen is touched, the plates come together, creating a resistor divider along the first plate (X plate). The point that creates the voltage, which represents the position on the X-plate, is sensed through the Y+. The process is then repeated by exciting the Y- plate and sensing the Y position through the X+ side. The formula is shown as follow:

$$V_{y+} = V_{REF} * \frac{R_{x-}}{R_{x(TOTAL)}} \quad (20)$$

$$V_{x+} = V_{REF} * \frac{R_{y-}}{R_{y(TOTAL)}} \quad (21)$$

where V_{REF} is the voltage of the power supply.

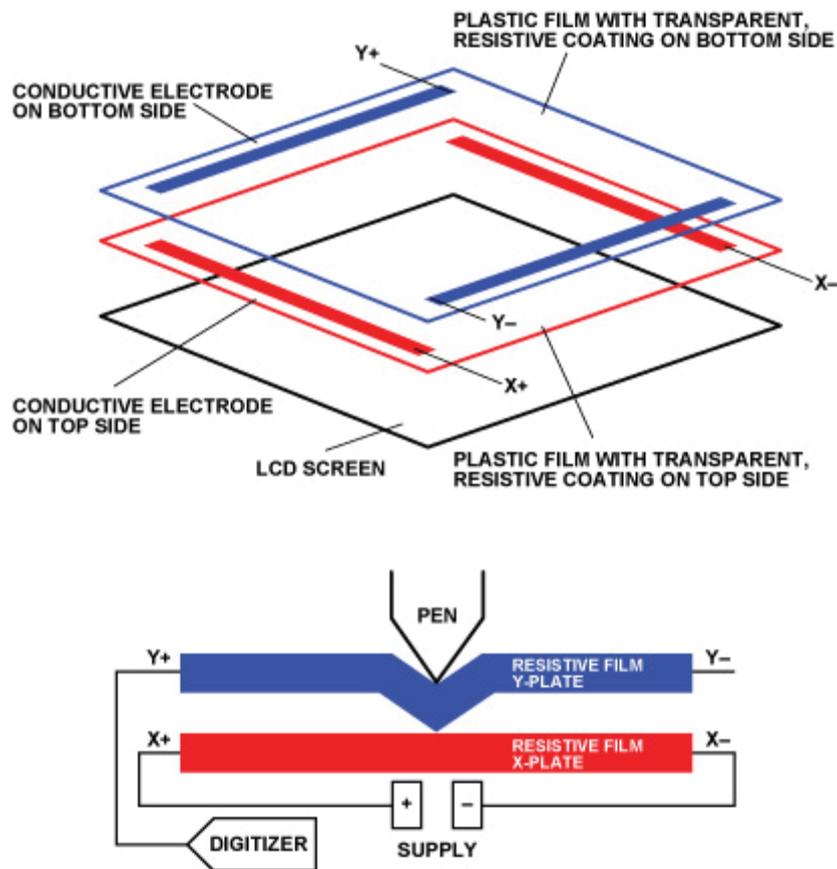


Figure 4.28: The principle of touch screen operation [56]

Analog 4-wire Resistive touch screen

Analog 4-wire resistive sensing is the most fundamental sensing method of resistive technology. The top and the bottom transparent conductive sheets that have uniform resistance value are facing each other with a gap. When the top sheet is touched, the touched point of the top sheet yields, and contacts the bottom sheet. The contact point conducts, and its location is sensed [56]. Figure 4.29 presents the principle of 4 wire touch screen.

The sensing process (5 V voltage as example) [57]

1. In the figure 4.28 the voltage is applied between the electrode Y+ and Y- on the top sheet. An equipotential distribution that is parallel to the Y+ and Y-.
2. Assuming that the electrode Y+ is 0 V (Ground), then apply 5 V to the electrode Y-. If the central point between the right and left electrodes is touched, 2.5 V would be measured by the bottom sheet. If a point 1/5 away from Y+ (4/5 away from X-) is touched, 1 V would be measured by the bottom sheet. The Y-coordinate point is detected in this way.
3. After detecting the coordinate point in Y direction, voltage is applied between the electrode X+ and X- on the bottom sheet. The top sheet would measure the point between X+ and X- (X coordinate), in the same manner as Y coordinate in steps 1-2.
4. As the set of step 1 to 3 is repeated, the X and Y coordinate points of touched locations keeps being detected.

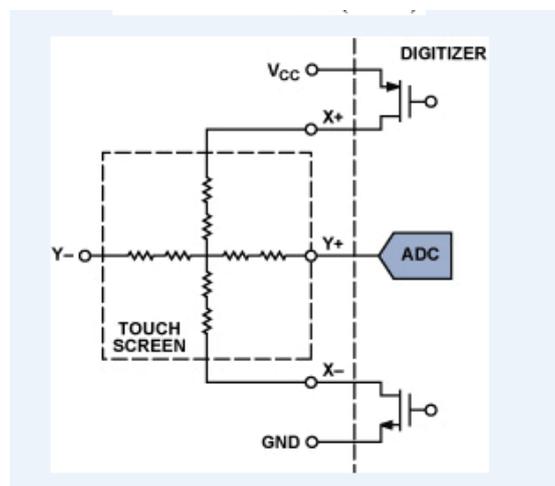


Figure 4.29: 4-wire touch screen

4.4 Protection System and Circuits

The protection system can adjust the maximum range of the arm movement. As can be seen in figure 4.30, a steel pipe attaches with two little adjustable circle buttons. There are two triggers on the right side of the arm. When the triggers touch the circular buttons, the microcontroller will recognize the limits of the start and stop range of the user. The distance between the top circle button and bottom circle button is the working range of robotic arm. The working principle of the protection system is by using optical coupler (Figure 4.31).



Figure 4.30: Protect system

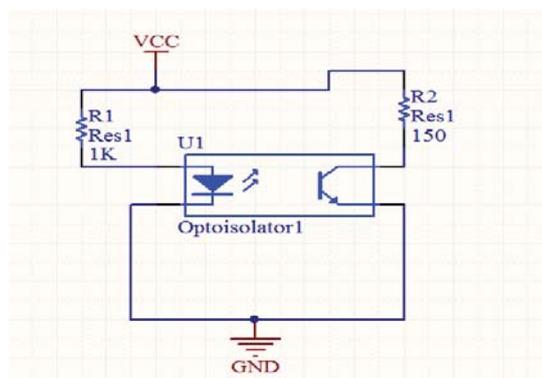


Figure 4.31: The schematic of the protection system [57]

4.5 Schematic and PCB

All the schematics of this project are shown in figures 4.34 and 4.35. Before manufacturing the PCB, the technician Ken (electronics specialist) helped me to make sure that the component were connected to the appropriate pins so that the circuit functioned as intended. Almost every custom footprint had to be created as they were not available in the Massey libraries, except the footprints like Nano, DB15 and some

connectors. The designed PCB can be seen in the figure 4.36 (top layer) and figure 4.37 (bottom layer) with the majority of the components surface mounted to fit within the available space.

The component layouts were implemented on the PCB based on the PCB design guidelines of Massey University, which are as follows:

- 20 mil track into surface mount pads
- At least 15 mil track through rest of board
- All components have decoupling capacitors connected to the supply pin and must be near the component
- Pour polygon on the ground so that it can reduce noise and impedance.
- Filtering capacitors on the incoming load cell lines were placed not far away from the ADC to prevent as much noise as possible from going through before the signal was digitized
- Positioning of components so the least amount of jumpers was required.

Due to the complexity of the PCB, we felt that it is necessary to illustrate some other PCB rules other than those mentioned in the guideline of Massey.

When laying out components for a mixed-signal PCB, certain considerations are critical to achieve optimum performance. Mixed-signal is particularly tricky to design since analogue devices possess different characteristics compared to digital components: different power ratings, current, voltage and heat dissipation requirements, to name a few [79].

In this PCB, there are both analogue and digital signals (stepper motor driver). Thus, a careful design of the mixed signal PCB should be one of the main focus.

Noise generated in the L6472 stepper motor driver can be a major cause which corrupts the results of the ADC. In order to circumvent its effect, the Nano microcontroller, situated between the analogue and the digital circuit, can be regarded as a buffer. Figure 4.32 shows the layout of the blocks on the PCB. To get better results for the ADC, it is located just near the DB15 connector.

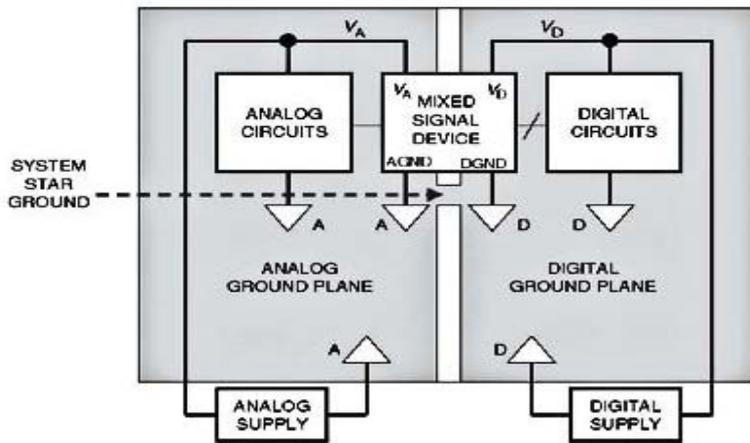


Figure 4.32: The formatting of mixed signal[58]

In this project the operating frequency is very low (under 1 MHz). If the ADC frequency is very high (higher than 10 MHz), two things need to be taken care of - the analogue ground (AGND) should connect to digital ground (DGND) just at a single point and then connect with the GND of the power supply. Between the AGND and DGND, at the single point, a 0Ω resistor or a bead should be added to reduce the effect of ripple generated from the ADC side for the digital part (Figure 4.33). Secondly, the track of the ADC should be as short as possible and close to the DB15 connector. Figure 4.34 shows the principle of the formatting of the mixed signal components for high frequency PCB.

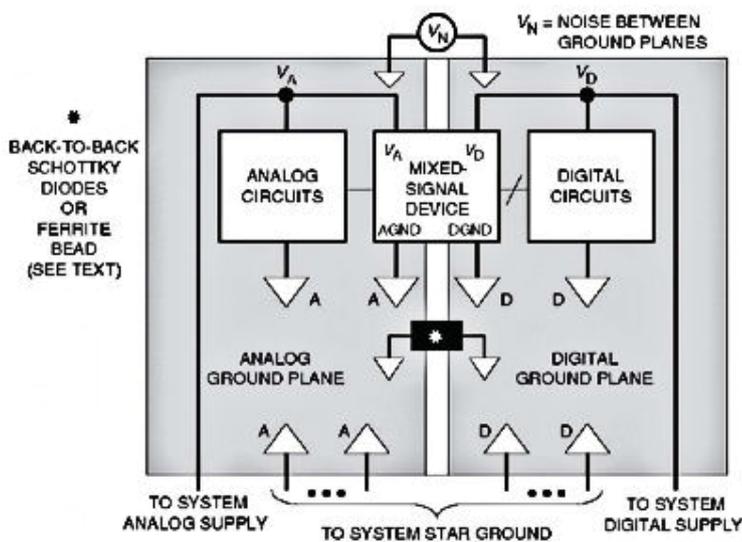


Figure 4.33: The diagram of mixed signal [58]

The reason for “polygon fill”

In electronics, the term "polygons pour" refers to an area on a printed circuit board filled with copper (the metal used to make connections in printed circuit boards). Copper pour is commonly used to create a ground plane[59]. Another reason for using copper pour is to reduce the amount of etching fluid used during manufacturing [60].

PCB designers today almost invariably use completely solid areas of the copper pour that completely cover the remaining area outside those tracks, pads, and stand-off regions. Many early PCBs have a "hatched copper pour", sometimes called a "cherry pie lattice." [61]

While solid copper pour provides better resistive characteristics, hatched copper pour is used to balance the heat and dilatation on both sides of the board to avoid warping of the substrate [62]. Heating might cause gas bubbles between the solid copper pour and certain substrates [63] Furthermore, it might be possible to adjust the impedance of high-frequency traces by using hatched copper pour to reach better signal quality [69].

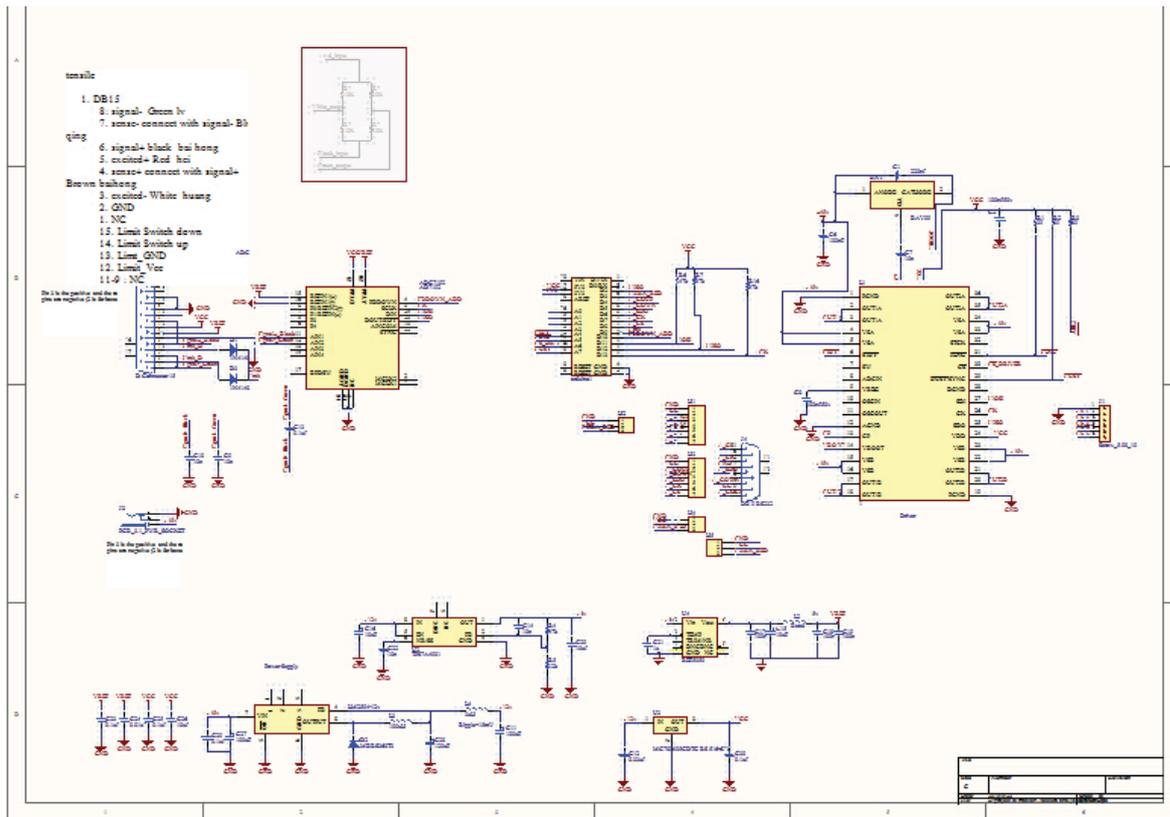


Figure 4.34: The complete schematic of the Master board[58]

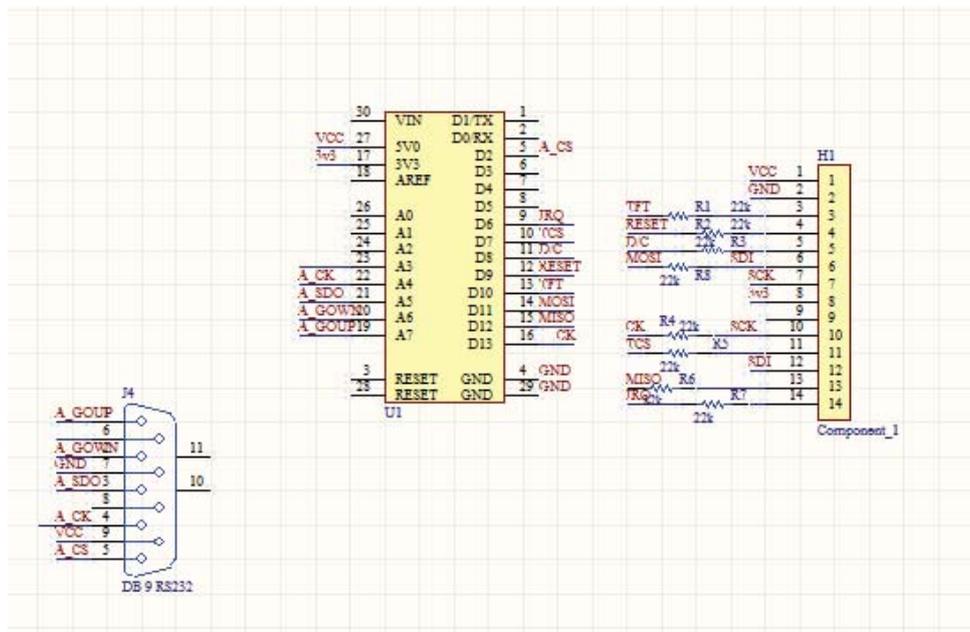


Figure 4.35: The schematic of the Slave board

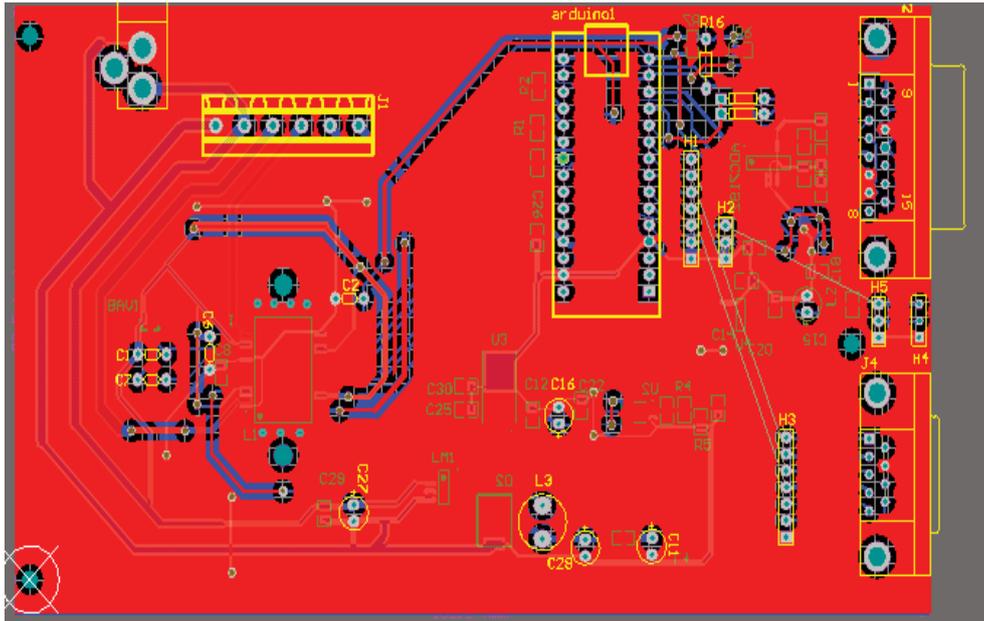


Figure 4.36: Top Layer of the Master Board

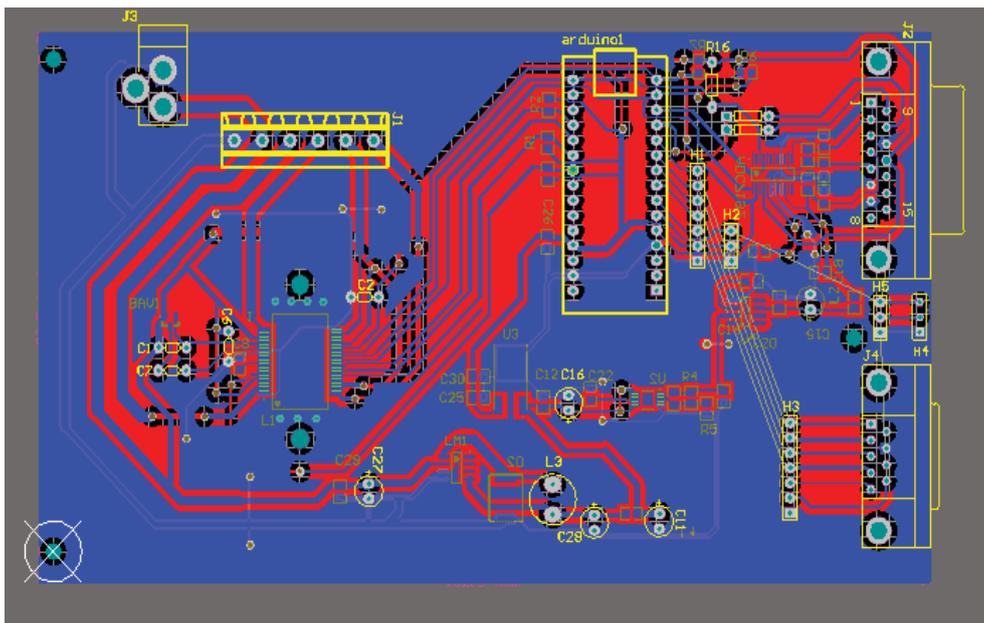


Figure 4.37: Bottom Layer of the Master Board

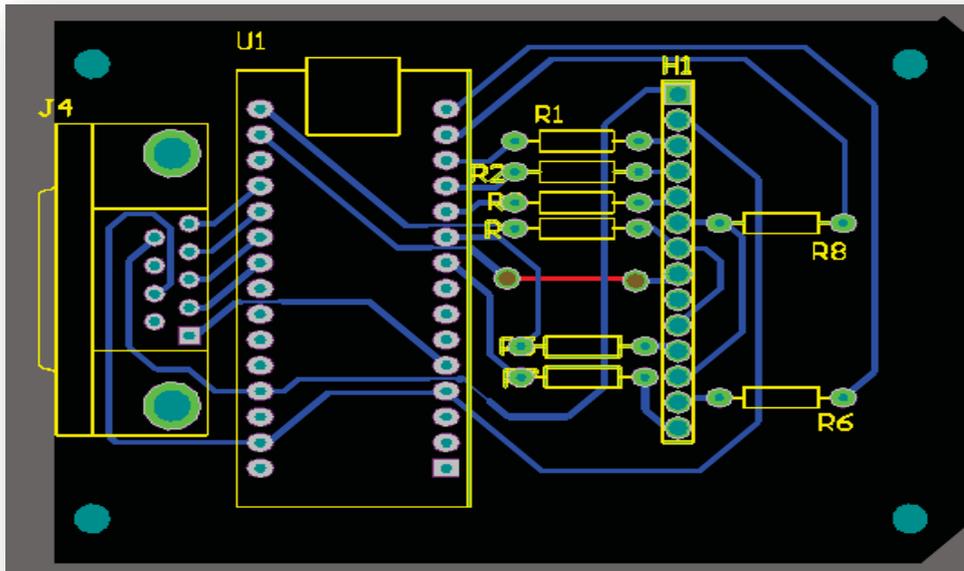


Figure 4.38: The PCB design of the Slave board

4.6 Summary

This chapter explains in details the function and selection of all the components that were used to make this project complete, along with the integration of the components and the rules of the PCB board design. Testing of each component required a number of different experiments to be conducted. The results continually improved with the implementation of different circuits. Before integrating all the components into one board, a small PCB board, just for L6472 was manufactured, to check whether the circuit worked as expected. The AD converter design worked correctly and the effect of noise was insignificant. Several tests for the AD converter were done in order to identify the appropriate programming code.

The touch screen can display the button and basic status of the whole machine. Users also can control the whole equipment by using the touch screen. The integration of the Master board and the slave board was successfully tested and the whole system functioned as envisaged.

Chapter 5

Software Implementation

There are two parts in the software programming. One is for the hardware, that includes the microcontroller and the ADC, and the other one is for the PC, which can transfer information between the Arduino Nano board and the PC, and display the data and real-time graphs on the screen.

Hardware programming includes the code for the stepper motor controller/driver, the ADC, the touchscreen, and the command interpreter. The next subsections will provide the information in detail. The SPI protocol is used to interface with all the peripherals (ADC, stepper motor driver, and touch screen). To begin with, the principles of SPI communication are explained in details.

5.1 SPI Bus

The Serial Peripheral Interface (SPI) bus is a synchronous serial communication interface specification used for short distance communication, primarily in embedded systems [64]. The interface was developed by Motorola [65]. Typical applications include sensors, secure digital cards, and liquid crystal displays (LCD) [65].

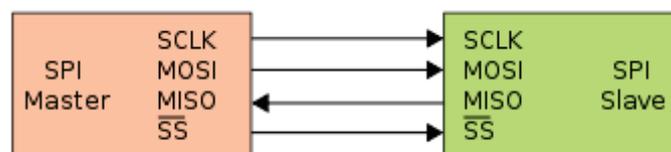


Figure 5.1: SPI bus connections between Master and Slave devices

In a SPI connection, there is always one master device (usually a microcontroller) which controls the peripheral devices (slaves). Typically, as shown in Figure 5.1 , there are four lines common to all the devices [66]:

- MISO (Master In Slave Out) - The Slave line for sending data to the Master

Table 5.1 illustrates the list of configurable registers.

Table 5.1: The registers of L6472 (R: Readable, WH: writable only when outputs are in high-impedance, WS: writable only when the motor is stopped, WR: always writable.)

Address [Hex]	Register name	Register function	Len. [bit]	Reset [Hex]	Reset value	Remarks ⁽¹⁾
h01	ABS_POS	Current position	22	000000	0	R, WS
h02	EL_POS	Electrical position	9	000	0	R, WS
h03	MARK	Mark position	22	000000	0	R, WR
h04	SPEED	Current speed	20	00000	0 step/tick (0 step/s)	R
h05	ACC	Acceleration	12	08A	$125.5e-12 \text{ step/tick}^2$ (2008 step/s ²)	R, WS
h06	DEC	Deceleration	12	08A	$125.5e-12 \text{ step/tick}^2$ (2008 step/s ²)	R, WS
h07	MAX_SPEED	Maximum speed	10	041	$248e-6 \text{ step/tick}$ (991.8 step/s)	R, WR
h08	MIN_SPEED	Minimum speed	13	000	0 step/tick (0 step/s)	R, WS
h15	FS_SPD	Full-step speed	10	027	$150.7e-6 \text{ step/tick}$ (602.7 step/s)	R, WR
h09	TVAL_HOLD	Holding current	7	29	1.3125 A	R, WR
h0A	TVAL_RUN	Constant speed current	7	29	1.3125 A	R, WR
h0B	TVAL_ACC	Acceleration starting current	7	29	1.3125 A	R, WR
h0C	TVAL_DEC	Deceleration starting current	7	29	1.3125 A	R, WR
h0D	RESERVED	Reserved address	16			
h0E	T_FAST	Fast decay/fall step time	8	19	1 μ s / 5 μ s	R, WH
h0F	TON_MIN	Minimum ON time	7	29	20.5 μ s	R, WH
h10	TOFF_MIN	Minimum OFF time	7	29	20.5 μ s	R, WH
h11	RESERVED	Reserved address	8			
h12	ADC_OUT	ADC output	5	XX ⁽²⁾		R
h13	OCD_TH	OCD threshold	4	8	3.38 A	R, WR
h14	RESERVED	Reserved address	8			
h16	STEP_MODE	Step mode	8	7 ⁽³⁾	16 microsteps, no synch.	R, WH
h17	ALARM_EN	Alarms enable	8	FF	All alarms enabled	R, WS

The host microcontroller can configure the L6472 device and control the motor motion quite easily by using a comprehensive set of commands which are listed in Table 5.2.

Table 5.2: Command set of L6472

	[7 ... 5]	[4]	[3]	[2 ... 1]	[0]	
NOP	000	0	0	00	0	Nothing
SetParam (PARAM, VALUE)	000	[PARAM]				Writes VALUE in the PARAM register
GetParam (PARAM)	001	[PARAM]				Returns the stored value in the PARAM register
Run (DIR, SPD)	010	1	0	00	DIR	Sets the target speed and the motor direction
StepClock (DIR)	010	1	1	00	DIR	Puts the device into step-clock mode and imposes DIR direction
Move (DIR, N_STEP)	010	0	0	00	DIR	Makes N_STEP (micro) steps in DIR direction (non-performable when motor is running)
GoTo (ABS_POS)	011	0	0	00	0	Brings motor in ABS_POS position (minimum path)
GoTo_DIR (DIR, ABS_POS)	011	0	1	00	DIR	Brings motor in ABS_POS position forcing DIR direction
GoUntil (ACT, DIR, SPD)	100	0	ACT	01	DIR	Performs a motion in DIR direction with speed SPD until SW is closed, the ACT action is executed then a SoftStop takes place
ReleaseSW (ACT, DIR)	100	1	ACT	01	DIR	Performs a motion in DIR direction at minimum speed until the SW is released (open), the ACT action is executed then a HardStop takes place
GoHome	011	1	0	00	0	Brings the motor in HOME position
GoMark	011	1	1	00	0	Brings the motor in MARK position
ResetPos	110	1	1	00	0	Resets the ABS_POS register (set HOME position)
ResetDevice	110	0	0	00	0	Device is reset to power-up conditions
SoftStop	101	1	0	00	0	Stops motor with a deceleration phase
HardStop	101	1	1	00	0	Stops motor immediately
SoftHiZ	101	0	0	00	0	Puts the bridges in high-impedance status after a deceleration phase
HardHiZ	101	0	1	00	0	Puts the bridges in high-impedance status immediately
GetStatus	110	1	0	00	0	Returns the STATUS register value
RESERVED	111	0	1	01	1	RESERVED COMMAND
RESERVED	111	1	1	00	0	RESERVED COMMAND

The code for the stepper motor driver has been shown in Appendix 4. The main functions implemented for motor control are:

void dSPIN_Run (byte dir, unsigned long spd)

It is the motor run function. The motor runs forward if *dir* is set 1, and backward if it is set 0. Also the *spd* variable can be configured to modify the speed. The unit of speed is step/s.

dSPIN_GoHome()

Brings the motor to *Home* position.

void dSPIN_Move (byte dir, unsigned long n_step)

Makes *n_step* (micro) steps in *dir* direction. This function is used when the probe touches the food.

void dSPIN_SoftStop()

Stops the motor with a deceleration phase

unsigned int dSPIN_GetStatus()

Returns the status of the motor driver.

unsigned long dSPIN_Get_Param(byte param)

Returns the stored value in the “*param*” register. Variable *param* is the address of the register wanted to visit.

5.2.2 Analogue to Digital Converter

To convert the analogue signal generated from the load cell to a digital signal, a 24-bit ADC, AD7192, is used in this project. There are two modes of the AD converter, they are:

Continuous Conversion Mode

In this mode, the AD7192 converts continuously. If CS is low the RDY bit in the status register goes low each time a conversion is completed. To read a conversion, the user writes to the communications register, indicating that the next operation is a read of the data register. After the data has been read, from the data register, RDY will go high. This timing diagram is shown in figure 5.3:

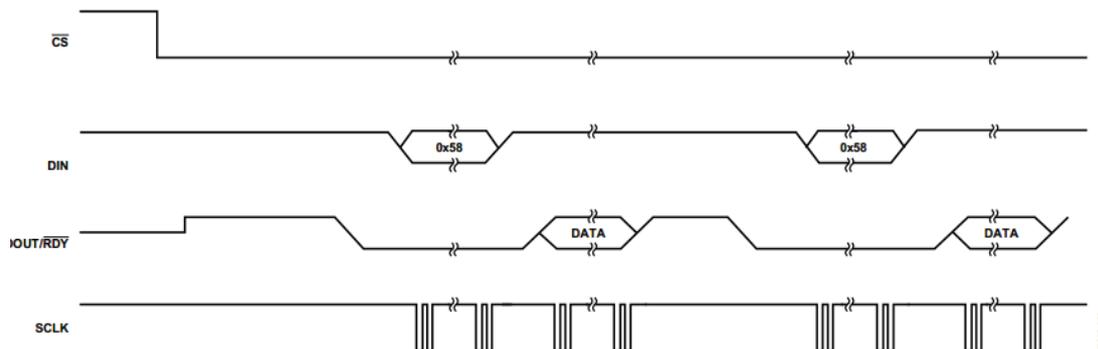


Figure 5.3: Continuous Conversion Mode

Continuous read mode

Rather than writing to the communications register each time a conversion is complete to access the data, this mode can be configured so that the conversions are placed on the RDY line automatically [40]. By writing 0x5c to the communications register, the user needs only apply the appropriate number of SCLK cycles to the ADC, and the conversion word is automatically placed on the RDY line when a conversion is complete. The timing diagram of continuous read is illustrated in figure 5.4:

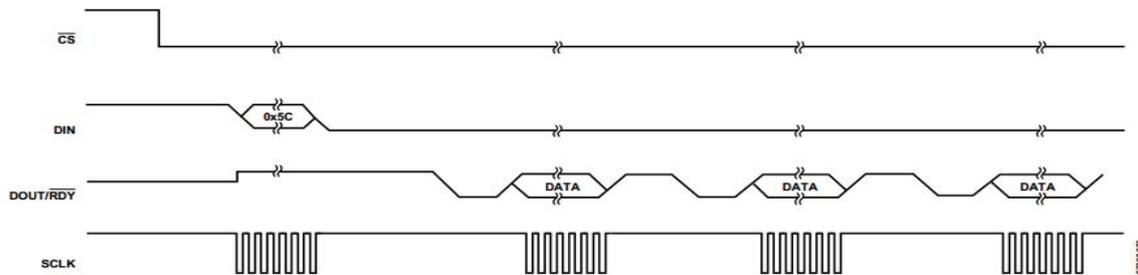


Figure 5.4: Continuous Read

Both of them will be used in this project in different places. Continuous Conversion Mode will be used when robotic arm descends initially, and Continuous Read will be used when the robotic arm has touched the sample being tested.

ADC programming

Initially, some of the ADC registers need to be configured. In the mode register (Table 5.3), the clock of the ADC is chosen as the internal clock (bit 19 – bit 18). The sample speed is configured as 1 kHz, which according to the datasheet, is the most stable sample rate for this ADC. The last three bits (bits 21 – 23) are set to 0, which set the ADC in the continuous conversion mode. In the configuration register (Table 5.4), the bits 15 to 8 are the channel selection bits; these bits are utilized to select which channels are enabled on the AD7192. In this project, the AIN1 and AIN2 are used for receiving the analogue signal from the load cell. Bit 3 (Table 5.5) is the polarity select bit. When this bit is set, unipolar operation is selected. When this bit is cleared, bipolar operation is selected. In this project, the ADC is used as a unipolar

input device. Hence bit 3 is set to 1. Also bits 2 to 0 are programmed to set the gain. These bits are written by the user to select the ADC input range. According to the specifications of the load cell (section 3.2.3), the signal output at capacity is $2 \pm 2 \text{ mV/V}$. The reference voltage of ADC is 5 V, hence the signal output at capacity is:

$$2 \text{ mV} * 5 \text{ V} = 10 \text{ mV} \quad (22)$$

The maximum output signal will be:

$$128 * 10 \text{ mV} = 1.28 \text{ V} \quad (23)$$

Hence, by using the maximum gain (128), the resulting signal is still within the range of the ADC input and will give the maximum resolution. Table 5.4 shows the table used to set the gain of the ADC.

Table 5.3: Programming the channel selection bits for the ADC

Channel Enable Bits in the Configuration Register								Channel Enabled		Status Register Bits CHD[2:0]	Calibration Register Pair
CH7	CH6	CH5	CH4	CH3	CH2	CH1	CH0	Positive Input AIN(+)	Negative Input AIN(-)		
						1	1	AIN1	AIN2	000	0
					1			AIN3	AIN4	001	1
				1				Temperature sensor		010	None
		1	1					AIN2	AIN2	011	0
	1							AIN1	AINCOM	100	0
								AIN2	AINCOM	101	1
								AIN3	AINCOM	110	2
1								AIN4	AINCOM	111	3

Table 5.4: Setting the gain for the ADC

CON2 to CON0	G2 to G0	Gain select bits. These bits are written by the user to select the ADC input range as follows:				
		G2	G1	G0	Gain	ADC Input Range (5V Reference)
		0	0	0	1	$\pm 5 \text{ V}$
		0	0	1	Reserved	
		0	1	0	Reserved	
		0	1	1	8	$\pm 625 \text{ mV}$
		1	0	0	16	$\pm 312.5 \text{ mV}$
		1	0	1	32	$\pm 156.2 \text{ mV}$
		1	1	0	64	$\pm 78.125 \text{ mV}$
		1	1	1	128	$\pm 39.06 \text{ mV}$

Table 5.5: Polarity select bit

CON3	$\overline{\text{U/B}}$	Polarity select bit. When this bit is set, unipolar operation is selected. When this bit is cleared, bipolar operation is selected.

The code for the ADC is presented in the Appendix 4.

5.2.3 Touch Screen

There are two sections in the programming of the touch screen. One is the display driving code, the other is the code for touch function. On the touch screen, the buttons are ‘painted’ for the users to control the whole system. The code for the touch screen can be download freely from the following link:

<https://github.com/gmtii/ili9341-arduino>

The code has to be modified to fit in the Arduino Nano. There are a large amount of functions provided in this code and proved to be useful to start with. Detailed study of the touch screen manuals helped to find more advanced programming options. Figure 5.5 presents what is done on the touch screen for this project.



Figure 5.5: The visual buttons of the touch screen

5.2.4 Control Modes and the Interpreter

After the commands from the PC interface are received by the microcontroller, an interpreter can analyse and process these commands. There are two modes that can be used:

- (1) **Program Control mode**, in which the user writes a *script* using a set of commands. The commands are interpreted by the interpreter and executed one by one in sequence.
- (2) **Interactive Control mode**, in which the regular graphical user interface (GUI) is used to control the equipment and do the measurements.

The commands are combined into a string and transferred to the microcontroller. A series of new commands have been introduced as follows:

1. **ResetPos**: Rest position, the motor will reset to the zero position.
2. **Reset**: Reset all

3. **HardStop**: Stop motor immediately
4. **SoftStop**: Stop motor with a deceleration phase
5. **GoHome**: The GoHome command produces a motion to the HOME position (zero position)
6. **xR+**: Run forward
7. **xR-**: Run backward
8. **xM+**: move n steps forward
9. **xM-**: Move n steps backward
10. **ACC**: set the parameter of acceleration
11. **DEC**: set the parameter of deceleration
12. **Delay**: Delay n ms
13. **mode_1**: activate Interactive Control mode
14. **P_Speed**: pre-test speed
15. **T_Speed**: test speed
16. **Distance**: the distance of pressing
17. **GO_Up**: go up at a constant speed
18. **GO_Down**: go down at a constant speed
19. **Stop**: stop the motor;
20. **GetPosition**: Get the absolute position of the stepper motor

Users can program these commands on a PC and create a *script* to control the action of the texture analyser. A few examples of command scripts are shown below:

```
xR+50;  
Delay,5000;  
xR-50;  
Delay,5000;  
xM+300;  
xM-400;
```

Initially, for the first 5 seconds the motor will go forward, with 50 steps/s speed, and then go backward, when the speed is 50 steps/s for the next 5 seconds. Then the motor

will move 300 steps forward and 400 steps backward.

The second example code is shown below:

```
P_Speed,3000;  
T_Speed,600;  
Distance,10;
```

The robotic arm will descend at a speed of 3000 steps/s, which is called the *pre-test* speed. When the infra-red sensor detects the arm, the speed turns to 600 steps/s, which is the *test* speed. The robotic arm presses the food and travels by 10 mm. It then rises up at the same test speed (i.e. 600 steps/s). When the infra-red sensor cannot detect the robotic arm's presence, the arm will travel back to the original position at the pre-test speed (i.e. 3000 steps/s). The flow of operations is shown in figure 5.6.

The advantage of this new code is that users can use any RS232 serial port software to control the whole machine, and do not need to install any specialised software. This is a novel contribution of this project.

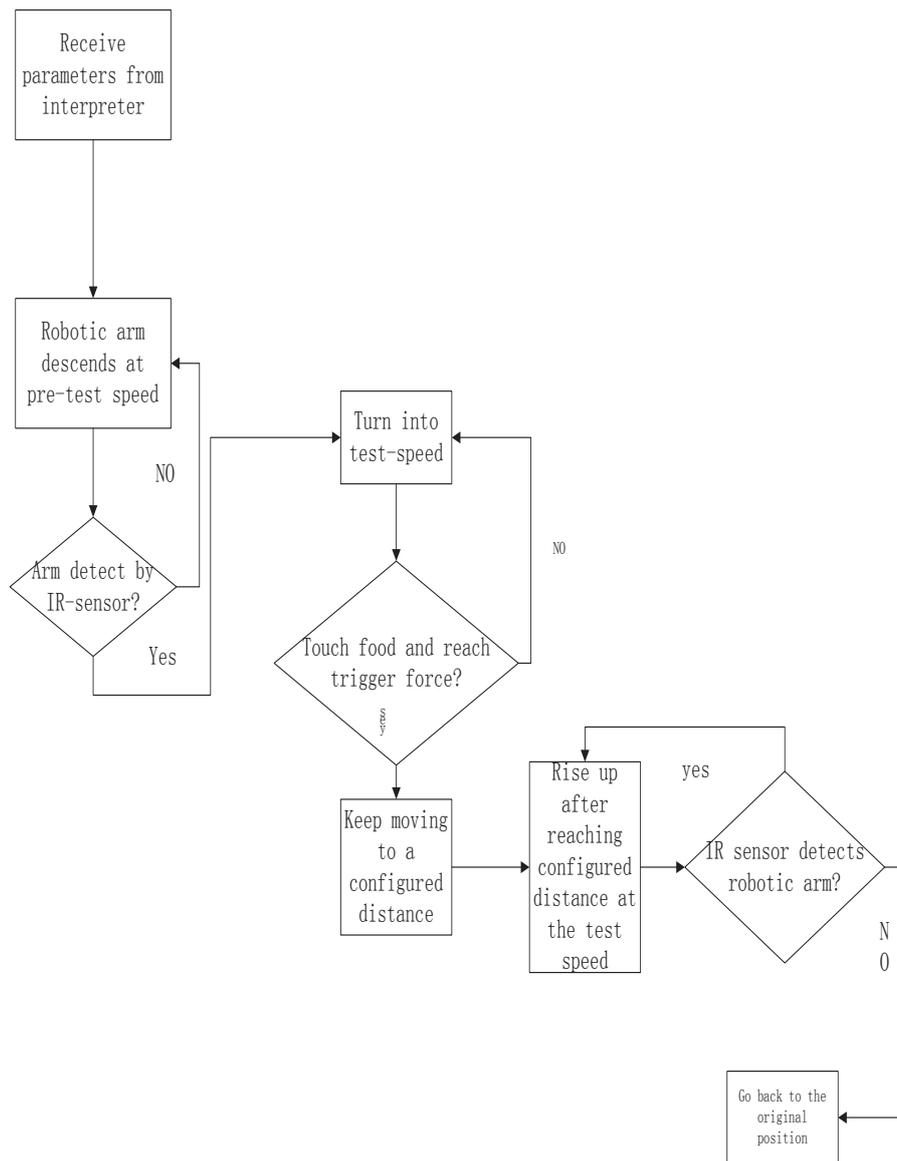


Figure 5.6:Program Control mode structure

The principle of Interpreter

Recursion:

Before explaining how the interpreter works, the methodology of recursion is explained in detail below:

Recursion is the process of repeating items in a self-similar way [67]. For instance, when the surfaces of two mirrors are exactly parallel with each other, the nested images that occur are a form of infinite recursion. The term has a variety of meanings specific to a variety of disciplines ranging from linguistics to logic [68-70].

In C programming language, when a function calls itself over and over again, that function is known as recursive function. The process of function calling itself repeatedly is called recursion. Figure 5.7 shows an example of Fibonacci series using recursion that is written in C.

```
#include<stdio.h>
int factorial(unsigned int i)
{
    if(i<=1)
    {
        return 1;
    }
    return ( i*factorial(i-1) );
}
int main()
{
    inti=15;
    printf("Factorial of %d is %d\n",i, factorial(i));
    return 0;
}
```

Figure 5.7: An example of recursive code in C

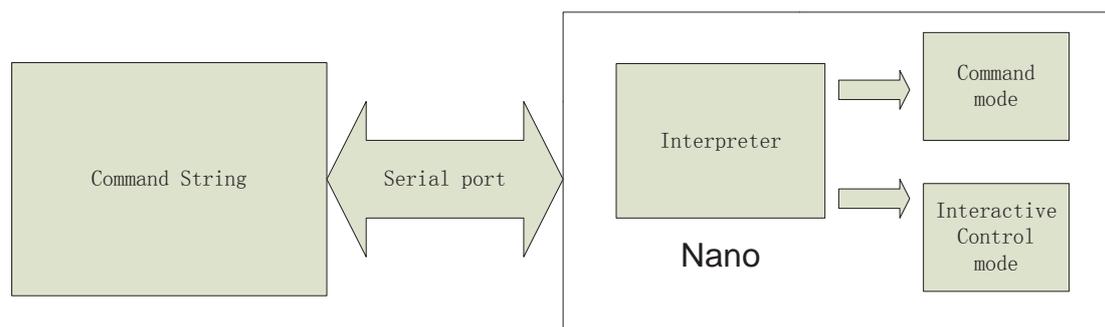


Figure 5.8: The structure of the software design

Figure 5.8 presents the structure of the software design. At the heart of the processing is the interpreter or command parser. After typing the commands on the PC and pressing the <Enter> key, the commands are transferred to the microcontroller. The parser will seek the first semi-colon after receiving the complete command string.

Then the command before the first semicolon will be cut from the whole command and processed by the command interpreter. Then the program will seek the first semi-colon from the rest of the command string and this process will continue recursively till the end of the string.

Figure 5.9 below shows the snippet of code segment which parses the command string and figure 5.10 shows how the commands are concatenated into one string and sent to the microcontroller over the RS232 serial port.

```
else if(Part.startsWith("P_Speed"))
{
    value = part.substring((Part.indexOf(',')+1),(Part.indexOf(';')));
    PT_Speed = value.toInt();value="";
}
else if(Part.startsWith("Distance"))
{
    value = Part.substring((Part.indexOf(',')+1),(Part.indexOf(';')));
    Distance = value.toInt();value="";
}
else if(Part.startsWith("T_Speed"))
{
    value = Part.substring((Part.indexOf(',')+1),(Part.indexOf(';')));
    T_Speed = value.toInt();value="";
}
```

Figure 5.9 : Snippet of code to parse the command string at the microcontroller end

```
Mode_1.WriteLine("mode_1;" + "P_Speed," + Speed[0].ToString() + ";" +
"T_Speed," + Speed[1].ToString() + ";" + "Distance," + textBox5.Text +
";");
```

Figure 5.10: Code to send command string on RS232 port

5.3 Graphical User Interface for Instrument Control

A very easy and intuitive graphical user interface (GUI) has been developed for controlling the instrument using either the Program Control mode or the Interactive Control mode. The default is the Interactive Control Mode. When in the Program Control mode, the command **mode_1** will put the control in the Program mode.

The software is written using C# using Visual Studio 2014. The details of the GUI are in the following sections.

5.3.1 Functions and Features of the Graphical User Interface

Figure 5.11 shows the user interface. The widgets (buttons, text boxes, pull-down lists etc) to the left of the screen are used to directly interact with the texture analyser and control it. The textbox at the right side is for the programming control mode.

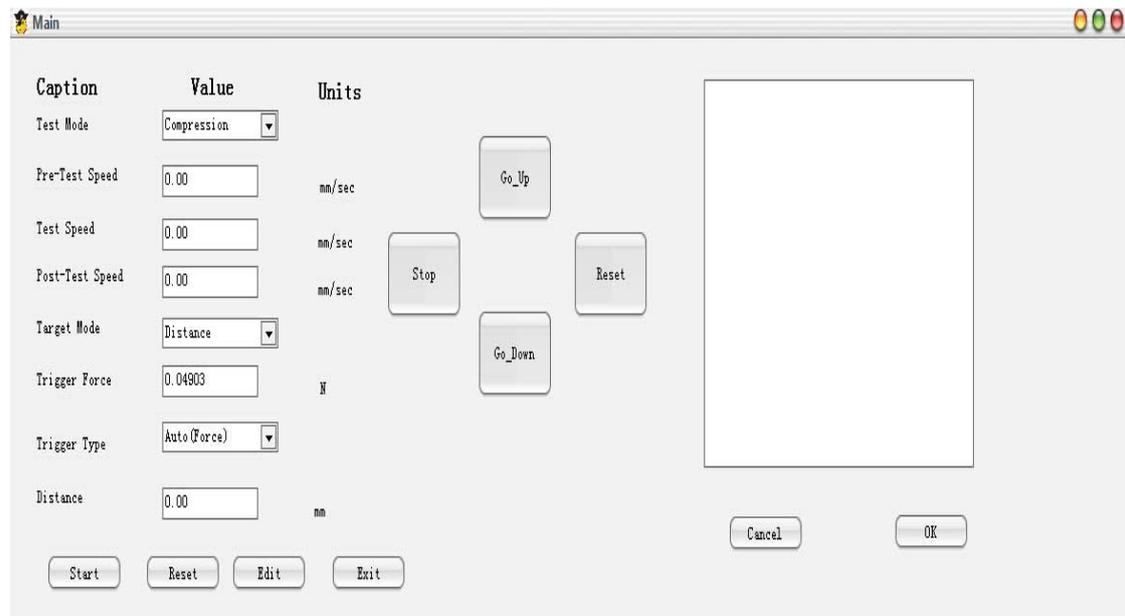


Figure 5.11: The Graphical User Interface (GUI) for the instrument

Interactive Control mode

In the Interactive Control mode the arm can be moved up or down using the buttons. The user can use the widgets to set the various speeds (pre-test speed, test speed, and post-test speed), test distance, trigger force etc., and transfer the settings to the microcontroller when the <Start> button is pressed. The user interface then automatically turns to receive mode. If measurement data from the microcontroller is detected, it will be shown on the screen and a real-time graph will be plotted, as

shown in figure 5.12.

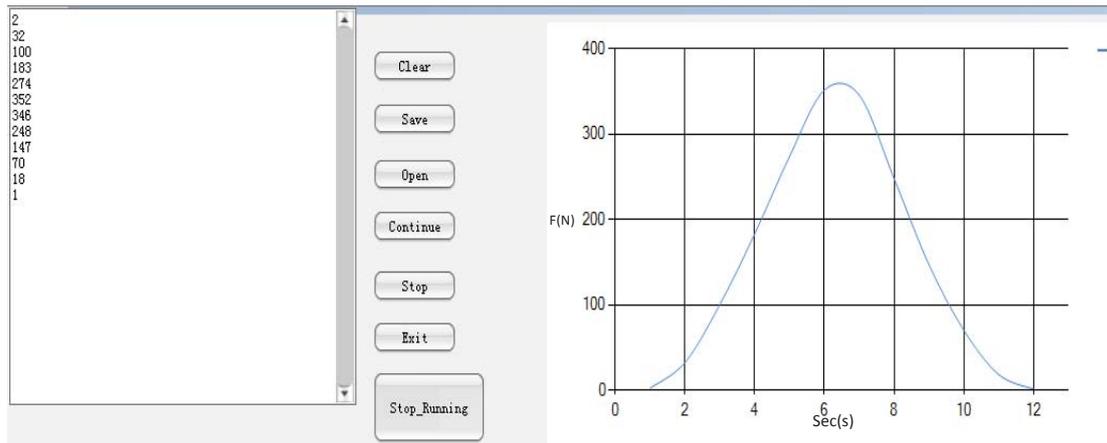


Figure 5.12: Real time measurement data and graph

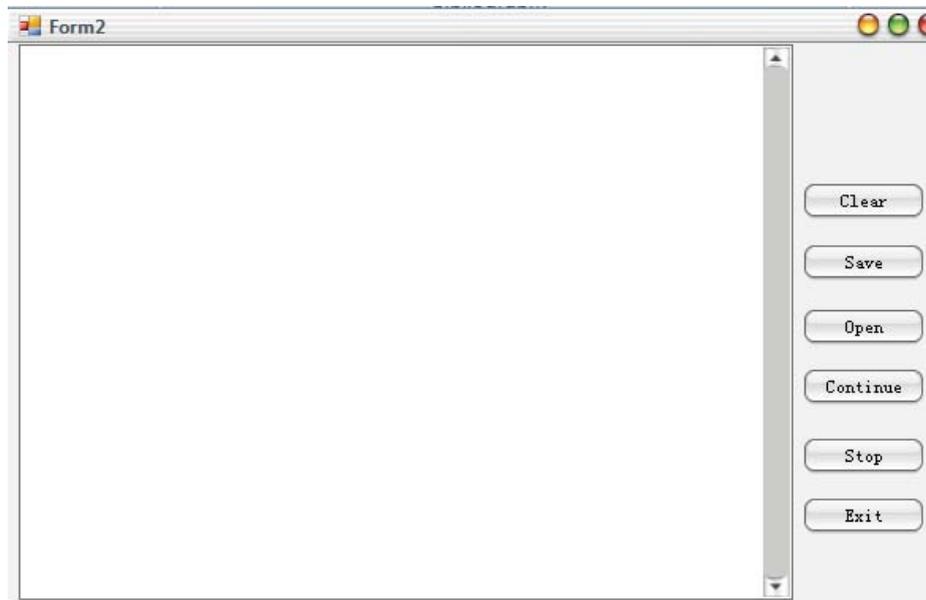


Figure 5.13: The textbox for displaying the data from the load cell

The text box, shown in figure 5.13, displays the data from the load cell. The Clear button clears the data from the text box, whereas the Save button can save the text box data to a file. Data can be saved in two different formats - as a TXT file or a CSV (comma separated variable format used for Excel) file. The Open button is for the user to open the data file (.TXT or .CSV) and show the contents in the text box. Clicking the Stop button will close the serial port and no new data will be transferred to the PC and shown on the screen. Clicking the Continue button resumes the data transfer. **The user must click the Stop button before clicking the Exit button to ensure the Serial port is closed properly.**

Program Control mode

The text box on the right of the screen (see figure 5.8) is used to write a *script* which is essentially a series of commands to control the instrument. This facility helps to automate repetitive measurements and the user can save a lot of time by reusing scripts for a specific measurement.

After the script has been written, the command string will be sent to the microcontroller when the OK button is clicked. Then the microcontroller will analyse the code and execute the commands using the interpreter which has been explained earlier. **There is no function to check the syntax/grammar of the script. The microcontroller simply ignores an incorrect command and goes to the next one.**

5.3.2 Serial Port

There is an inbuilt serial port class in Visual Studio that is used to control the I/O (input and output) on the serial port. Figure 5.14 shows the example code for setting up the serial port for communication at 14400 baud rate and timeout for write operation of 10 ms .

```
try
{
    SerialPort Mode_1 = newSerialPort();
    Mode_1.BaudRate = 14400;
    Mode_1.WriteTimeout = 10000;
    Mode_1.Open();
    if (Mode_1.IsOpen)
    {
        Mode_1.WriteLine("Rest;");
        Mode_1.Close();
    }
}
catch (Exception a)
{
    MessageBox.Show(a.Message);
}
```

Figure 5.14: Example code of serial port initialization

5.5 Summary

In this chapter, the software, including the code for the microcontroller and the code running on the PC, has been presented. Because the code size is very large, code optimization is imperative. Lot of time was spent on optimising the code to ensure that the microcontroller resources are utilised efficiently.

A recursive function on the microcontroller parses the command string received from the PC, interprets the commands, and executes them. The user interface on the PC allows the user to control the instrument either interactively, using the widgets, or by executing a command script.

The measurement data is also received and depicted on the user screen including a real time plot of the data. The measurement data can be stored in a file as text or in the CSV format for later retrieval and use.

The programming of the movement of the robotic arm and capturing measurement data has been an important component of this study. Although the software is working well, in the microcontroller part there will always be room for improvement.

Chapter 6

Experiments and Results

After finishing the design and implementation of the equipment, it is necessary to test it and compare its performance with an existing texture analyser with the aim of evaluating its accuracy. The existing texture analyser used was from the Massey University food lab. The range of force for the equipment is between 0 kg and 20 kg. Tests using a squeeze ball and several fruits have been conducted and these are reported in this chapter in subsequent sections.

6.1 Initial force test using pressure ball

At first a squeeze/bouncy ball has been used for testing because the ball can be compressed easily and it can recover quickly after being pressed. This enables exactly the same tests to be performed on the ball by pressing it at the same point using two different texture analysers. The test conditions of the experiments are presented in table 6.1. The data from all the measurements reported in this chapter are presented in Appendix 3.

Table 6.1: The conditions of the pressure ball test

Test sample	Bouncy ball (figure 6.1)
Test equipment	Newly designed instrument and the standard texture analyser in the food lab of Massey University (Model: TA.XT plus Texture Analyser)
Test method	Compression test
Probe	A professional probe (figure 6.2)
Pressing point	Top of the bouncy ball
Pre-test speed	5 mm/s
Test speed	5 mm/s
Distance	5 mm



Figure 6.1: Squeeze/Bouncy ball used for initial experimentation



Figure 6.2: The compression probe used with the squeeze ball

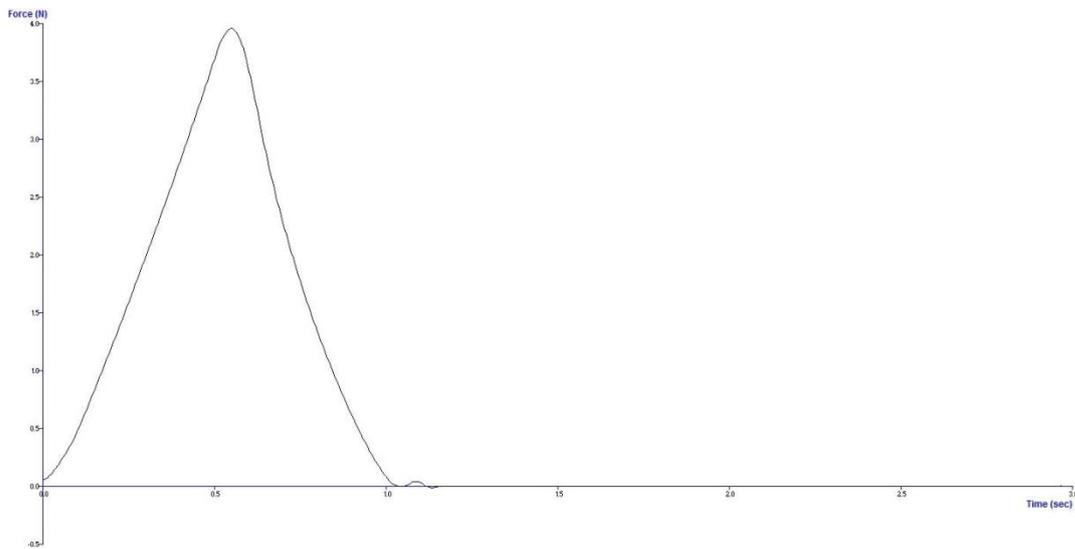


Figure 6.3: The result from tests done using standard texture analyser (force vs. time)

In figure 6.3, the x axis represents time (in Seconds) and the y axis represents force (in Newton). The maximum force is 4 N (0.407 kg). In this test, the important observable points are the maximum force and the trend of the curve. Figure 6.4 shows the results achieved by repeating the same test using the developed equipment. The measured data and the graph plotted in real time are seen in this picture.

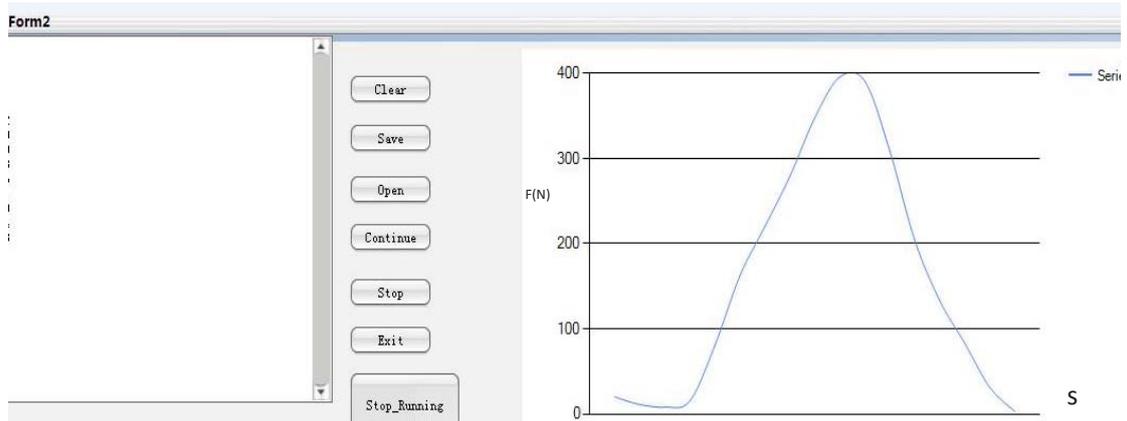


Figure 6.4: The result from tests done using the newly developed texture analyser

The curve in figure 6.4 suggests that the maximum force is 0.399 kg (3.913 N) which is almost the same as measured by the standard texture analyser. However, the noise due to switching cannot be eliminated completely. In order to minimise the effect of noise the sample rate is lowered to 1 kHz, the speed recommended for AD7192.

Table 6.2 shows the measurement data (i.e. force in Newton) for the tests done using the standard and the new instrument respectively. From the data, the minimum, maximum, and mean errors have been calculated which are very low. Additionally, the standard deviation of the error is also very low (~0.035 N or 0.00357 kg), meaning the results from the two instruments are very close to each other (for the range of 0 to 0.4 kg)

Table 6.2: The maximum, minimum, mean error and standard deviation for measurements done on squeeze ball with the standard and the new instrument

Force (N)		Error (N)
Standard Instrument	New Instrument	
0.388597819	0.37	0.018598
0.590994751	0.57	0.020995
0.770760123	0.76	0.01076
0.952563408	0.95	0.002563
1.17834271	1.17	0.008343
1.408841388	1.37	0.038841
1.6428796	1.66	-0.01712
1.802265843	1.78	0.022266
2.044241189	2.04	0.004241
2.289970585	2.23	0.059971
2.579139705	2.54	0.03914
2.747535668	2.72	0.027536

3.006457869	3.01	-0.00354
3.269670413	3.25	0.01967
3.538245886	3.43	0.108246
3.808108462	3.82	-0.01189
3.974251995	4.1	-0.12575
3.953872866	3.99	-0.03613
3.703745868	3.69	0.013746
3.282326925	3.24	0.042327
2.851791003	2.85	0.001791
2.476171472	2.44	0.036171
2.144527957	2.11	0.034528
1.847314445	1.84	0.007314
1.57359056	1.57	0.003591
1.321961942	1.32	0.001962
1.087601955	1.076	0.011602
0.871261408	0.85	0.021261
0.666290271	0.66	0.00629
0.480625676	0.46	0.020626
0.311049869	0.31	0.00105
0.16035157	0.14	0.020352
Maximum Error (N)	0.108245886	
Minimum Error (N)	-0.125748005	
Mean Error (N)	0.012792225	
Standard Deviation (N)	0.03506309	

6.2 Repeat tests and comparison

The tests, as explained in section 6.1, were repeated to evaluate the repeatability of the new instrument. The same experiment was performed twice on the standard analyser and the new equipment. The test results have been plotted in the graph shown in figure 6.5. As the plot shows, the curves coincide very closely.

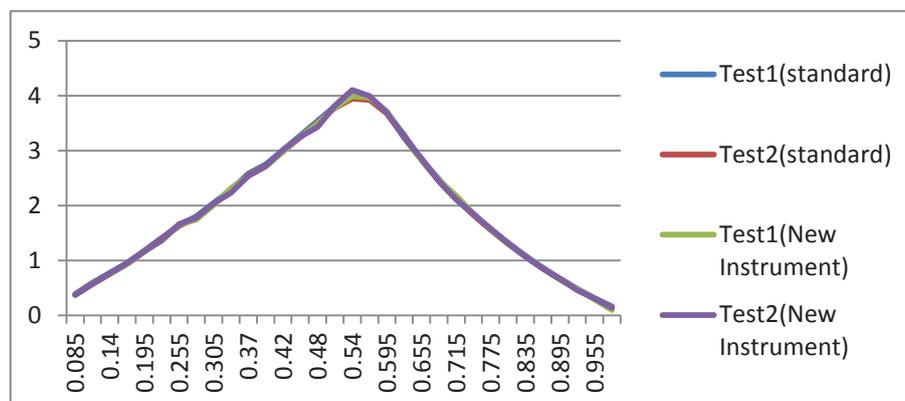


Figure 6.5: Coinciding the test curves

6.3 Experimentations with fruits

There are various types of foods that can be used as samples for testing. After testing the bouncy ball, tests were done on actual fruits such as avocado, kiwi fruit, and persimmon. The reason for choosing these fruits is because they can cover the full range of force of the load cell (0 kg ~ 20 kg).

6.3.1 Avocado

The first fruit sample is avocado and the conditions for the test are summarised in table 6.3. Figures 6.6 and 6.7 show the avocado being tested using the standard texture analyser and the new instrument respectively.

Table 6.3: The conditions of the avocado test

Test sample	Avocado
Test equipment	Newly designed instrument and the standard texture analyser in the food lab of Massey University (Model: TA.XT plus Texture Analyser)
Test method	Penetration test
Probe	A professional probe (diameter of tip is 5 mm)
Pressing point	Top of the avocado fruit
Pre-test speed	5 mm/s
Test speed	5 mm/s
Distance	5 mm



Figure 6.6: Testing avocado using standard texture analyser



Figure 6.7: Testing avocado using the new texture analyser

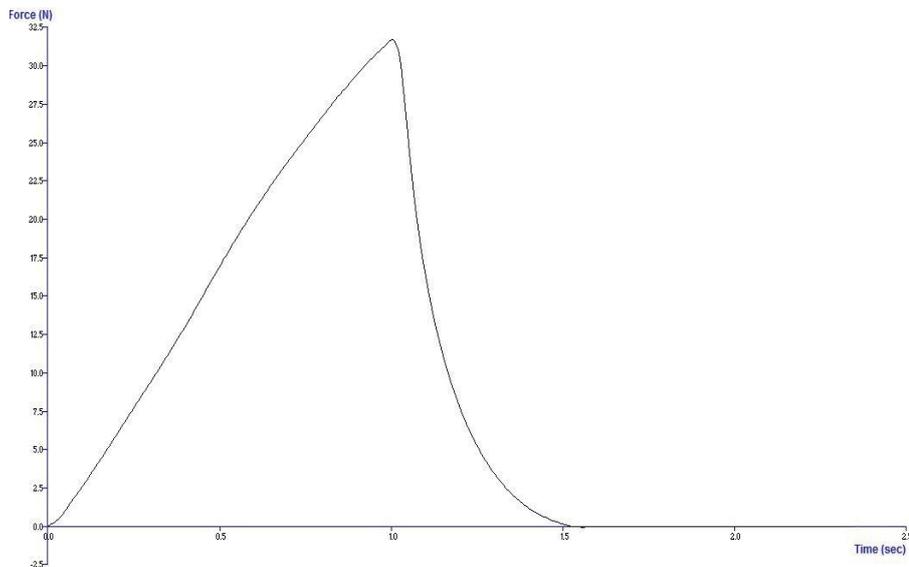


Figure 6.8: Results of force measurement of avocado using the standard texture analyser

The results of force measurement of avocado using the standard texture analyser is shown in figure 6.8. When the robotic arm presses the avocado, the curve seems to rise smoothly and slower than that when the robotic arm releases from the fruit. The maximum force is approximately 32.43 N (3.31 kg).

Figure 6.9 shows the results that were obtained using the new instrument. The results are very similar to those obtained using the standard texture analyser. The maximum force is approximately 32.32 N (3.23 kg). It must be noted that because the test is a penetration/puncture test, the two tests (using the standard texture analyser and the new instrument) cannot be done on the same point of the fruit. This explains the slight variation in the maximum force measured by the two instruments.

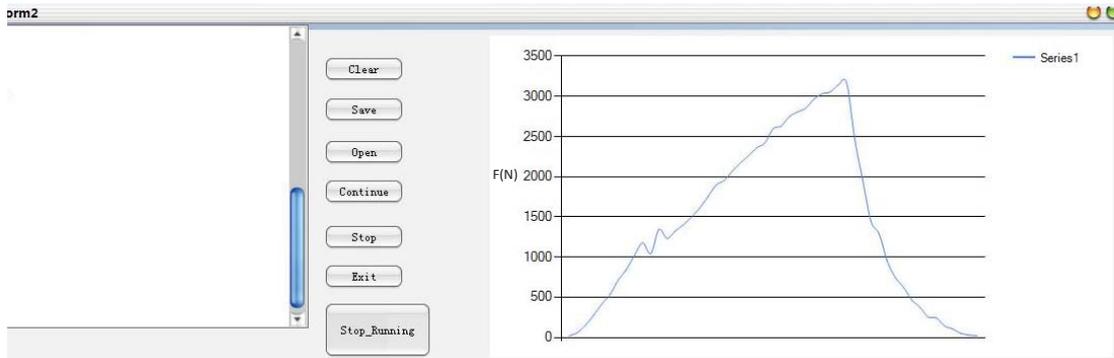


Figure 6.9: Results of force measurement of avocado using the new texture analyser

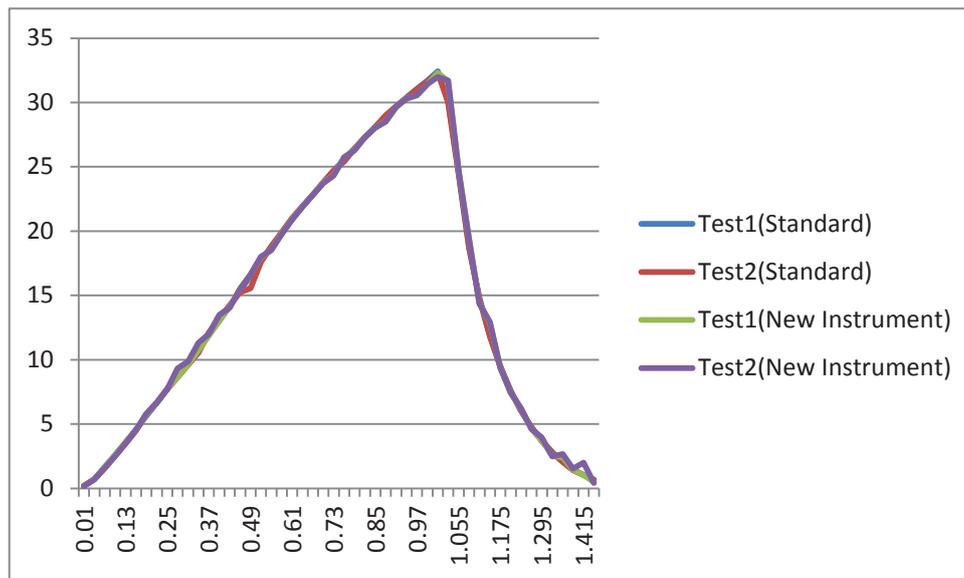


Figure 6.10: Combining the results of the texture analyser and the new instrument for avocado

Two sets of experiments were repeated using the two instruments and the results are plotted in figure 6.10.

Table 6.4 shows the measurement data (i.e. force in Newton) for the tests done on avocado using the standard and the new instrument respectively. From the data, the minimum, maximum, and mean errors have been calculated which are very low. Additionally, the standard deviation of the error is also very low (~0.33 N or 0.0337 kg), meaning the results from the two instruments are very close to each other (for the range of 0 kg to 5 kg)

Table 6.4: The maximum, minimum, mean error and standard deviation for measurements done on avocado with the standard and the new instrument

Force (N)		Error (N)
Standard Instrument	New Instrument	
0.199282505	0.2	-0.000717495
0.727860702	0.72	0.007860702
1.674186182	1.63	0.044186182
2.59600098	2.6	-0.00399902
3.594544871	3.62	-0.025455129
4.589891717	4.52	0.069891717
5.632128564	5.76	-0.127871436
6.678628138	6.71	-0.031371862
7.736850213	7.75	-0.013149787
8.758839104	8.66	0.098839104
9.77763095	9.63	0.14763095
10.83585302	10.74	0.095853025
11.93457101	11.87	0.06457101
13.0151724	13.04	-0.024827597
14.17463425	14.11	0.064634253
15.34262156	15.54	-0.197378442
16.52126568	16.64	-0.118734319
17.67859617	17.94	-0.261403832
18.7922337	18.54	0.252233698
19.87709782	19.83	0.047097819
20.91080921	20.92	-0.009190789
21.89656492	21.92	-0.02343508
22.8546129	22.85	0.004612901
23.77962474	23.76	0.019624744
24.68545431	24.34	0.345454315
25.56464184	25.76	-0.195358161
26.43210686	26.32	0.112106863
27.28465234	27.34	-0.055347659
28.13080373	28.06	0.070803727
28.89489761	28.54	0.354897612
29.6824365	29.65	0.032436497
30.40603447	30.32	0.086034472
31.05929744	30.55	0.509297444
31.71682314	31.43	0.286823144
32.43643785	32.32	0.11643785
30.09378969	31.67	-1.57621031
24.4222309	24.64	-0.217769102
18.73255551	19.43	-0.697444485
14.81830609	14.41	0.408306089

11.8354626	12.85	-1.014537402
9.481371397	9.43	0.051371397
7.6142968	7.42	0.1942968
6.059466985	6.21	-0.150533015
4.761466494	4.65	0.111466494
3.707507147	3.74	-0.032492853
2.83791076	2.53	0.30791076
2.113247104	2.43	-0.316752896
1.516465269	1.43	0.086465269
1.037974119	1.04	-0.002025881
0.690561837	0.5	0.190561837
Maximum Error (N)	0.509297444	
Minimum Error (N)	-1.57621031	
Mean Error (N)	0.190242465	
Standard Deviation (N)	0.32996538	

6.3.2 Kiwifruit

To ensure that the measurement of force in the range 5 kg to 10 kg is reliable, kiwi fruit was used as the next sample. The conditions for the test are summarised in table 6.5. Figures 6.11 and 6.12 show the kiwifruit being tested using the standard texture analyser and the new instrument respectively.

Table 6.5: The conditions of testing kiwifruit

Test sample	Kiwi fruit
Test equipment	Newly designed instrument and the standard texture analyser in the food lab of Massey University (Model: TA.XT plus Texture Analyser)
Test method	Penetration test
Probe	A professional probe (the diameter of tip is 5 mm)
Pressing point	Mid-point of kiwi fruit (figure 6.10)
Pre-test speed	5 mm/s
Test speed	5 mm/s
Distance	5 mm

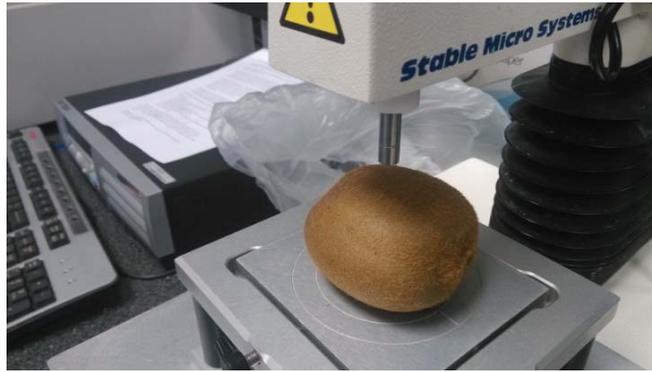


Figure 6.11: Testing kiwifruit using standard texture analyser

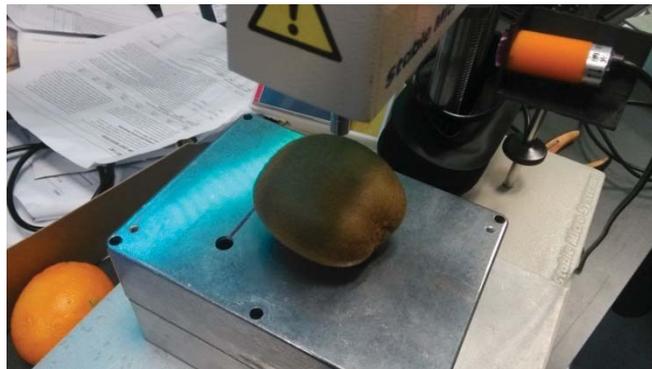


Figure 6.12: Testing kiwifruit using the new analyser

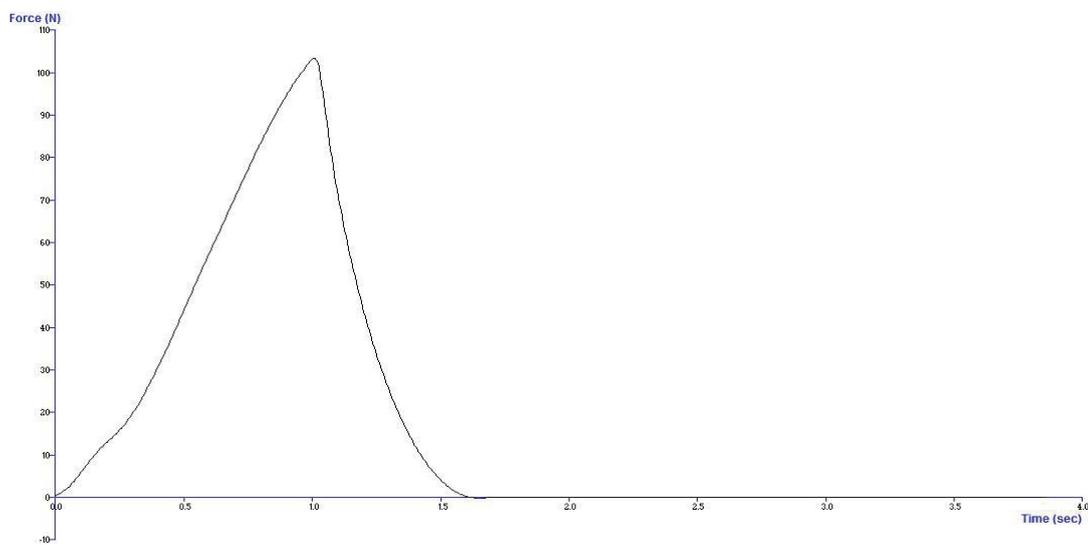


Figure 6.13: Results of force measurement of kiwifruit using the standard texture analyser

The results of force measurement of kiwifruit using the new instrument is shown in figure 6.13. The curve is shaper than that of avocado, and the maximum force is 103.45 N (10.56 kg). Figure 6.14 shows the results that were obtained using the new instrument. The results are very similar to those obtained using the standard texture analyser (figure 6.15). The maximum force is approximately 102.43 N (10.45 kg).

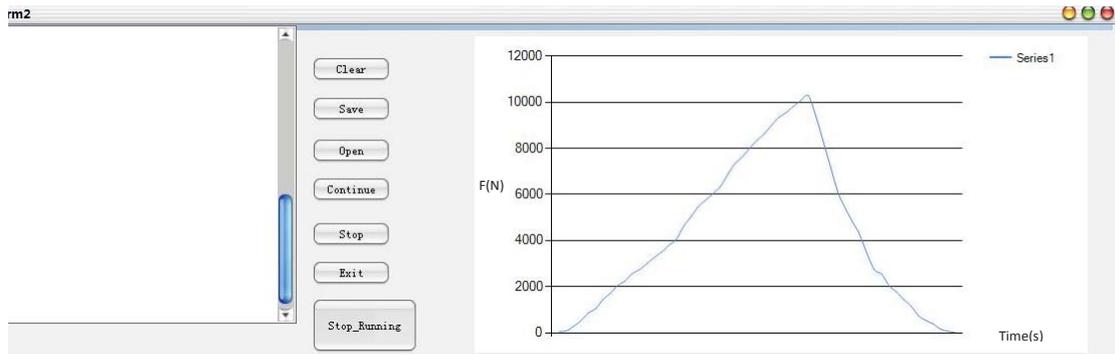


Figure 6.14: Results of force measurement of kiwifruit using the new texture analyser

Figure 6.15 shows the two sets of data combined into one plot.

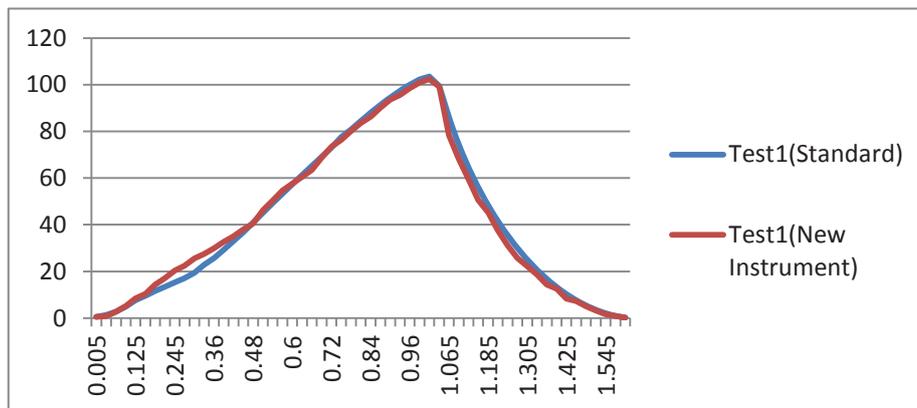


Figure 6.15: Combining the results of the texture analyser and the new instrument for kiwifruit

Table 6.6 shows the measurement data (i.e. force in Newton) for the tests done on kiwifruit using the standard and the new instrument respectively. From the data, the minimum, maximum, and mean errors have been calculated which are very low. The standard deviation of the error is more than that for avocado but still very low (~2.78 N or 0.283 kg) for the range 5 to 10 kg, which is larger than avocado.

Table 6.6: The maximum, minimum, mean error and standard deviation for measurements done on kiwifruit with the standard and the new instrument

Force (N)		Error (N)
Standard Instrument	New Instrument	
0.574403	0.53	0.044403
1.365138	0.76	0.605138
2.798481	2.78	0.018481
4.961815	5.23	-0.26819
7.693157	8.54	-0.84684
9.622041	10.43	-0.80796
11.67454	14.34	-2.66546
13.38603	17.12	-3.73397
15.38205	20.43	-5.04795

17.03386	22.42	-5.38614
19.45935	25.64	-6.18065
22.84289	27.43	-4.58711
25.68933	30.01	-4.32067
29.24124	32.65	-3.40876
32.94875	35.04	-2.09125
36.82464	37.97	-1.14536
40.92218	40.54	0.382183
45.06662	46.23	-1.16338
49.17589	50.34	-1.16411
53.2809	54.75	-1.4691
57.31024	57.54	-0.22976
61.2085	60.43	0.778503
65.12488	63.45	1.674883
69.10201	68.65	0.452008
73.06208	73.43	-0.36792
77.60082	76.31	1.290821
80.79041	80.14	0.650407
84.4766	83.54	0.9366
87.95605	86.34	1.616051
91.35451	90.13	1.224511
94.52172	93.54	0.981717
97.3916	95.65	1.741598
99.93858	98.41	1.528578
102.3587	100.9	1.458741
103.4575	102.43	1.027459
99.47181	99.21	0.261809
86.0975	78.3	7.797502
74.3441	68.32	6.024097
64.53236	59.43	5.102364
55.96641	50.65	5.316414
48.39261	45.32	3.072613
41.58397	37.54	4.043971
35.48614	30.98	4.50614
30.02559	25.76	4.265586
25.12132	22.32	2.801318
20.71366	18.54	2.173658
16.7781	14.32	2.458095
13.28692	12.54	0.746921
10.23055	8.33	1.900546
7.653727	7.2	0.453727
5.460554	5.12	0.340554
3.566837	3.24	0.326837

2.079145	1.63	0.449145
0.96977	0.94	0.02977
0.23445	0.2	0.03445
Maximum Error (N)		7.797502
Minimum Error (N)		-6.18065
Mean Error (N)		0.429691
Standard Deviation (N)		2.786301

6.3.2 Persimmon

The last step is to ensure the accuracy of measurement in the range 10 kg to 20 kg. This requirement can be fulfilled by testing a persimmon. The conditions for the test are summarised in table 6.7. Figure 6.16 shows the persimmon fruit being tested using the standard texture analyser.

Table 6.7: The conditions of testing persimmon

Test sample	Persimmon
Test equipment	Newly designed instrument and the standard texture analyser in the food lab of Massey University (Model: TA.XT plus Texture Analyser)
Test method	Penetration test
Probe	A professional probe (The diameter of the tip is 5 mm)
Pressing point	Top of the persimmon (figure 6.14)
Pre-test speed	5 mm/s
Test speed	5 mm/s
Distance	5 mm

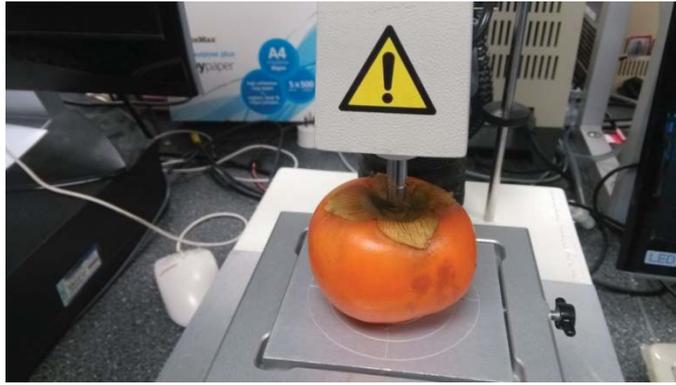


Figure 6.16: Persimmon being tested using a standard texture analyser

The results obtained from testing persimmon using a standard texture analyser is shown in figure 6.17. As can be seen, the maximum force is 205.23 N (20.927 kg).

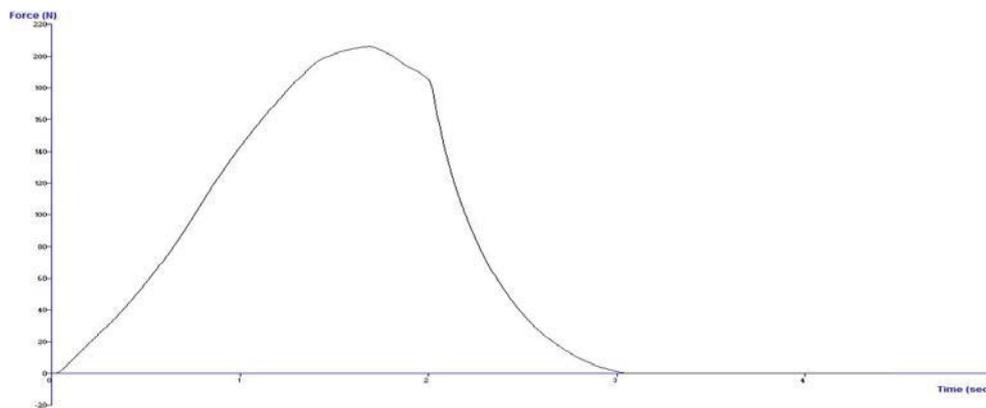


Figure 6.17: Results of force measurement of persimmon using the standard texture analyser

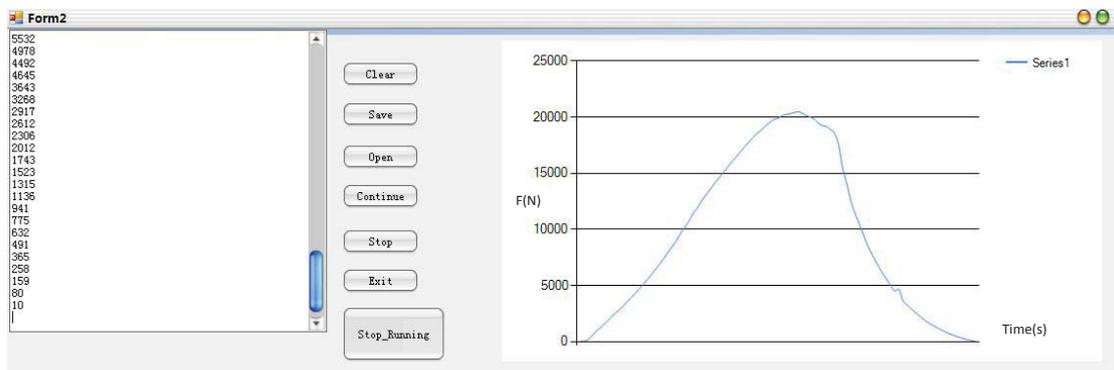


Figure 6.18: Results of force measurement of persimmon using the new texture analyser

Figure 6.18 shows the results obtained from testing persimmon using the new instrument. The curve is very similar to the standard one. The maximum force is 204.98 N (20.902 kg).

Another set of measurement was done using the standard texture analyser. The results of the various tests have been shown in a combined plot in figure 6.19.

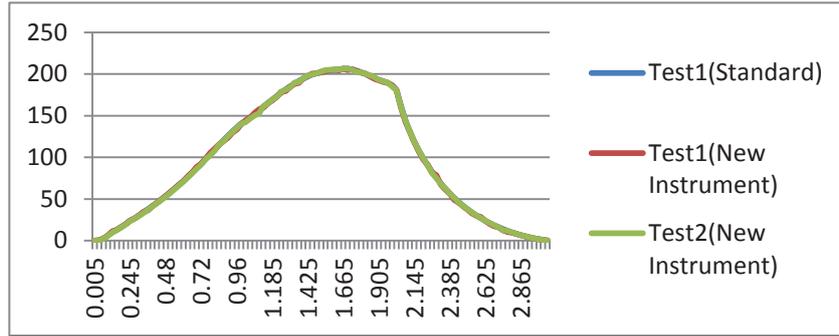


Figure 6.19: Combining the results of the texture analyser and the new instrument for persimmon

Table 6.8 shows the measurement data (i.e. force in Newton) for the tests done on persimmon using the standard and the new instrument respectively. From the data, the minimum, maximum, and mean errors have been calculated which are very low. The standard deviation of the error is very low (~0.934 N or 0.095 kg) for the range 10 to 20 kg.

Table 6.8: The maximum, minimum, mean error and standard deviation for measurements done on persimmon with the standard and the new instrument

Force (N)		Error (N)
Standard Instrument	New Instrument	
0.095911	0.0084	0.087511
0.474228	0.4542	0.020028
2.816597	2.92	-0.1034
6.240633	6.32	-0.07937
10.35736	11.43	-1.07264
13.20273	13.23	-0.02727
16.61611	16.71	-0.09389
20.01883	20.13	-0.11117
23.93308	24.43	-0.49692
26.82641	26.43	0.396409
30.34422	30.32	0.024225
34.54195	34.564	-0.02205
37.64308	36.431	1.21208
41.45396	41.431	0.022958
45.40231	45.413	-0.01069
49.48067	49.531	-0.05033
53.69438	53.631	0.06338
58.0381	58.341	-0.3029
62.46494	62.433	0.031941
67.08467	67.0418	0.042872
71.84934	71.941	-0.09166

76.77492	77.431	-0.65608
81.80494	82.413	-0.60806
87.01932	88.531	-1.51168
92.32215	92.413	-0.09085
98.69386	98.5455	0.148362
103.3594	105.413	-2.05358
109.0352	110.4352	-1.39996
114.7132	115.324	-0.61081
120.3496	119.432	0.917582
125.792	123.54	2.25202
131.0064	129.455	1.551401
135.9618	133.541	2.420821
140.7638	139.6424	1.121384
143.0923	144.3445	-1.2522
147.6214	147.434	0.187447
152.1186	153.341	-1.22238
156.5092	157.435	-0.92577
160.8498	159.5434	1.306355
165.0699	164.343	0.726855
169.2633	168.432	0.831314
173.4173	172.435	0.982341
177.5192	178.543	-1.02385
181.5282	179.5456	1.982646
184.9523	184.434	0.518282
188.0651	188.054	0.011138
191.5478	189.4345	2.113287
194.8386	194.654	0.184612
197.2886	197.54	-0.25139
199.2601	200.43	-1.16987
200.7979	200.64	0.157905
202.1641	201.98	0.184109
203.2245	203.54	-0.31554
204.126	204.54	-0.41397
205.0212	204.99	0.031202
205.6713	204.3	1.371268
206.1391	206.45	-0.3109
206.3714	204.64	1.731421
205.5839	205.765	-0.18112
203.7637	203.53	0.233698
201.9606	201.546	0.414564
200.0732	200.564	-0.49076
197.5071	197.435	0.07208
195.0869	194.43	0.656916

193.011	192.45	0.560968
191.2824	190.343	0.939432
189.2683	189.354	-0.08571
186.8002	186.345	0.455174
180.8089	180.343	0.465911
161.3858	159.433	1.952793
143.9598	142.43	1.529764
130.4309	130.53	-0.09907
118.8331	118.34	0.493117
108.4576	107.43	1.027639
99.04234	97.54	1.50234
90.44975	91.4345	-0.98475
82.53812	81.545	0.993125
75.27444	78.543	-3.26856
68.59687	67.34	1.256875
62.42125	61.34	1.081249
56.70813	56.5675	0.140628
51.42767	49.345	2.082675
46.54259	45.686	0.856589
42.00705	41.454	0.553047
37.83597	37.43	0.405968
33.9441	32.567	1.377098
30.33996	30.13	0.209962
27.02676	28.455	-1.42824
23.95759	23.77	0.187594
21.13354	20.15	0.983537
18.53754	17.54	0.997536
16.10991	16.3456	-0.23569
13.90821	12.545	1.363214
11.85571	10.53	1.325711
9.982242	9.56	0.422242
8.297399	8.12	0.177399
6.721255	6.943	-0.22174
5.323081	5.21	0.113081
4.060248	3.97	0.090248
2.923165	2.73	0.193165
1.909702	1.834	0.075702
1.062485	0.934	0.128485
0.357003	0.345	0.012003
Maximum Error(N)		2.420821
Minimum Error(N)		-3.26856
Mean Error(N)		0.239707
Standard Deviation(N)		0.934364

The data and plots of the rest of the tests done on gala apple and orange are presented in Appendix 3.

6.2 Summary

In this chapter, the comparison of experimental results obtained using a standard texture analyser and the newly designed instrument has been presented. The avocado, kiwifruit, and persimmon were used as examples to test the performance of the new equipment. Results show that the machine designed for this project can be as accurate as the standard one. The complete range of force of the load cell, from 5 kg to 20 kg, has been tested. However, there is still some room for improvement. For example, the effect of noise needs to be addressed. On a few occasions, noise has resulted in inaccurate readings. Moreover the nature of the noise has been very unpredictable and has necessitated restarting the machine. However, as future work, software code for noise reduction can be added to the existing project.

Chapter 7

Summary and Future Possibilities

The objective of the research and development project was to develop a texture analyser to be used in the food texture measurement which uses several specific probes and a load cell to determine the texture of food. This was accomplished by designing the machinery part consisting of ball screw shaft and stepper motor. In the electronic part, it includes a 24-bit sigma-delta analogue to digital converter, a powerful stepper motor driver, L6472, and an ATmega328 microcontroller. The components were reviewed thoroughly before purchasing (which took a considerable amount of time) to ensure that the system used high quality components and would last numerous seasons in the demanding environment of a food lab.

The novel contributions of the project are:

1. Implement a new programmable system that a user can use to debug and control the whole system. The programming method uses a new command language written in the form of a script. The language is generic and can be used in any other application where stepper motor control is required.
2. Using advanced technology, both hardware schematic design and PCB design were done. The new PCB board is much smaller than the original one and combines the motor driver, analogue-to-digital converter, power supply and the embedded microcontroller into one.
3. A touch screen based user interface has been developed. The touch screen has visual buttons to control the basic operations of the instrument.
4. The real time graph of the measurement data can be displayed on the computer screen while the testing is in progress.

The design of the whole equipment has gone through a few iterations and appropriate changes done in each round.

Initially the selection of ball screw, shaft, stepper motor, and load cell were considered. Then, according to the features of the selected motor and the load cell, the

electronic parts were decided.

The PCB board has gone through a few design phases to fit the base of the texture analyser. The touch screen is used for the visual button. The infra-red sensor is to detect the position of the robotic arm, so that the robotic arm can be slowed down from pre-test speed to test speed before compressing/penetrating the test sample, which could otherwise cause damage to the food. A new command language was developed so that the user can manage the machine by just using simple UART software. A simple intuitive graphical user interface has been developed to show the measurement data and real time graphs.

After implementing and integrating the hardware and software components, some sample fruits have been used to test the performance of the equipment. As mentioned in chapter 6, the results are very accurate and reliable. However more experiments should be done to ensure this equipment is stable and useful over a long period of time with repetitive experiments.

Future work will involve calibration of load cell data, using new algorithms like Kalman filter that can reduce the noise produced by the motor, and make the data more accurate and stable. The touch screen will show more information that includes not only visual buttons but also the real time graph combined with the data transferred from the load cell.

Nowadays, in the era of modern and powerful microcontrollers, STM32, the microcontroller based on ARM architecture (Cortex-M3), is a very popular industrial controller. In future research, it is recommended that this kind of microcontroller be used in such projects to accomplish more complicated tasks. Every time the microcontroller (Nano) needs to wait for the data from the ADC and then transfer it to the touch screen and PC terminal, which means that the CPU would be stuck on the point of collecting data from ADC rather than doing anything else. Utilizing the technology called DMA (Direct memory access) the data from ADC can be transferred directly to the USART without the intervention of the microcontroller. Once the processor has set up the transfer it can do something else while the transfer

is in progress or wait to be notified when the transfer has finished, which means that more of the resources of the microcontroller can be used for other aspects such as filtering, touch screen control, and motor control.

The comparison of the machine developed for this project is done with the standard texture analyser and presented below in table 7.1.

Table 7.1: Comparison between two texture analysers

Machine developed for the project	The original texture analyser
Open source (software)	Proprietary software
Programmable pre-test speed, faster than test speed	At least equal or less than the test speed
Cheap (less than 1000 dollars)	>10,000 NZD
Programmable	Non-programmable
Good for small company for quick testing	For University, Research Institute, or large industry
Quick response time (less than 100 ms)	Very slow (4~5 s)
Does not rely on unique software	Must install specialized software
Real time graph generation	Drawing of graph takes place after the experiment has been done
Touch screen visual buttons	Real (hardware) button

In the software area, for multi-tasking of data collection, USART, stepper motor driver and touch screen displaying, a real time operating system is required to coordinate the relationships among different tasks. The UCOSII RTOS (real-time operating system) might be a possibility. This will allow multi-tasking and timely execution of high-priority tasks such as data capture on the serial port.

References

- [1] M. Bourne, *Food texture and viscosity: concept and measurement*: Academic press, 2002.
- [2] S. A. Surmacka, "The whys and whats of objective texture measurements," *Canadian Institute of Food Technology Journal*, vol. 2, pp. 150-156, 1969.
- [3] R. D. Brown, "Food Texture Analysis," *American Laboratory*, vol. 01, May 01 2010.
- [4] A. J. Rosenthal, "Food texture: measurement and perception," 1999.
- [5] M. C. Bourne, "Basic principles of food texture measurement," in *Dough rheology and baked product texture*, ed: Springer, 1990, pp. 331-341.
- [6] H. Wium, K. Qvist, and M. Gross, "UNIAXIAL COMPRESSION OF UF - FETA CHEESE RELATED TO SENSORY TEXTURE ANALYSIS," *Journal of Texture Studies*, vol. 28, pp. 455-476, 1997.
- [7] T. Chang and C.-C. Kuo, "Texture analysis and classification with tree-structured wavelet transform," *Image Processing, IEEE Transactions on*, vol. 2, pp. 429-441, 1993.
- [8] L. Rolle, R. Siret, S. R. Segade, C. Maury, V. Gerbi, and F. Jourjon, "Instrumental texture analysis parameters as markers of table-grape and winegrape quality: A review," *American Journal of Enology and Viticulture*, p. ajev. 2011.11059, 2011.
- [9] M. Tuceryan and A. K. Jain, "Texture analysis," *The handbook of pattern recognition and computer vision*, vol. 2, pp. 207-248, 1998.
- [10] TAP. (2015). *Measure Excludability- stable Mirco systems*. Available: www.stablemicrosystems.com/MeasureExtrudability.htm
- [11] E. Katz and T. Labuza, "Effect of water activity on the sensory crispness and mechanical deformation of snack food products," *Journal of Food Science*, vol. 46, pp. 403-409, 1981.
- [12] F. T. a. V. C. a. M. (n.d.). Available: https://books.google.com/books/about/Food_Texture_and_Viscosity.html?id=YMjvdbQu...
- [13] H. H. Friedman, J. E. WHITNEY, and A. S. SZCZESNIAK, "The texturometer—a new instrument for objective texture measurement," *Journal of Food Science*, vol. 28, pp. 390-396, 1963.
- [14] H. Singh, A. Rockall, C. Martin, O. Chung, and G. Lookhart, "THE ANALYSIS OF STRESS RELAXATION DATA OF SOME VISCOELASTIC FOODS USING A TEXTURE ANALYZER*," *Journal of texture studies*, vol. 37, pp. 383-392, 2006.
- [15] *Stable Micro Systems | TA.XTplus Texture Analyser. (n.d.).* . Available: <http://www.stablemicrosystems.com/TAXTplus.htm>
- [16] T. technologies. (1998-2014). *TA.XTPlus Texture Analyzer*. Available: <http://www.texturetechnologies.com/>
- [17] *Detailed list of features of the TA.XTPlus Texture Analyzer ... (n.d.).* Available: <http://texturetechnologies.com/texture-analyzers/TA-XTPlus-texture-analyzer.php>
- [18] T. Technologies, "TA.HDPlus Texture Analyzer," ed, 1998-2014.
- [19] D. Henstenes, *New Foundations for Classical Mechanics.*: Dordrecht: Kluwer Academic, 1990.
- [20] "Rotation."
- [21] K. G. Budinski and M. K. Budinski, "Engineering materials" vol. 25, ed, 2009.
- [22] *Ball screw - Wikipedia, the free encyclopedia*. Available: http://en.wikipedia.org/wiki/Ball_screw
- [23] "The Stainless Steel Family," *International Stainless Steel*, Retrieved 8 December 2012.
- [24] *How Stainless Steel is made? | Yahoo Answers*. Available:

- <https://answers.yahoo.com/question/index?qid=20081225091856AAjubIT&p=%22stai>
- [25] K. G. Budinski and M. K. Budinski, *Engineering materials* vol. 25, 2009.
- [26] T. E. ToolBox. (2010). *Linear Temperature Expansion (inches/100 feet)*. Available: http://www.engineeringtoolbox.com/thermal-expansion-pipes-d_931.html
- [27] THK, "examples of selecting a ball screw," vol. 501, 2010.
- [28] C. H. Vonnegut, M. Khazaei, S. K. Mohan, E. A. Bansbach, and D. J. Miller, "Torque transfer clutch with ball screw actuator," ed: Google Patents, 2004.
- [29] *Loadstar sensors*. Available: <http://www.loadstarsensors.com/what-is-a-load-cell.html>
- [30] *What is a load cell? - Load Cell, Load Cells, Torque Sensors ..* Available: <http://www.loadstarsensors.com/what-is-a-load-cell.html>
- [31] *THE LOAD CELL AND STRAIN GAUGING SPECIALISTS*. Available: http://www.pcm-uk.com/products_faultfinding.html
- [32] (2014). *Arduino*. Available: <http://www.arduino.cc/>
- [33] A. J. Sedriks, "Corrosion of stainless steel, 2," 1996.
- [34] *Arduino – ArchWiki – Arch Linux*. . Available: <https://wiki.archlinux.org/index.php/Arduino>
- [35] nano. Available: <http://www.arduino.cc/en/Main/ArduinoBoardNano>
- [36] ST.life.augmented. dSPIN fully integrated microstepping motor driver. 1.
- [37] Element14. Available: <http://nz.element14.com/stmicroelectronics/l6472pd/motor-driver-microstpng-7a-36powerso/dp/2309414>
- [38] M. Zaeh, T. Oertli, and J. Milberg, "Finite element modelling of ball screw feed drive systems," *CIRP Annals-Manufacturing Technology*, vol. 53, pp. 289-292, 2004.
- [39] *Load cell type, weight-measuring device - Tokyo Electric Co ... (n.d.)*. Available: <http://www.freepatentsonline.com/4796212.html>
- [40] A. D. Datasheet. 4.8 kHz, Ultralow Noise, 24-Bit Sigma-Delta ADC with PGA.
- [41] Z. Y. Wu, K. Q. Hu, Z. Pan, and X. D. Hu, "Design and Implementation of Yarn Tension Measurement System during Weft Insertion on Air-Jet Loom," *Advanced Materials Research*, vol. 765, pp. 2123-2127, 2013.
- [42] B. Baker, "How delta-sigma ADCs work," p. 13, 2011.
- [43] A. AD, A. AD, and A. AD, "Tutorial on Technical and Performance Benefits of AD719x Family."
- [44] "4.8 kHz Ultralow Noise 24-Bit Sigma-Delta ADC with PGA. (n.d.).".
- [45] *About Infra-Red | Pax Inspections.* "Insert Name of Site in Italics. N.p., n.d. Web. 29 Jun. 2015. Available: <http://paxinspections.com/roof-inspections/>
- [46] N. Semiconductor, "LM2594 datasheet," ed, 1999.
- [47] *3.3V Mini Power Supply - Circuitlib Electronics. (n.d.)*. . Available: <http://www.circuitlib.com/index.php/schematics/product/13-3-3v-mini-power-supply>
- [48] T. Instruments. (2010). *+36v,+150mA Ultralow-Noise, Positive LINEAR REGULATOR*.
- [49] D. I. Dunthorn, "Virtual button for touch screen," ed: Google Patents, 1990.
- [50] *TOUCH SCREENS app for Windows in the Windows Store. (n.d.)*. Available: from <http://apps.microsoft.com/windows/en-us/app/touch-screens/ff171b5b-5806-427b-813>
- [51] *Touchscreen - Wikipedia, the free encyclopedia. (n.d.)*. . Available: <http://en.wikipedia.org/wiki/Touchscreen>
- [52] ILITEK, "ILI9341 datasheet," a.-S. T. L. S. C. Driver and R. R. a. K. color, Eds., 1.11 ed.
- [53] *ILI9341 DS V1.10 20110415 - Display Future. (n.d.)*. . Available:

- <http://www.displayfuture.com/Display/datasheet/controller/ILI9341.pdf>
- [54] *New Touch-Screen Controllers Offer Robust Sensing for ...* (n.d.). Available: http://lark.tu-sofia.bg/ntt/pesu/readings/touch_screen.pdf
- [55] G. Finn, "New Touch-Screen Controllers Offer Robust Sensing for Portable Displays," vol. 44, 2010.
- [56] *Technologies of Touch Screen (Analog 4-wire Resistive ...* (n.d.). Available: <http://www.dmcoltd.com/english/museum/touchscreens/technologies/4-wire.asp>
- [57] D. Co.Ltd. (2004-2011). *Touch Screen Museum*. Available: <http://www.dmcoltd.com/english/museum/touchscreens/technologies/4-wire.asp>
- [58] W. Kester. (2010 11 07). *Single-card grounding for multocard systems*. Available: <http://www.embedded.com/design/system-integration/4211327/Tips-about-PCB-design--Part-2---Single-card-grounding-for-multocard-systems->
- [59] *copper pour : definition of copper pour and synonyms of ...* (n.d.). Available: <http://dictionary.sensagent.com/copper%20pour/en-en/>
- [60] *copper pour : definition of copper pour and synonyms of ...* (n.d.). Available: <http://dictionary.sensagent.com/copper%20pour/en-en/>
- [61] P. d. f. W. w. polygons. Available: http://techref.massmind.org/techref/app/pwb_design_flow.htm#polygons
- [62] Matt. (2007-08-01). *Copper pour or traces?* Available: http://www.electronicpoint.com/threads/copper-pour-or-traces.72199/#post_message_556731
- [63] Sam. (2003-09-20). *PADS: hatch vs pour*. Available: <http://forum.allaboutcircuits.com/newsgroups/viewtopic.php?p=8563#8563>
- [64] M. T. C. G. S. Gupta, *Embedded Programming with field programmable Mixed-signal uControllers* vol. 3: Silicon LABS, 2012.
- [65] F. Leens, "An introduction to I 2 C and SPI protocols," *Instrumentation & Measurement Magazine, IEEE*, vol. 12, pp. 8-13, 2009.
- [66] NANO. *SPI library*. Available: <http://www.arduino.cc/en/Reference/SPI>
- [67] B. W. Kernighan, D. M. Ritchie, and P. Ekelint, *The C programming language* vol. 2: prentice-Hall Englewood Cliffs, 1988.
- [68] G. E. Sacks, *Higher recursion theory*: Springer Publishing Company, Incorporated, 2010.
- [69] P. Odifreddi, *Classical recursion theory: The theory of functions and sets of natural numbers*: Elsevier, 1992.
- [70] wikipedia. *Recursion*. Available: <http://en.wikipedia.org/wiki/Recursion>
- [79] "Design Considerations for Mixed-Signal How to Design a PCB Layout." from https://www.sparkfun.com/datasheets/BreakoutBoards/mixed_signal_design.pdf.

Appendix

Appendix 1: Critical Component Data Sheets

AD7192 Datasheet



4.8 kHz, Ultralow Noise, 24-Bit Sigma-Delta ADC with PGA

AD7192

FEATURES

- RMS noise: 11 nV @ 4.7 Hz (gain = 128)
- 15.5 noise-free bits @ 2.4 kHz (gain = 128)
- Up to 22 noise-free bits (gain = 1)
- Offset drift: 5 nV/°C
- Gain drift: 1 ppm/°C
- Specified drift over time
- 2 differential/4 pseudo differential input channels
- Automatic channel sequencer
- Programmable gain (1 to 128)
- Output data rate: 4.7 Hz to 4.8 kHz
- Internal or external clock
- Simultaneous 50 Hz/60 Hz rejection
- 4 general-purpose digital outputs
- Power supply
 - AV_{DD}: 3 V to 5.25 V
 - DV_{DD}: 2.7 V to 5.25 V
- Current: 4.35 mA
- Temperature range: -40°C to +105°C
- Package: 24-lead TSSOP

INTERFACE

- 3-wire serial
- SPI, QSPI™, MICROWIRE™, and DSP compatible
- Schmitt trigger on SCLK

APPLICATIONS

- Weigh scales
- Strain gage transducers
- Pressure measurement

- Temperature measurement
- Chromatography
- PLC/DCS analog input modules
- Data acquisition
- Medical and scientific instrumentation

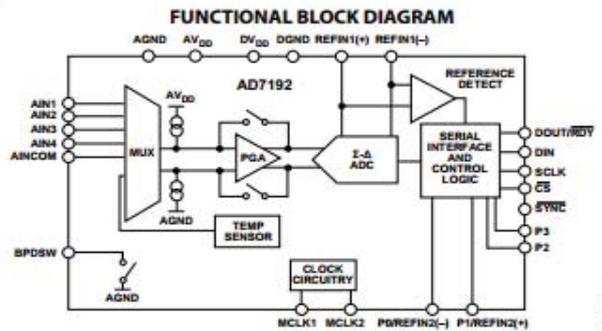
GENERAL DESCRIPTION

The AD7192 is a low noise, complete analog front end for high precision measurement applications. It contains a low noise, 24-bit sigma-delta (Σ - Δ) analog-to-digital converter (ADC). The on-chip low noise gain stage means that signals of small amplitude can be interfaced directly to the ADC.

The device can be configured to have two differential inputs or four pseudo differential inputs. The on-chip channel sequencer allows several channels to be enabled, and the AD7192 sequentially converts on each enabled channel. This simplifies communication with the part. The on-chip 4.92 MHz clock can be used as the clock source to the ADC or, alternatively, an external clock or crystal can be used. The output data rate from the part can be varied from 4.7 Hz to 4.8 kHz.

The device has two digital filter options. The choice of filter affects the rms noise/noise-free resolution at the programmed output data rate, the settling time, and the 50 Hz/60 Hz rejection. For applications that require all conversions to be settled, the AD7192 includes a zero latency feature.

The part operates with a power supply from 3 V to 5.25 V. It consumes a current of 4.35 mA. It is housed in a 24-lead TSSOP package.



Rev. A
Information furnished by Analog Devices is believed to be accurate and reliable. However, no responsibility is assumed by Analog Devices for its use, nor for any infringements of patents or other rights of third parties that may result from its use. Specifications subject to change without notice. No license is granted by implication or otherwise under any patent or patent rights of Analog Devices. Trademarks and registered trademarks are the property of their respective owners.

One Technology Way, P.O. Box 9106, Norwood, MA 02062-9106, U.S.A.
Tel: 781.329.4700 www.analog.com
Fax: 781.461.3113 ©2009 Analog Devices, Inc. All rights reserved.

The full datasheet for the AD7192 24bit ADC can be found at:

http://www.analog.com/static/imported-files/data_sheets/AD7191.pdf accessed on 11

April 2014

L6472 Datasheet:

Datasheet - production data



Features

- Operating voltage: 8 - 45 V
- 7.0 A output peak current (3.0 A *r.m.s.*)
- Low $R_{DS(on)}$ Power MOSFETs
- Programmable speed profile
- Programmable Power MOSFET slew rate
- Up to 1/16 microstepping
- Predictive current control with adaptive decay
- Non dissipative current sensing
- SPI interface
- Low quiescent and standby currents
- Programmable non dissipative overcurrent protection on all Power MOSFETs
- Two levels of overtemperature protection

Applications

- Bipolar stepper motor

Description

The L6472 device, realized in analog mixed signal technology, is an advanced fully integrated solution suitable for driving two-phase bipolar stepper motors with microstepping. It integrates a dual low $R_{DS(on)}$ DMOS full bridge with all of the power switches equipped with an accurate on-chip current sensing circuitry suitable for non dissipative current control and overcurrent protection. Thanks to a new current control, a 1/16 microstepping is achieved through an adaptive decay mode which outperforms traditional implementations. The digital control core can generate user defined motion profiles with acceleration, deceleration, speed or target position, easily programmed through a dedicated register set.

All application commands and data registers, including those used to set analog values (i.e. current control value, current protection trip point, deadtime, etc.) are sent through a standard 5-Mbit/s SPI.

A very rich set of protections (thermal, low bus voltage, overcurrent) makes the L6472 device "bullet proof", as required by the most demanding motor control applications.

Table 1. Device summary

Order codes	Package	Packing
L6472H	HTSSOP28	Tube
L6472HTR	HTSSOP28	Tape and reel
L6472PD	POWERSO36	Tube
L6472PDTR	POWERSO36	Tape and reel

The full datasheet for the L6472 stepper motor driver can be found at:

<http://www.farnell.com/datasheets/1922760.pdf>

December 1999

National Semiconductor

LM2594/LM2594HV SIMPLE SWITCHER® Power Converter 150 kHz 0.5A Step-Down Voltage Regulator

General Description

The LM2594/LM2594HV series of regulators are monolithic integrated circuits that provide all the active functions for a step-down (buck) switching regulator, capable of driving a 0.5A load with excellent line and load regulation. These devices are available in fixed output voltages of 3.3V, 5V, 12V, and an adjustable output version, and are packaged in a 8-lead DIP and a 8-lead surface mount package.

Requiring a minimum number of external components, these regulators are simple to use and feature internal frequency compensation, a fixed-frequency oscillator, and improved line and load regulation specifications.

The LM2594/LM2594HV series operates at a switching frequency of 150 kHz thus allowing smaller sized filter components than what would be needed with lower frequency switching regulators. Because of its high efficiency, the copper traces on the printed circuit board are normally the only heat sinking needed.

A standard series of inductors (both through hole and surface mount types) are available from several different manufacturers optimized for use with the LM2594/LM2594HV series. This feature greatly simplifies the design of switch-mode power supplies.

Other features include a guaranteed $\pm 4\%$ tolerance on output voltage under all conditions of input voltage and output load conditions, and $\pm 15\%$ on the oscillator frequency. External shutdown is included, featuring typically 85 μ A standby current. Self protection features include a two stage frequency reducing current limit for the output switch and an over temperature shutdown for complete protection under fault conditions.

The LM2594HV is for applications requiring an input voltage up to 60V.

Features

- 3.3V, 5V, 12V, and adjustable output versions
- Adjustable version output voltage range, 1.2V to 37V (57V for the HV version) $\pm 4\%$ max over line and load conditions
- Available in 8-pin surface mount and DIP-8 package
- Guaranteed 0.5A output current
- Input voltage range up to 60V
- Requires only 4 external components
- 150 kHz fixed frequency internal oscillator
- TTL Shutdown capability
- Low power standby mode, I_C typically 85 μ A
- High Efficiency
- Uses readily available standard inductors
- Thermal shutdown and current limit protection

Applications

- Simple high-efficiency step-down (buck) regulator
- Efficient pre-regulator for linear regulators
- On-card switching regulators
- Positive to Negative converter

Typical Application (Fixed Output Voltage Versions)

SIMPLE SWITCHER and Switches Their Simple™ are registered trademarks of National Semiconductor Corporation.

© 1999 National Semiconductor Corporation DS012439 www.national.com

LM2594/LM2594HV SIMPLE SWITCHER Power Converter 150 kHz 0.5A Step-Down Voltage Regulator

The full datasheet for the LM2594 can be found at

<http://www.farnell.com/datasheets/1896094.pdf>

+36V, +150mA, Ultralow-Noise, Positive LINEAR REGULATOR

FEATURES

- Input Voltage Range: +3V to +36V
- Noise:
 - 12.7 μ V_{RMS} (20Hz to 20kHz)
 - 15.4 μ V_{RMS} (10Hz to 100kHz)
- Power-Supply Ripple Rejection:
 - 72dB (120Hz)
 - \geq 52dB (10Hz to 400kHz)
- Adjustable Output: +1.194V to +33V
- Output Current: 150mA
- Dropout Voltage: 260mV at 100mA
- Stable with Ceramic Capacitors \geq 2.2 μ F
- CMOS Logic-Level-Compatible Enable Pin
- Built-In, Fixed, Current-Limit and Thermal Shutdown Protection
- Available in High Thermal Performance MSOP-8 PowerPAD™ Package
- Operating Temperature Range: –40°C to +125°C

APPLICATIONS

- Supply Rails for Op Amps, DACs, ADCs, and Other High-Precision Analog Circuitry
- Audio
- Post DC/DC Converter Regulation and Ripple Filtering
- Test and Measurement
- RX, TX, and PA Circuitry
- Industrial Instrumentation
- Base Stations and Telecom Infrastructure

DESCRIPTION

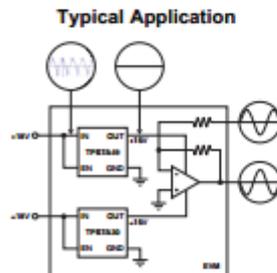
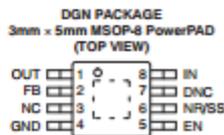
The TPS7A49xx series of devices are positive, high-voltage (+36V), ultralow noise (15.4 μ V_{RMS}, 72dB PSRR) linear regulators capable of sourcing a load of 150mA.

These linear regulators include a CMOS logic-level-compatible enable pin and capacitor-programmable soft-start function that allows for customized power-management schemes. Other features available include built-in current limit and thermal shutdown protection to safeguard the device and system during fault conditions.

The TPS7A49xx family is designed using bipolar technology, and is ideal for high-accuracy, high-precision instrumentation applications where clean voltage rails are critical to maximize system performance. This design makes it an excellent choice to power operational amplifiers, analog-to-digital converters (ADCs), digital-to-analog converters (DACs), and other high-performance analog circuitry.

In addition, the TPS7A49xx family of linear regulators is suitable for post dc/dc converter regulation. By filtering out the output voltage ripple inherent to dc/dc switching conversion, maximum system performance is provided in sensitive instrumentation, test and measurement, audio, and RF applications.

For applications where both positive and negative high-performance rails are required, consider TI's TPS7A30xx family of negative high-voltage, ultralow-noise linear regulators as well.



Post DC/DC Converter Regulation for High-Performance Analog Circuitry

Please be aware that an important notice concerning availability, standard warranty, and use in critical applications of Texas Instruments semiconductor products and disclaimers thereto appears at the end of this data sheet. PowerPAD is a trademark of Texas Instruments. All other trademarks are the property of their respective owners.

PRODUCTION DATA information is current as of publication date. Products conform to specifications per the terms of the Texas Instruments standard warranty. Production processing does not necessarily include testing of all parameters.

Copyright © 2010, Texas Instruments Incorporated

The full datasheet for the TPS7A4901 can be found at:

<http://www.farnell.com/datasheets/1857485.pdf>

BAV99 Datasheet

Surface Mount Switching Diode

COMCHIP
www.comchip.com.tw



BAV99 Thru BAW56 Voltage: 70 Volts Current: 215mA

Features

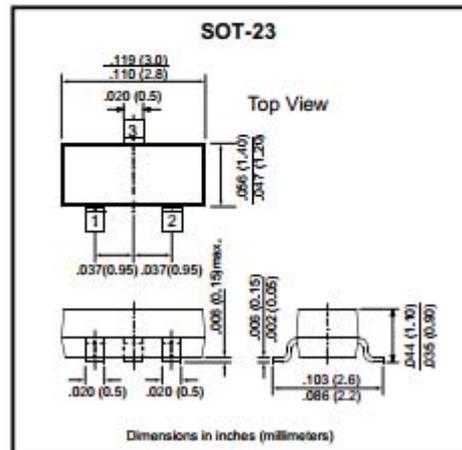
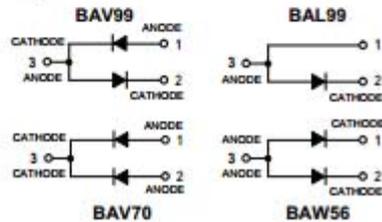
Fast Switching Speed
Surface Mount Package Ideally Suited for Automatic Insertion
For General Purpose Switching Applications
High Conductance

Mechanical data

Case: SOT -23, Plastic

Approx. Weight: 0.008 gram

This diodes is also available in other configurations including a dual common cathode with type designation BAV70, a dual common anodes with type designation BAW56 and single chip inside with type Designation BAL99



Maximum Ratings

Rating	Symbol	Value	Units
Continuous Reverse Voltage	V_R	70	Vdc
Peak Forward Current	I_F	215	mAdc
Peak Forward Surge Current	$I_{FM}(surge)$	500	mAdc

Thermal Characteristics

Characteristic	Symbol	Max	Units
Total Device Dissipation FR-5 Board(1) $T_A = 25^\circ C$	P_D	225	mW
Derate above 25°C		1.8	mW/°C
Thermal Resistance, Junction to Ambient	$R_{\theta JA}$	556	°C/W
Total Device Dissipation Alumina Substrate,(2) $T_A = 25^\circ C$	P_D	300	mW
Derate above 25°C		2.4	mW/°C
Thermal Resistance, Junction to Ambient	$R_{\theta JA}$	417	°C/W
Junction and Storage Temperature	T_J, T_{STG}	-55 to +150	°C

Electrical Characteristics ($T_A = 25^\circ C$ unless otherwise noted)

Characteristic (OFF CHARACTERISTICS)	Symbol	Min	Max	Units
Reverse Breakdown Voltage ($I_{RR} = 100 \mu A$)	V_{BR}	70	-	Vdc
Reverse Voltage Leakage Current $V_R = 25 \text{ Vdc}, T_J = 150^\circ C$ $V_R = 70 \text{ Vdc}$ $V_R = 70 \text{ Vdc}, T_J = 150^\circ C$	I_R	-	30	μA
		-	2.5	μA
		-	50	μA
Diode Capacitance ($V_R = 0, f = 1.0 \text{ MHz}$)	C_D		1.5	pF
Forward Voltage $I_F = 1.0 \text{ mAdc}$ $I_F = 10 \text{ mAdc}$ $I_F = 50 \text{ mAdc}$ $I_F = 150 \text{ mAdc}$	V_F	-	715	mV
		-	855	mV
		-	1000	mV
		-	1250	mV
Reverse Recovery Time ($I_F = I_R = 10 \text{ mAdc}, I_{RR} = 1.0 \text{ mAdc}, R_L = 100 \Omega$)	T_{rr}		6.0	nS

1.FR-5 = 1.0 X 0.75X 0.062 in. 2.Aluminum = 0.4X 0.3X 0.024 in. 99.5% aluminum.

MDS0210001A

Page 1

The full datasheet for the BAV99 can be found at:

<http://www.farnell.com/datasheets/1822674.pdf>

REF5050 Datasheet:



REF5010, REF5020
REF5025, REF5030
REF5040, REF5045, REF5050

www.ti.com

SBOS410F – JUNE 2007 – REVISED DECEMBER 2013

Low-Noise, Very Low Drift, Precision Voltage Reference

Check for Samples: REF5010, REF5020, REF5025, REF5030, REF5040, REF5045, REF5050

FEATURES

- **LOW TEMPERATURE DRIFT:**
 - High-Grade: 3ppm/°C (max)
 - Standard-Grade: 8ppm/°C (max)
- **HIGH ACCURACY:**
 - High-Grade: 0.05% (max)
 - Standard-Grade: 0.1% (max)
- **LOW NOISE:** 3µV_{PP}/V
- **EXCELLENT LONG-TERM STABILITY:**
 - 45ppm/1000hr (typ) after 1000 hours
- **HIGH OUTPUT CURRENT:** ±10mA
- **TEMPERATURE RANGE:** –40°C to +125°C

APPLICATIONS

- 16-BIT DATA ACQUISITION SYSTEMS
- ATE EQUIPMENT
- INDUSTRIAL PROCESS CONTROL
- MEDICAL INSTRUMENTATION
- OPTICAL CONTROL SYSTEMS
- PRECISION INSTRUMENTATION

DESCRIPTION

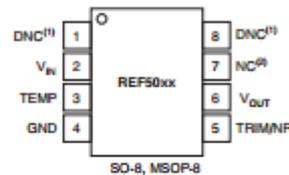
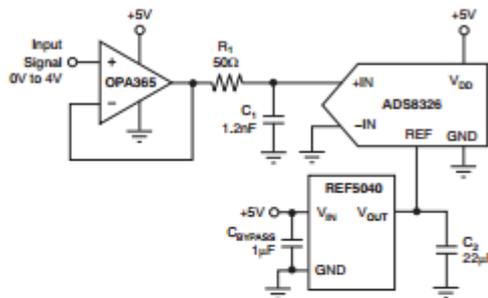
The REF50xx is a family of low-noise, low-drift, very high precision voltage references. These references are capable of both sinking and sourcing, and are very robust with regard to line and load changes.

Excellent temperature drift (3ppm/°C) and high accuracy (0.05%) are achieved using proprietary design techniques. These features, combined with very low noise, make the REF50xx family ideal for use in high-precision data acquisition systems.

Each reference voltage is available in both standard- and high-grade versions. They are offered in MSOP-8 and SO-8 packages, and are specified from –40°C to +125°C.

REF50xx Family

MODEL	OUTPUT VOLTAGE
REF5020	2.048V
REF5025	2.5V
REF5030	3.0V
REF5040	4.096V
REF5045	4.5V
REF5050	5.0V
REF5010	10.0V



NOTES: (1) DNC = Do not connect.
(2) NC = No internal connection.



Please be aware that an important notice concerning availability, standard warranty, and use in critical applications of Texas Instruments semiconductor products and disclaimers thereto appears at the end of this data sheet.

All trademarks are the property of their respective owners.

PRODUCTION DATA information is current as of publication date. Products conform to specifications per the terms of the Texas Instruments standard warranty. Production processing does not necessarily include testing of all parameters.

Copyright © 2007–2013, Texas Instruments Incorporated

The full datasheet for the ref5050 voltage reference can be found at:

<http://www.farnell.com/datasheets/1885920.pdf>

ATmega328 Datasheet:

Features

- High Performance, Low Power AVR[®] 8-Bit Microcontroller
- Advanced RISC Architecture
 - 131 Powerful Instructions – Most Single Clock Cycle Execution
 - 32 x 8 General Purpose Working Registers
 - Fully Static Operation
 - Up to 20 MIPS Throughput at 20 MHz
 - On-chip 2-cycle Multiplier
- High Endurance Non-volatile Memory Segments
 - 4/8/16/32K Bytes of In-System Self-Programmable Flash program memory (ATmega48PA/88PA/168PA/328P)
 - 256/512/512/1K Bytes EEPROM (ATmega48PA/88PA/168PA/328P)
 - 512/1K/1K/2K Bytes Internal SRAM (ATmega48PA/88PA/168PA/328P)
 - Write/Erase Cycles: 10,000 Flash/100,000 EEPROM
 - Data retention: 20 years at 85°C/100 years at 25°C⁽¹⁾
 - Optional Boot Code Section with Independent Lock Bits
 - In-System Programming by On-chip Boot Program
 - True Read-While-Write Operation
 - Programming Lock for Software Security
- Peripheral Features
 - Two 8-bit Timer/Counters with Separate Prescaler and Compare Mode
 - One 16-bit Timer/Counter with Separate Prescaler, Compare Mode, and Capture Mode
 - Real Time Counter with Separate Oscillator
 - Six PWM Channels
 - 8-channel 10-bit ADC in TQFP and QFN/MLF package
 - 6-channel 10-bit ADC in PDIP Package
 - Temperature Measurement
 - Programmable Serial USART
 - Master/Slave SPI Serial Interface
 - Byte-oriented 2-wire Serial Interface (Philips I²C compatible)
 - Programmable Watchdog Timer with Separate On-chip Oscillator
 - On-chip Analog Comparator
 - Interrupt and Wake-up on Pin Change
- Special Microcontroller Features
 - Power-on Reset and Programmable Brown-out Detection
 - Internal Calibrated Oscillator
 - External and Internal Interrupt Sources
 - Six Sleep Modes: Idle, ADC Noise Reduction, Power-save, Power-down, Standby, and Extended Standby
- I/O and Packages
 - 23 Programmable I/O Lines
 - 28-pin PDIP, 32-lead TQFP, 28-pad QFN/MLF and 32-pad QFN/MLF
- Operating Voltage:
 - 1.8 - 5.5V for ATmega48PA/88PA/168PA/328P
- Temperature Range:
 - -40°C to 85°C
- Speed Grade:
 - 0 - 20 MHz @ 1.8 - 5.5V
- Low Power Consumption at 1 MHz, 1.8V, 25°C for ATmega48PA/88PA/168PA/328P:
 - Active Mode: 0.2 mA
 - Power-down Mode: 0.1 µA
 - Power-save Mode: 0.75 µA (Including 32 kHz RTC)



8-bit AVR[®]
Microcontroller
with 4/8/16/32K
Bytes In-System
Programmable
Flash

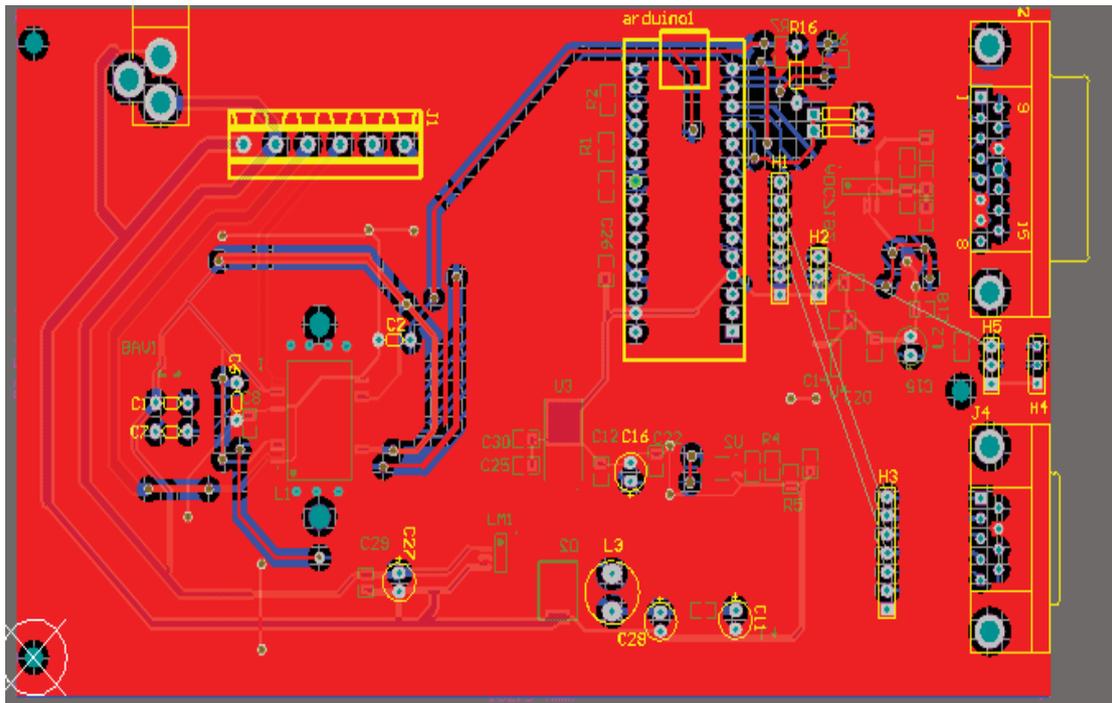
ATmega48PA
ATmega88PA
ATmega168PA
ATmega328P

Rev. 8161D-AVR-10/09

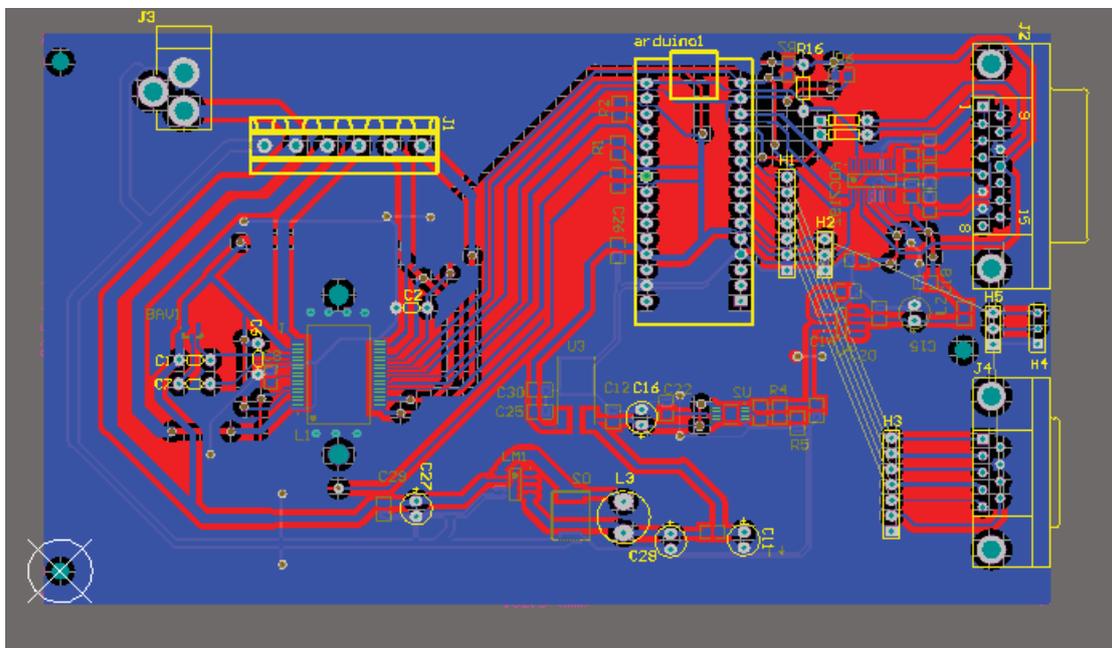


The full datasheet for the ATmega328 microcontroller can be found at
<http://www.atmel.com/images/doc8161.pdf>

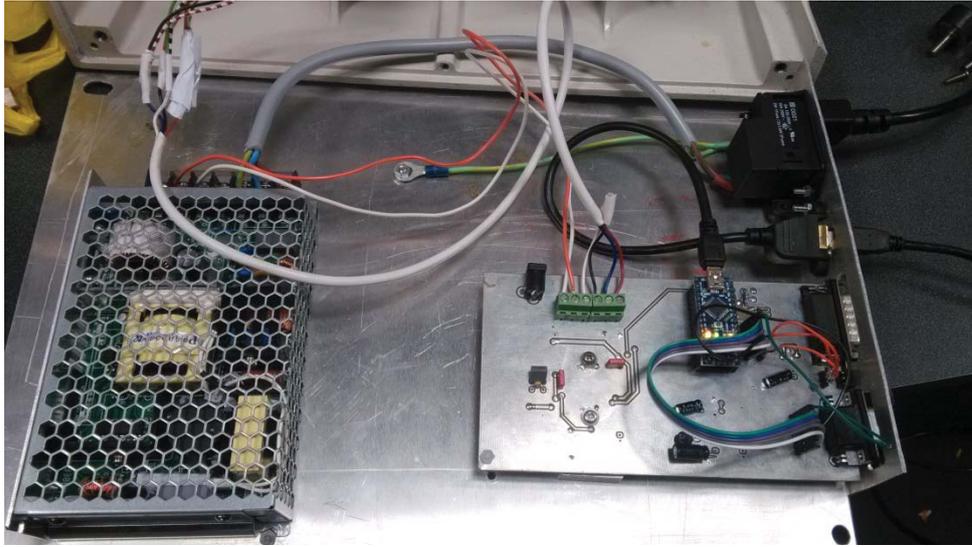
Appendix 2: PCB design



Top layer of main PCB



The bottom layer of main PCB



Electronic parts and assembly of texture analyser

Appendix 3: Test results

Results of tests on pressure ball:

Test1 (standard) and Test 2 (standard) is the result from the standard texture analyser, whereas Test1 (new instrument)and Test 2 (new instrument) are the two tests on the new texture analyser.

Test1 (standard) (N)	Test2 (Standard) (N)	Test1(Standard) (N)	Test2(Standard) (N)	Time(s)
0.388597819	0.395475344	0.37	0.37	0.085
0.590994751	0.583049343	0.57	0.54	0.115
0.770760123	0.764545893	0.75	0.76	0.14
0.952563408	0.965847934	0.94	0.95	0.165
1.17834271	1.169475841	1.17	1.17	0.195
1.408841388	1.418439575	1.36	1.37	0.225
1.6428796	1.658490759	1.65	1.66	0.255
1.802265843	1.817438957	1.74	1.78	0.275
2.044241189	2.032453545	2.01	2.04	0.305
2.289970585	2.268935454	2.31	2.23	0.335
2.579139705	2.578935704	2.54	2.54	0.37
2.747535668	2.945390543	2.71	2.72	0.39
3.006457869	2.995748785	2.98	3.01	0.42
3.269670413	3.269849075	3.24	3.25	0.45
3.538245886	3.589465604	3.49	3.43	0.48
3.808108462	3.795475949	3.78	3.82	0.51
3.974251995	3.945478756	3.99	4.1	0.54
3.953872866	3.589406798	3.96	3.99	0.565
3.703745868	3.758475493	3.72	3.69	0.595
3.282326925	3.238923579	3.23	3.24	0.625
2.851791003	2.854438959	2.83	2.85	0.655
2.476171472	2.543564933	2.46	2.44	0.685
2.144527957	2.134697594	2.18	2.11	0.715
1.847314445	1.853975943	1.85	1.84	0.745
1.57359056	1.635843957	1.56	1.57	0.775
1.321961942	1.323589407	1.3	1.32	0.805
1.087601955	1.084497583	1.08	1.076	0.835
0.871261408	0.885437543	0.86	0.85	0.865
0.666290271	0.639859493	0.65	0.66	0.895
0.480625676	0.493758933	0.48	0.46	0.925
0.311049869	0.325543853	0.29	0.31	0.955
0.16035157	0.158946745	0.1	0.14	0.985

Results of tests on avocado:

Test1 (standard) and Test 2 (standard) is the result from the standard texture analyser, whereas Test1 (new instrument) and Test 2 (new instrument) are the two tests on the new texture analyser.

Test1 (Standard) (N)	Test2 (Standard) (N)	Test2 (New Instrument) (N)	Test2 (New Instrument) (N)	Time (s)
0.199282505	0.21	0.2	0.18	0.01
0.727860702	0.69	0.72	0.7	0.04
1.674186182	1.59	1.63	1.59	0.07
2.59600098	2.53	2.6	2.5	0.1
3.594544871	3.49	3.62	3.52	0.13
4.589891717	4.49	4.52	4.53	0.16
5.632128564	5.79	5.76	5.81	0.19
6.678628138	6.67	6.71	6.67	0.22
7.736850213	7.7	7.75	7.72	0.25
8.758839104	8.63	8.66	9.32	0.28
9.77763095	9.61	9.63	9.87	0.31
10.83585302	10.55	10.74	11.32	0.34
11.93457101	12.12	11.87	12.01	0.37
13.0151724	13.21	13.04	13.5	0.4
14.17463425	14.23	14.11	14.05	0.43
15.34262156	15.23	15.54	15.49	0.46
16.52126568	15.56	16.64	16.62	0.49
17.67859617	17.59	17.94	18.01	0.52
18.7922337	18.82	18.54	18.51	0.55
19.87709782	19.92	19.83	19.78	0.58
20.91080921	21.02	20.92	20.89	0.61
21.89656492	21.93	21.92	21.89	0.64
22.8546129	22.83	22.85	22.83	0.67
23.77962474	23.8	23.76	23.73	0.7
24.68545431	24.72	24.34	24.32	0.73
25.56464184	25.42	25.76	25.74	0.76
26.43210686	26.4	26.32	26.28	0.79
27.28465234	27.31	27.34	27.32	0.82
28.13080373	28.12	28.06	28.03	0.85
28.89489761	29.01	28.54	28.52	0.88
29.6824365	29.72	29.65	29.67	0.91
30.40603447	30.38	30.32	30.29	0.94
31.05929744	31.02	30.55	30.57	0.97
31.71682314	31.65	31.43	31.45	1

32.43643785	32.3	32.32	31.98	1.01
30.09378969	29.99	31.67	31.72	1.03
24.4222309	24.39	24.64	24.67	1.055
18.73255551	18.72	19.43	19.39	1.085
14.81830609	14.79	14.41	14.36	1.115
11.8354626	11.81	12.85	12.92	1.145
9.481371397	9.52	9.43	9.39	1.175
7.6142968	7.58	7.42	7.49	1.205
6.059466985	6.03	6.21	6.19	1.235
4.761466494	4.75	4.65	4.62	1.265
3.707507147	3.69	3.74	3.97	1.295
2.83791076	2.78	2.53	2.49	1.325
2.113247104	2.05	2.43	2.67	1.355
1.516465269	1.42	1.43	1.54	1.385
1.037974119	1.04	1.04	2	1.415
0.690561837	0.68	0.5	0.43	1.445

Results of tests on kiwifruit:

Test1 (standard) and Test 2 (standard) is the result from the standard texture analyser, whereas Test1 (new instrument) and Test 2 (new instrument) are the two tests on the new texture analyser.

Test1 (Standard) (N)	Test1(new instrument) (N)	Time (s)
0.574402516	0.53	0.005
1.365138447	0.76	0.03
2.798480531	2.78	0.06
4.961814682	5.23	0.09
7.693157257	8.54	0.125
9.622041401	10.43	0.15
11.67454464	14.34	0.18
13.38602969	17.12	0.21
15.38205179	20.43	0.245
17.03385865	22.42	0.27
19.45935053	25.64	0.3
22.8428904	27.43	0.335
25.68932661	30.01	0.36
29.24124421	32.65	0.39
32.94875136	35.04	0.42
36.82463624	37.97	0.45
40.92218294	40.54	0.48
45.06661965	46.23	0.51
49.17588885	50.34	0.54
53.28089533	54.75	0.57
57.31023839	57.54	0.6
61.20850259	60.43	0.63
65.12488338	63.45	0.66
69.10200803	68.65	0.69
73.06208178	73.43	0.72
77.60082077	76.31	0.755
80.79040654	80.14	0.78
84.47660005	83.54	0.81
87.95605128	86.34	0.84
91.35451069	90.13	0.87
94.52171714	93.54	0.9
97.39159836	95.65	0.93
99.93857797	98.41	0.96
102.3587414	100.9	0.99
103.4574594	102.43	1.005

99.47180932	99.21	1.035
86.09750214	78.3	1.065
74.34409704	68.32	1.095
64.53236427	59.43	1.125
55.96641358	50.65	1.155
48.39261269	45.32	1.185
41.58397137	37.54	1.215
35.48613984	30.98	1.245
30.02558605	25.76	1.275
25.12131819	22.32	1.305
20.71365807	18.54	1.335
16.77809501	14.32	1.365
13.28692127	12.54	1.395
10.23054574	8.33	1.425
7.653727028	7.2	1.455
5.460553786	5.12	1.485
3.566837143	3.24	1.515
2.079145284	1.63	1.545
0.969770481	0.94	1.575
0.234450006	0.2	1.605

Results of tests on persimmon:

Test (standard) is the result from standard texture analyser, whereas Test (new instrument) is the test on new texture analyser.

Test1 (Standard) N	Test1 (New Instrument) N	Test2 (New Instrument) N	Time (s)
0.095911366	0.0084	0.1	0.005
0.474228422	0.4542	0.2	0.03
2.816597123	2.92	2.34	0.06
6.240632899	6.32	5.75	0.09
10.35736188	11.43	9.75	0.125
13.20273241	13.23	12.65	0.15
16.61611137	16.71	16.08	0.18
20.0188335	20.13	19.52	0.21
23.93308293	24.43	23.42	0.245
26.82640915	26.43	26.43	0.27
30.34422492	30.32	29.53	0.3
34.54194572	34.564	33.54	0.335
37.6430799	36.431	37.21	0.36
41.45395818	41.431	40.82	0.39
45.40230943	45.413	44.79	0.42
49.48067386	49.531	48.81	0.45
53.69437988	53.631	53.01	0.48
58.03809909	58.341	57.31	0.51
62.46494149	62.433	61.71	0.54
67.0846723	67.0418	66.32	0.57
71.84933584	71.941	71.03	0.6
76.77491734	77.431	76.01	0.63
81.80493566	82.413	81.21	0.66
87.01931694	88.531	86.21	0.69
92.32214981	92.413	91.41	0.72
98.69386158	98.5455	97.72	0.755
103.3594167	105.413	102.52	0.78
109.0352382	110.4352	108.12	0.81
114.7131911	115.324	114.84	0.84
120.3495824	119.432	119.34	0.87
125.7920196	123.54	125.33	0.9
131.0064009	129.455	130.34	0.93
135.9618215	133.541	135.17	0.96
140.7637839	139.6424	140.13	0.99
143.0922987	144.3445	142.4	1.005
147.6214466	147.434	146.34	1.035

152.118624	153.341	150.32	1.065
156.5092332	157.435	152.43	1.095
160.8497553	159.5434	161.54	1.125
165.0698554	164.343	164.34	1.155
169.2633135	168.432	169.43	1.185
173.4173414	172.435	172.34	1.215
177.5191508	178.543	178.34	1.245
181.5282459	179.5456	181.43	1.275
184.9522817	184.434	183.43	1.305
188.0651383	188.054	189.86	1.335
191.5477866	189.4345	190.45	1.365
194.8386122	194.654	194.53	1.395
197.2886147	197.54	197.95	1.425
199.2601262	200.43	199.11	1.455
200.7979051	200.64	200.88	1.485
202.1641092	201.98	203.23	1.515
203.2244626	203.54	204.53	1.545
204.1260295	204.54	205.01	1.575
205.0212022	204.99	205.3	1.605
205.6712682	204.3	205.34	1.635
206.1391025	206.45	206.11	1.665
206.3714211	204.64	206.44	1.695
205.5838822	205.765	204.93	1.725
203.7636976	203.53	202.43	1.755
201.960564	201.546	201.8	1.785
200.0732414	200.564	200.12	1.815
197.5070795	197.435	198.43	1.845
195.086916	194.43	196.34	1.875
193.0109678	192.45	193.03	1.905
191.2824318	190.343	191.13	1.935
189.2682932	189.354	189.86	1.965
186.800174	186.345	185.21	1.995
180.8089106	180.343	180.46	2.025
161.3857933	159.433	160.12	2.055
143.9597637	142.43	144.23	2.085
130.4309327	130.53	130.37	2.115
118.8331171	118.34	119.03	2.145
108.4576387	107.43	108.53	2.175
99.04233954	97.54	99.03	2.205
90.4497468	91.4345	90.64	2.235
82.53812477	81.545	81.45	2.265
75.2744373	78.543	75.31	2.295
68.59687484	67.34	68.03	2.325

62.42124853	61.34	62.64	2.355
56.70812815	56.5675	56.62	2.385
51.42767459	49.345	51.36	2.415
46.54258901	45.686	46.12	2.445
42.00704706	41.454	41.99	2.475
37.83596831	37.43	37.76	2.505
33.94409821	32.567	33.43	2.535
30.3399622	30.13	30.26	2.565
27.02675733	28.455	27.01	2.595
23.95759361	23.77	24.12	2.625
21.13353672	20.15	21.13	2.655
18.53753574	17.54	18.49	2.685
16.10991249	16.3456	16.21	2.715
13.90821379	12.545	12.58	2.745
11.85571055	10.53	12.02	2.775
9.982241865	9.56	10.01	2.805
8.297398864	8.12	8.13	2.835
6.721255412	6.943	6.73	2.865
5.323080828	5.21	5.31	2.895
4.060247839	3.97	3.91	2.925
2.923165308	2.73	3.02	2.955
1.909701871	1.834	2.12	2.985
1.062484802	0.934	0.98	3.015
0.357003419	0.345	0.29	3.045
75.2744373	78.543	75.31	2.295
68.59687484	67.34	68.03	2.325
62.42124853	61.34	62.64	2.355
56.70812815	56.5675	56.62	2.385
51.42767459	49.345	51.36	2.415
46.54258901	45.686	46.12	2.445
42.00704706	41.454	41.99	2.475
37.83596831	37.43	37.76	2.505
33.94409821	32.567	33.43	2.535
30.3399622	30.13	30.26	2.565
27.02675733	28.455	27.01	2.595
23.95759361	23.77	24.12	2.625
21.13353672	20.15	21.13	2.655
18.53753574	17.54	18.49	2.685
16.10991249	16.3456	16.21	2.715
13.90821379	12.545	12.58	2.745
11.85571055	10.53	12.02	2.775
9.982241865	9.56	10.01	2.805
8.297398864	8.12	8.13	2.835

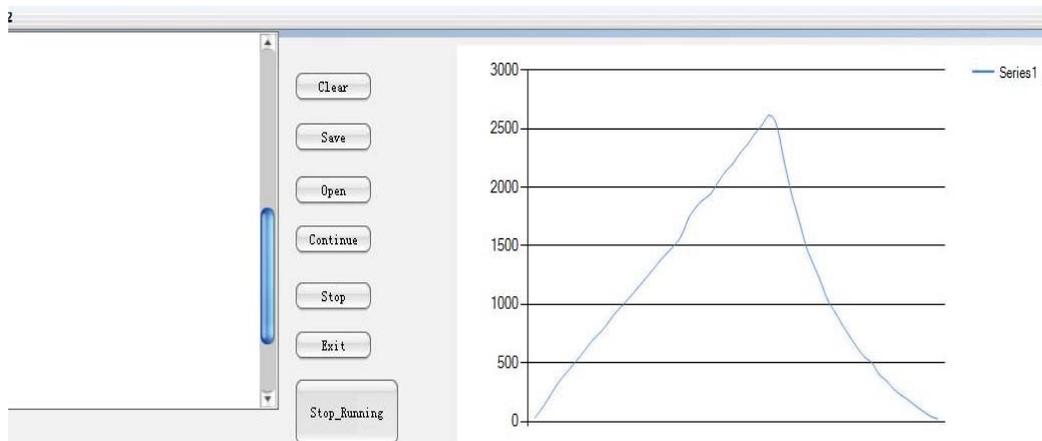
6.721255412	6.943	6.73	2.865
5.323080828	5.21	5.31	2.895
4.060247839	3.97	3.91	2.925
2.923165308	2.73	3.02	2.955
1.909701871	1.834	2.12	2.985
1.062484802	0.934	0.98	3.015
0.357003419	0.345	0.29	3.045

Results of tests on orange:

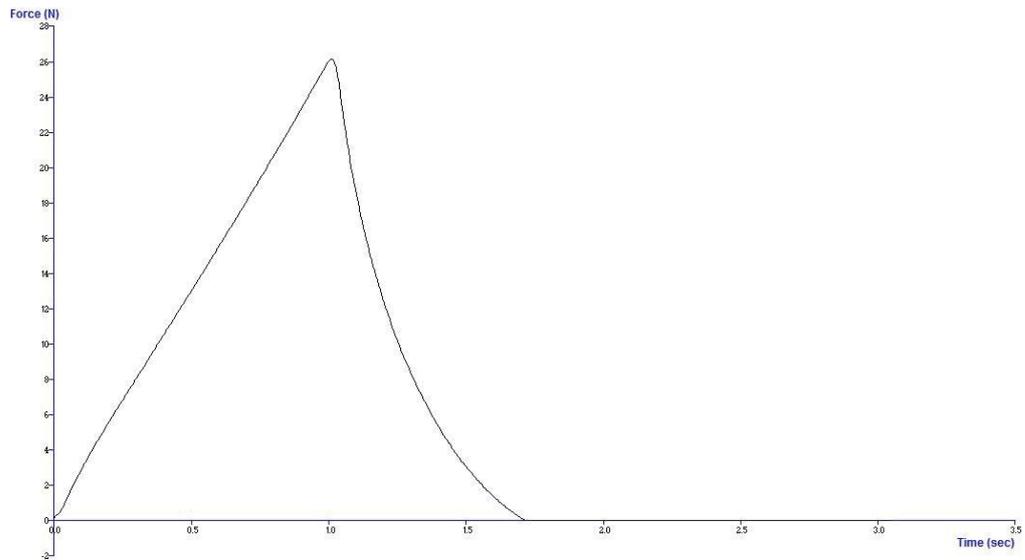
Test (standard) is the result from standard texture analyser, whereas Test (new instrument) is the test on new texture analyser.

Test (standard) N	Test (new instrument) N	Time (s)
0.100174094	0.11	0
0.529643878	0.53	0.025
1.124294349	1.13	0.045
1.942738008	1.93	0.07
2.680189846	2.65	0.095
3.386736911	3.36	0.12
4.080495794	4.03	0.145
4.750809676	4.71	0.17
5.425386285	5.39	0.195
6.046678802	6.03	0.22
6.653051774	6.65	0.245
7.270081563	7.28	0.27
7.899899535	8.01	0.295
8.495615688	8.51	0.32
9.112645478	9.13	0.345
9.759514359	9.76	0.37
10.38187256	10.36	0.395
10.96906326	10.98	0.42
11.59355282	11.62	0.445
12.20099147	12.22	0.47
12.82441535	12.89	0.495
13.44144514	13.43	0.52
13.95297243	14.01	0.54
14.43998903	14.5	0.56
15.07087269	15.11	0.585
15.7102818	15.72	0.61
16.3614134	16.35	0.635
16.97098342	16.94	0.66
17.62637776	17.65	0.685
18.28923187	18.32	0.71
18.90519597	18.88	0.735
19.56272167	19.53	0.76
20.21385328	20.19	0.785
20.86391921	20.86	0.81
21.50545968	21.56	0.835
22.16937947	22.12	0.86

22.86207267	22.91	0.885
23.53132087	23.56	0.91
24.2165543	24.23	0.935
24.88686818	24.84	0.96
25.57423298	25.56	0.985
26.12305913	26.14	1.01
25.21509819	25.32	1.035
22.5199888	22.64	1.06
20.04547555	20.05	1.085
18.05158481	18.03	1.11
16.2910784	16.31	1.135
14.73944563	14.62	1.16
13.33913968	13.01	1.185
12.1349192	12.72	1.21
10.97332598	10.95	1.235
9.959862546	9.88	1.26
8.987960701	8.92	1.285
8.121561359	8.11	1.31
7.289263837	7.33	1.335
6.530498361	6.55	1.36
5.83780516	5.85	1.385
5.161097187	5.21	1.41
4.550461489	4.53	1.435
3.971796245	3.89	1.46
3.434692594	3.51	1.485
2.933822126	2.94	1.51
2.484104386	2.51	1.535
2.054634602	2.06	1.56
1.644347091	1.67	1.585
1.283080944	1.31	1.61
0.947391162	0.95	1.635



The curve of testing orange on new instrument.



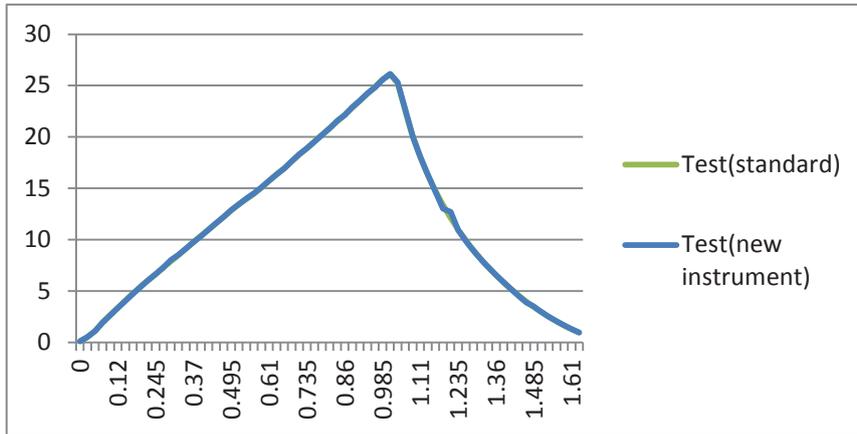
The curve of testing orange on standard instrument.

Test (standard) N	Test (new instrument) N	Error (N)
0.100174094	0.11	-0.009825906
0.529643878	0.53	-0.000356122
1.124294349	1.13	-0.005705651
1.942738008	1.93	0.012738008
2.680189846	2.65	0.030189846
3.386736911	3.36	0.026736911
4.080495794	4.03	0.050495794
4.750809676	4.71	0.040809676
5.425386285	5.39	0.035386285
6.046678802	6.03	0.016678802
6.653051774	6.65	0.003051774
7.270081563	7.28	-0.009918437
7.899899535	8.01	-0.110100465
8.495615688	8.51	-0.014384312
9.112645478	9.13	-0.017354522
9.759514359	9.76	-0.000485641
10.38187256	10.36	0.021872558
10.96906326	10.98	-0.010936744
11.59355282	11.62	-0.026447181
12.20099147	12.22	-0.019008528
12.82441535	12.89	-0.065584648
13.44144514	13.43	0.011445142
13.95297243	14.01	-0.057027571
14.43998903	14.5	-0.060010967

15.07087269	15.11	-0.039127313
15.7102818	15.72	-0.009718205
16.3614134	16.35	0.011413404
16.97098342	16.94	0.030983421
17.62637776	17.65	-0.023622243
18.28923187	18.32	-0.030768134
18.90519597	18.88	0.025195974
19.56272167	19.53	0.032721674
20.21385328	20.19	0.023853283
20.86391921	20.86	0.00391921
21.50545968	21.56	-0.054540318
22.16937947	22.12	0.049379473
22.86207267	22.91	-0.047927326
23.53132087	23.56	-0.028679126
24.2165543	24.23	-0.013445698
24.88686818	24.84	0.046868184
25.57423298	25.56	0.014232975
26.12305913	26.14	-0.016940873
25.21509819	25.32	-0.104901807
22.5199888	22.64	-0.120011199
20.04547555	20.05	-0.004524449
18.05158481	18.03	0.021584814
16.2910784	16.31	-0.018921598
14.73944563	14.62	0.119445632
13.33913968	13.01	0.329139685
12.1349192	12.72	-0.585080803
10.97332598	10.95	0.023325983
9.959862546	9.88	0.079862546
8.987960701	8.92	0.067960701
8.121561359	8.11	0.011561359
7.289263837	7.33	-0.040736163
6.530498361	6.55	-0.019501639
5.83780516	5.85	-0.01219484
5.161097187	5.21	-0.048902813
4.550461489	4.53	0.020461489
3.971796245	3.89	0.081796245
3.434692594	3.51	-0.075307406
2.933822126	2.94	-0.006177874
2.484104386	2.51	-0.025895614
2.054634602	2.06	-0.005365398
1.644347091	1.67	-0.025652909
1.283080944	1.31	-0.026919056
0.947391162	0.95	-0.002608838

Minimum Error	-0.585080803
Maximum Error	0.329139685
Mean Error	-0.008231455
Standard Deviation	0.092158953

The comparison between standard texture analyser and new instrument on orange test.

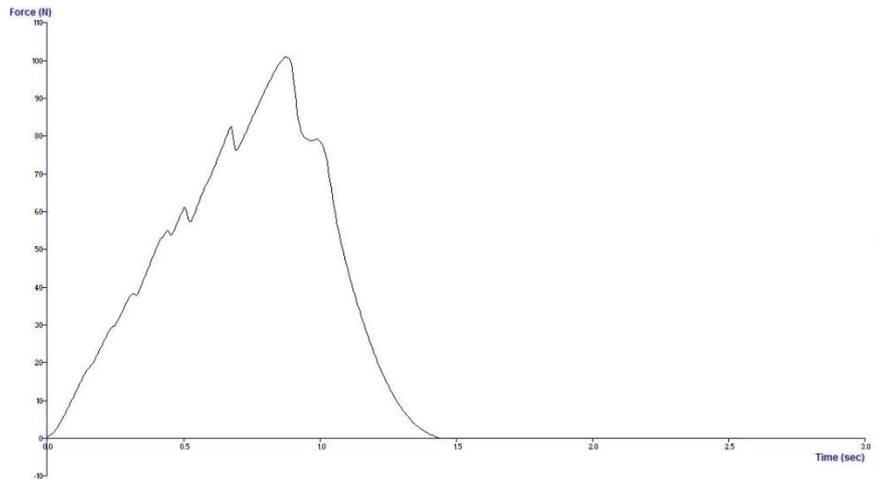


Results of tests on Gala Apple:

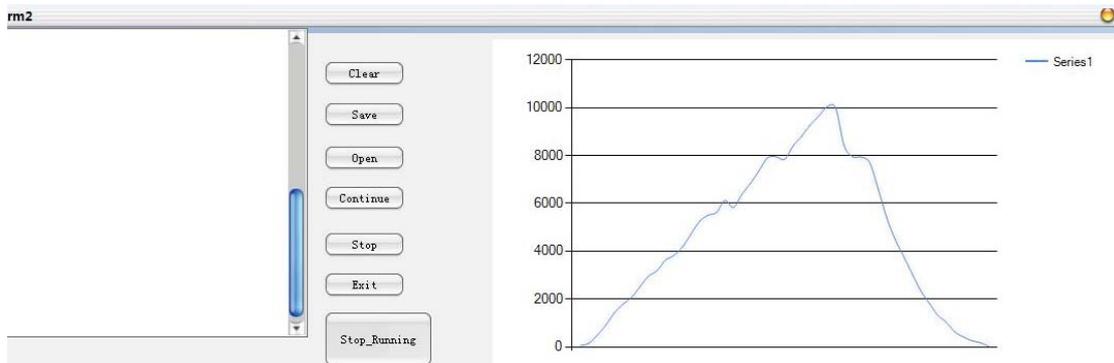
Test standard is the result from standard texture analyser, whereas Test1 is the test on new texture analyser.

Test (standard) (N)	Test (new instrument) (N)	Time (s)
0.385776829	0.5	0.013
1.527122087	1.48	0.025
4.869100361	4.93	0.055
8.989026383	9.05	0.085
14.18529107	14.21	0.12
17.87148458	17.79	0.145
20.64438875	20.63	0.175
24.99450205	25.1	0.205
29.47356286	27.51	0.24
31.79461792	32.84	0.265
36.269416	36.26	0.295
37.96278445	38.21	0.33
41.7289041	41.74	0.355
47.18626084	47.17	0.385
52.39318235	51.43	0.415
55.11813083	55.06	0.445
56.18914109	56.24	0.475
61.17226941	62.32	0.505
58.20967387	58.31	0.535
63.72244607	63.87	0.565
68.45407347	68.43	0.595
73.65246952	73.77	0.625
79.07359308	79.11	0.655
79.81743901	79.54	0.685
78.51730716	78.52	0.715
84.14197595	84.09	0.75
88.01253242	88.12	0.775
92.67915323	92.78	0.805
96.91630425	96.54	0.835
100.3595223	100.42	0.865
99.99186207	103.01	0.895
83.86383299	84.21	0.925
79.21852581	79.56	0.955
79.19614649	79.43	0.985
77.28324758	76.314	1.015
66.07120886	65.92	1.045

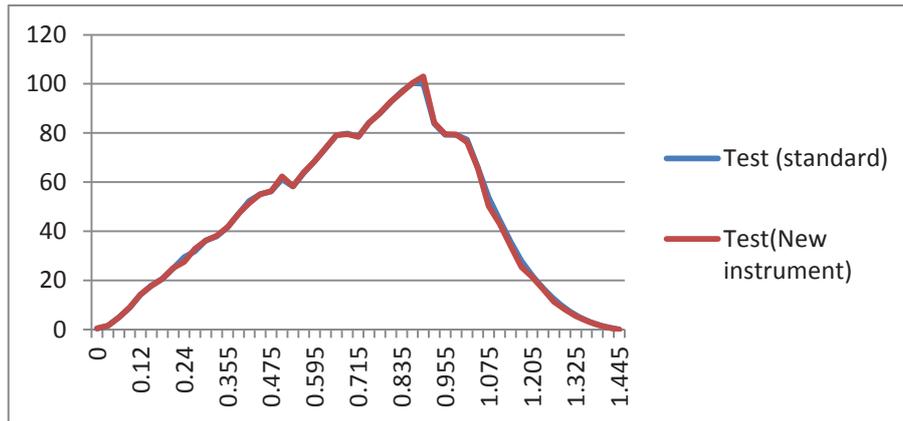
53.78602852	50.33	1.075
44.73945532	43.12	1.105
35.81863258	34.21	1.14
27.98267395	25.434	1.175
22.05322015	21.43	1.205
16.87294069	16.43	1.235
12.41412784	11.32	1.265
8.752445013	8.1	1.295
5.841002206	5.42	1.325
3.654223055	3.54	1.355
2.015204374	1.9	1.385
0.86533366	0.78	1.415
0.012788182	0.01	1.445



The curve of gala apple tested on standard instrument



The curve of gala apple tested on new instrument



Two curves coincide together.

Test (standard) (N)	Test (new instrument) (N)	Error (N)
0.385776829	0.5	-0.11422
1.527122087	1.48	0.047122
4.869100361	4.93	-0.0609
8.989026383	9.05	-0.06097
14.18529107	14.21	-0.02471
17.87148458	17.79	0.081485
20.64438875	20.63	0.014389
24.99450205	25.1	-0.1055
29.47356286	27.51	1.963563
31.79461792	32.84	-1.04538
36.269416	36.26	0.009416
37.96278445	38.21	-0.24722
41.7289041	41.74	-0.0111
47.18626084	47.17	0.016261
52.39318235	51.43	0.963182
55.11813083	55.06	0.058131
56.18914109	56.24	-0.05086
61.17226941	62.32	-1.14773
58.20967387	58.31	-0.10033
63.72244607	63.87	-0.14755
68.45407347	68.43	0.024073
73.65246952	73.77	-0.11753
79.07359308	79.11	-0.03641
79.81743901	79.54	0.277439
78.51730716	78.52	-0.00269
84.14197595	84.09	0.051976
88.01253242	88.12	-0.10747
92.67915323	92.78	-0.10085
96.91630425	96.54	0.376304

100.3595223	100.42	-0.06048
99.99186207	103.01	-3.01814
83.86383299	84.21	-0.34617
79.21852581	79.56	-0.34147
79.19614649	79.43	-0.23385
77.28324758	76.314	0.969248
66.07120886	65.92	0.151209
53.78602852	50.33	3.456029
44.73945532	43.12	1.619455
35.81863258	34.21	1.608633
27.98267395	25.434	2.548674
22.05322015	21.43	0.62322
16.87294069	16.43	0.442941
12.41412784	11.32	1.094128
8.752445013	8.1	0.652445
5.841002206	5.42	0.421002
3.654223055	3.54	0.114223
2.015204374	1.9	0.115204
0.86533366	0.78	0.085334
0.012788182	0.01	0.002788
Min Error	-3.018137935	
Max Error	3.456028523	
Mean Error	0.210333707	
Standard Deviation	0.924272863	

The comparison between standard texture analyser and new instrument on gala apple test.

Appendix 4 ADC code

```
#include <SPI.h>

#define CK 13

#define MISO 12

#define MOSI 11

#define AD_CS 10

#define AD_SYNC 9

#define AD_CS_ON() digitalWrite(AD_CS,LOW)

#define AD_CS_OFF() digitalWrite(AD_CS,HIGH)

//-----these are the configurations of registers--//

#define ST_R 0x44 //status read

#define MODE_W 0x08 //mode register

#define CR_W 0x10 //this is the configuration register..

#define DR_R_C 0x5c //Read data Consecutively

#define DR_R 0x58 //Read data uncontinuous

#define ID_R 0x60

//-----the adress of registers-----//

#define MR 0x08 //this is the mode register

#define CR 0x10 //this is the configuration register

#define DATA_R 0x18 //Data register/data register plus status
information

#define ID_R 0x20 // ID register

#define OFF_R 0x30 //offset register

#define FULL_SCALE 0x38 //full scale register

//-----the SPI driving
code-----//

byte ADC_Transfer(byte val)
{
    byte data_out= 0;

    AD_CS_ON();
```

```

    SPI.transfer(val);

    data_out = SPI.transfer(0xff);

    AD_CS_OFF();

    return data_out;
}

void ADC_Transfer_W(byte Adress_select, unsigned long val) // this
function is just for the 24bits
{
    AD_CS_ON();

    SPI.transfer(Adress_select);

    SPI.transfer(val>>16);

    SPI.transfer(val>>8);

    SPI.transfer(val);

    AD_CS_OFF();
}

unsigned long ADC_Transfer_R(byte Adress_select) // this function is just
for the 24bits
{
    unsigned long val = 0;

    AD_CS_ON();

    ADC_Transfer(Adress_select);

    val = ADC_Transfer(0x00);

    val=(val << 8)|ADC_Transfer(0x00);

    val=(val << 8)|ADC_Transfer(0x00);

    AD_CS_OFF();

    return val;
}

byte ADC_Transfer_R8(byte Adress_select) //this is for 8bit
{

    return ADC_Transfer(Adress_select);
}

```



```
}
```

```
void initialization()
```

```
{
```

```
  pinMode(AD_CS, OUTPUT);
```

```
  digitalWrite(AD_CS, HIGH);
```

```
  pinMode(MOSI, OUTPUT);
```

```
  pinMode(MISO, INPUT);
```

```
  pinMode(CK, OUTPUT);
```

```
  SPI.begin();
```

```
  SPI.setBitOrder(MSBFIRST);
```

```
  SPI.setClockDivider(SPI_CLOCK_DIV16); // or 2, 8, 16, 32, 64
```

```
  SPI.setDataMode(SPI_MODE3);
```

```
  Serial.begin(9600);
```

```
  ADC_Transfer_W(MODE_W,0x813ff);
```

```
  ADC_Transfer_W(CR_W,0x10f);
```

```
}
```

```
byte ADC_ID()
```

```
{
```

```
  byte val;
```

```
  AD_CS_ON();
```

```
  SPI.transfer(0x60);
```

```
  val = SPI.transfer(0xFF);
```

```
  AD_CS_OFF();
```

```
  return val;
```

```
}
```

```
void setup()
```

```

{
  initialization();
}

void loop()
{
  unsigned long val = 0;

  float data;

  AD_CS_ON();

  while(digitalRead(MISO)==1); //waiting for the output data

  SPI.transfer(0x58); //configure as continous mode

  val = SPI.transfer(0xff);

  val = (val<<8)|SPI.transfer(0xFF);

  val = (val<<8)|SPI.transfer(0xFF);

  Serial.println(val);

  delay(2);

  Serial.println("\n");

  delay(2);

  val = 0;

  AD_CS_OFF();
}

```